Università degli Studi di Ferrara

DOTTORATO DI RICERCA IN

"SCIENZE BIOMEDICHE E BIOTECNOLOGICHE"

CICLO XXX

Coordinatore Prof. Paolo Pinton

A JOURNEY THROUGH IN VITRO AND IN VIVO MODELS TO UNDERSTAND THE ROLE OF MAGMAS IN CANCER CHEMORESISTANCE

Settore Scientifico Disciplinare MED/13

Dottorando

Dott.ssa Riva Eleonora

Tutore

Prof.ssa Zatelli Maria Chiara

Anni 2014/2017

INDEX

1. INTRODUCTION

1.1MITOCHONDRIA

Mitochondria are maternally inherited, cytoplasmic organelles that originated from symbiotic bacteria around two billion years ago[1]. They co-evolved with their host, such that most mitochondrial proteins are nuclear encoded[2,3]. Cells have hundreds or thousands of these organelles and the number not only vary among species but also among tissue types[4]. Mitochondria are important bioenergetic and biosynthetic factories critical for normal cell function and human health[5]. Moreover, they are responsible for energy production in eukaryotes, including the synthesis of phospholipids and heme, calcium homeostasis, apoptotic activation and cell death[6,7,8]. Mitochondrial biogenesis is influenced by environmental stress such as exercise, caloric restriction, low temperature, oxidative stress, cell division, renewal and differentiation. Mitochondrial biogenesis is accompanied not only by variations in number, but also in size and mass[9].

1.1.1 MITOCHONDRIAL STRUCTURE AND FUNCTION

Mitochondria are generally described as static, rod-shaped structures ranging from 2 to 8 micrometers scattered throughout the cytoplasm.

Mitochondria are characterized by two membranes, the outer and the inner membrane (OM and IM, respectively). The two membranes delimit two aqueous compartments, the intermembrane space (IMS) between the OM and the IM and the matrix enclosed by the IM (Figure 1).

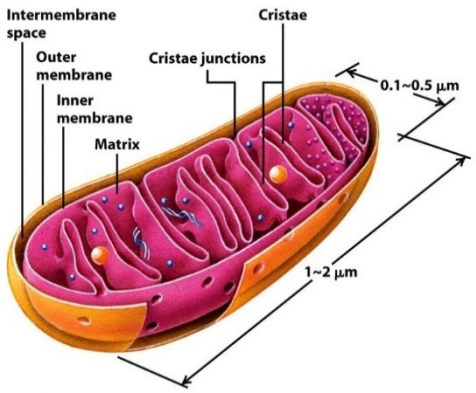

Figure 1: Mitochondrial structure

The OM is a semipermeable barrier prevalently enriched by porins that allow the free passage from/to cytosol of ions or up to 5-6 kDa small molecules.
The IMS, vice versa, is really selective, has a very high protein to phospholipids ratio (3:1) and is impermeable to molecules and even small ions. It contains multi-subunit complexes involved in generation of ATP (ATP synthase), in electron transport (cytochromes) and the Mitochondrial carriers (MCs) family, a highly represented group of solute and protein transporters[10]. It houses proteins involved in the assembly of respiratory chain components, in apoptotic signalling and protein import. The peculiarity of the IM is the folding into the *cristae mitochondrialis*, which enhance its surface area and thus the ability to produce ATP.
The matrix contains about one third of the total amount of mitochondrial proteins, since most of mitochondrial processes occur in the matrix (e.g. oxidation of pyruvate, of fatty acids, and Krebs' cycle). The solute environment of the matrix is dependent on the solutes and proteins transported across the IM.
Mitochondria retain a small 16,5 Kb double-stranded circular DNA genome (mtDNA) that encodes 37 genes: 22 tRNAs, 2 rRNAs and 13 proteins, which are core constituents of the mitochondrial respiratory complexes I-IV that are embedded in the inner membrane[9,11]. Mitochondria possess about 900 different proteins in yeast and about 1,500 different proteins in humans[12,13,14]. Ninety-nine percent of mitochondrial proteins is encoded by the nuclear DNA and synthesized on cytosolic ribosomes[15].
Within these organelles, sugars and long chain fatty acids are broken down, ADP is recycled back into ATP, steroids and lipids are synthesized, ancient DNA is replicated, transcribed and proteins are translated, along with numerous other reactions that are essential for human life[16].

1.1.2 MITOCHONDRIAL TARGETING SIGNALS

Biogenesis of mitochondria is under the control of two genetic systems, their own genome and that of the cell nucleus. However, contribution of the mitochondrial genome to the mitochondrial proteome is very limited and does not exceed 1% of the total number of proteins. The biogenesis of mitochondria, therefore, depends on the import of several hundreds of proteins from the cytosol. Mitochondrial precursor proteins are delivered to the organelle by virtue of specific targeting signals (MTS)[17,18]. These signals are highly divergent in nature but are all recognized by the specialized receptor proteins, which are located in the mitochondrial outer membrane and expose their hydrophilic receptor domains to the cytosol[19]. The information which directs specific targeting of newly synthesized precursor proteins (preproteins) to mitochondria is in the amino-terminal portion of the

presequence[20,21,22] . Presequences usually consist of 15 to 30 amino acid segments that are rich in positively charged and often hydroxylated amino acids[23]. Protein import into mitochondria is a highly regulated process that is coordinated by translocons on the outer membrane and the inner membrane[24] (Figure 2).

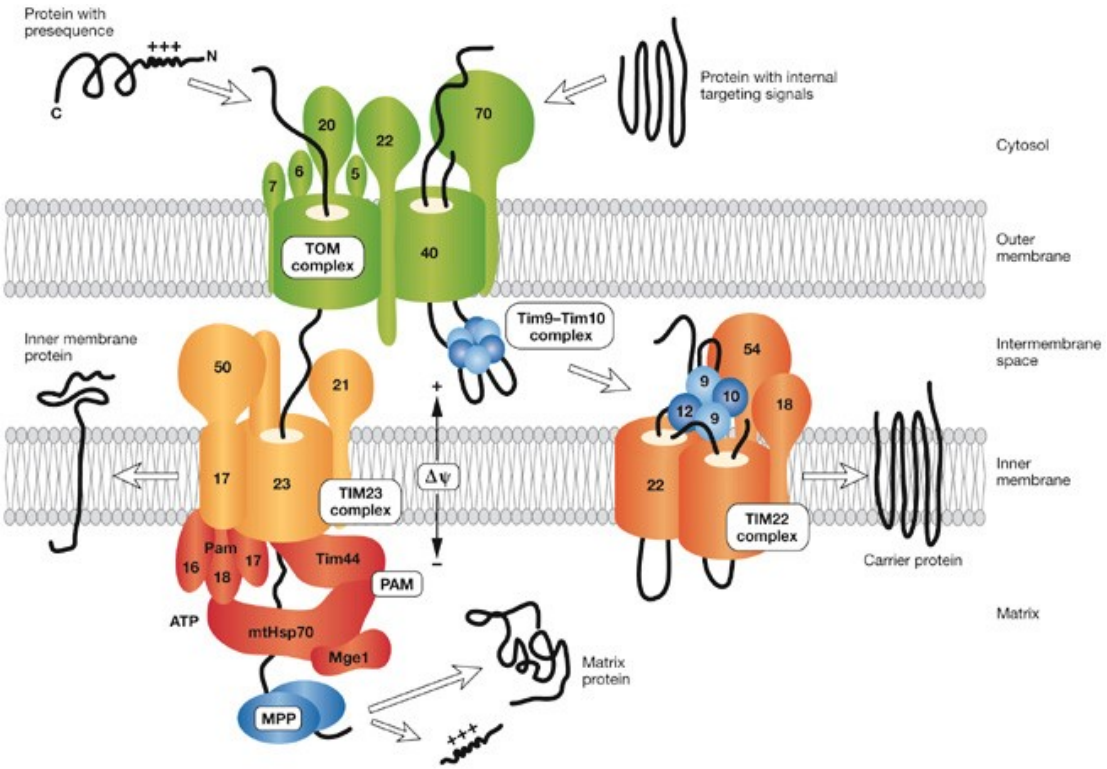

Figure 2: Two main protein import pathways of mitochondria. Presequences direct proteins through the TOM complex, TIM23 complex and motor PAM to the matrix; the mitochondrial processing peptidase (MPP) removes the presequences. Cleavable inner membrane proteins are laterally released from the TIM23 complex. Carrier precursors with internal targeting signals are recognized by the receptor Tom70, and translocated by the TOM complex and the Tim9–Tim10 chaperone of the intermembrane space. The TIM22 complex promotes insertion of carrier proteins into the inner membrane. MtHsp70, matrix heat shock protein 70; PAM, presequence translocase-associated motor; TIM, translocase of the inner membrane; TOM, translocase of the outer membrane[25].

The receptors deliver the precursor proteins to the translocation channel of the TOM (translocase of the outer membrane) complex through which the preproteins cross the outer membrane. TOM is the major gateway for proteins to enter the mitochondria and contains import receptors for the initial recognition of preproteins (Tom20, Tom22, and Tom70) and membrane-embedded components that form the general import pore which facilitates the translocation of preprotein across the outer membrane (Tom40, Tom5, Tom6, and Tom7)[26,27,28]. The Translocase of the Inner Membrane (TIM23) mediates import for proteins

that typically have an amino-terminal targeting sequence and reside in the matrix, whereas the TIM22 translocon directs the import of the carrier proteins. Together the translocation and assembly complexes coordinate assembly of the mitochondrion[23]. Tim50 is the first component of the TIM23 complex that interacts with precursors after they have been partially translocated across the outer membrane[29]. It is anchored into the mitochondrial inner membrane with a single transmembrane domain exposing its large C-terminal domain into the intermembrane space (IMS). Besides binding to the preproteins, this C-terminal domain also interacts with the N-terminal domain (amino acid residues 50–100) of Tim23, the other core complex of TIM23 together with Tim17. The TIM23 channel is formed by Tim17 and the C-terminal region of Tim23[30]. The accessory subunit Tim21 assembles with the TIM23 core complex to serve as a conduit to promote the transfer of substrates with a hydrophobic stop-transfer signal into the inner membrane in a membrane-potential dependent manner. The membrane potential $\Delta\psi$ serves as the initial driving force for protein translocation across the inner membrane by activating the Tim23 channel and promoting translocation of the positively charged presequences. For translocation of the entire preprotein into the matrix, a second driving force, the presequence translocase-associated motor (PAM), is essential[31]. Components of the PAM complex includes Tim44, mitochondrial Hsp70, the nucleotide exchange factor mGrpE (Mge1), and J-proteins Pam16 and Pam18. mtHsp70 is the central component of the PAM complex as it pulls the precursor into the matrix. mtHsp70 consists of an N-terminal nucleotide-binding domain and a C-terminal peptide-binding domain. Hsp70 chaperones use the energy of ATP hydrolysis at the nucleotide-binding domain to drive conformational changes of the peptide-binding domain, thereby altering its affinity for substrates[32]. In the case of mtHsp70, the substrates are the precursor polypeptides that are entering the mitochondrial matrix. The ATP-hydrolysis-driven cycle allows Hsp70 chaperones to associate with unfolded protein substrates in the ATP form and then bind them tightly upon hydrolysis to ADP. Release of ADP and rebinding of ATP triggers the release of the bound substrate[33].Co-chaperone Pam18 stimulates the ATPase activity of mtHsp70, whereas co-chaperone Pam16 regulates Pam18. Tim44 is crucial for mtHsp70 and J-protein binding and association of the PAM complex with the membrane[34]. Mge1 is the nucleotide exchange factor that is required for completion of the mtHsp70 reaction cycle. Repeated mtHsp70-binding cycles drive the complete translocation of the precursors into the matrix, where the presequence is proteolytically removed by the mitochondrial processing peptidase (MPP). Thus, the TIM23 translocon is a dynamic and highly regulated machine[3536]. TOM and TIM23 complexes do not appear to form a stable super complex in the absence of the precursor[19].

1.1.3 MITOCHONDRIA AND APOPTOSIS

Programmed cell death serves as a major mechanism for the precise regulation of cell numbers and as a defense mechanism to remove unwanted and potentially dangerous cells. Despite the striking heterogeneity of cell death induction pathways, the execution of the death program is often associated with characteristic morphological and biochemical changes, and this form of programmed cell death has been termed apoptosis[37].

Apoptosis is an evolutionary conserved, intrinsic program of cell death that occurs in various physiological and pathological situations and is characterized by typical morphological and biochemical hallmarks, including cell shrinkage, nuclear DNA fragmentation and membrane blebbing [3839]. The best characterized and the most prominent ones are called the extrinsic and intrinsic pathways. In both pathways, cysteine aspartyl-specific proteases (caspases) are activated, cleave cellular substrates, and this leads to the biochemical and morphological changes that are characteristic of apoptosis (Figure 3).

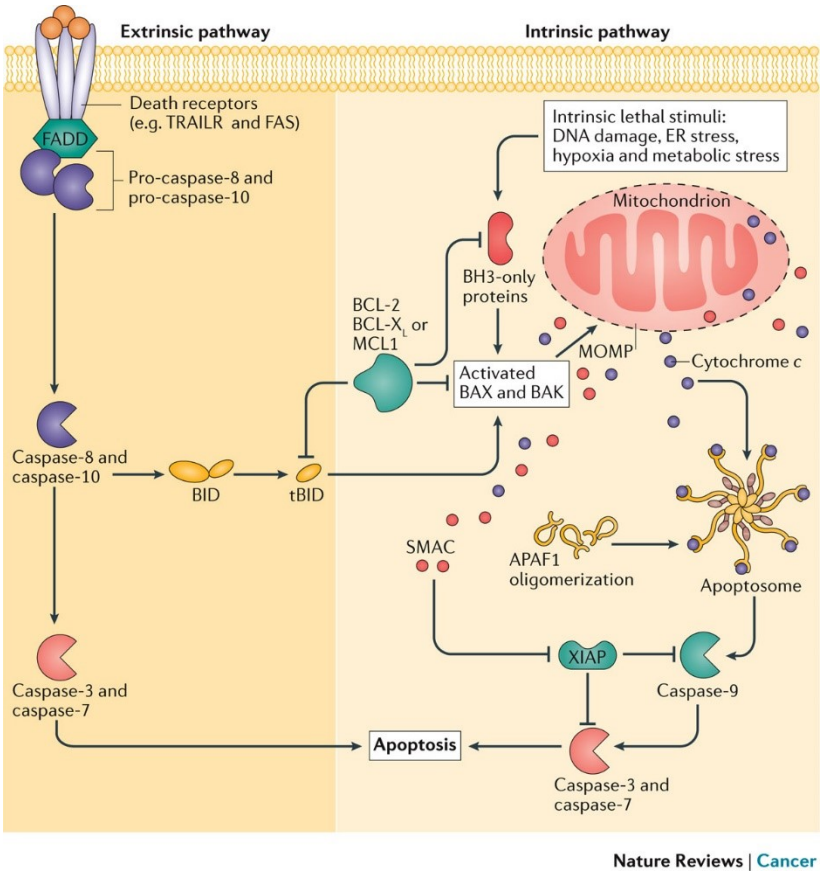

Figure 3: Extrinsic and intrinsic apoptotic signaling pathways[40].

In the **extrinsic pathway** (also known as "death receptor pathway"), apoptosis is triggered by the ligand-induced activation of death receptors at the cell surface. Death receptors are activated by their natural ligands, the TNF family[41]. When ligands bind to their respective death receptors, such as TNFR1-2, CD95, TRAIL-R1 (TNF-related apoptosis-inducing ligand-R1) or TRAIL-R2, the death domains (DD) attract the intracellular adaptor protein TRADD or FADD[4243] (Fas-associated death domain protein, also known as MORT1), which, in turn, recruits the inactive proforms of certain members of the caspase protease family. The caspases that are recruited to this death-inducing signaling complex (DISC)[44], caspase-8 and caspase-10, function as 'initiator' caspase for the signaling pathway[45,46,47].

In the **intrinsic pathway** (also called "mitochondrial pathway"), apoptosis results from an intracellular cascade of events in which mitochondrial outer membrane permeabilization (MOMP) plays a crucial role[48]. Upon cellular stress, the functional balance of proapoptotic BCL-2 (B-cell lymphoma 2) family members, such as BAX, BAK or BOK and anti-apoptotic Bcl-2 family members such as BCL-2 or BCL-XL is shifted in favor of the pro-apoptotic proteins. It appears that a third class of BH3-only proteins (BAD, BIK, BID, NOXA, PUMA, BNIP3 and BNIP3L[49]) and antiapoptotic BCL-2 proteins are positive and negative regulators of BAX/BAK, respectively[50,51,52]. It turns out a loss of mitochondrial transmembrane potential ($\Delta\Psi m$) with the formation of mitochondrial permeability transition (MPT) pores[53] and the release of pro-apoptotic proteins, normally sequestered from the intermembrane space, into the cytosol[50]. The BCL2-family members BAX, normally localized in the cytosol as a monomer, and BAK, normally localized in the mitochondria[54], directly activated by the tumor suppressor p53[55], form pores in the outer mitochondrial membrane (OMM), which releases several proteins, including cytochrome c and SMAC (second mitochondria-derived activator of caspases)/Diablo, from the intermembrane space into the cytosol[56]. Once in the cytosol, cytochrome c and SMAC/Diablo participate independently in activating caspases[57]. Cytochrome c binds and activates monomeric APAF1, promoting a conformational change with the replacement of ADP by dATP or ATP, that permits the formation of the APAF1 heptameric apoptosome able to recruit and activate caspase-9[58,59,60,61]. In the fully assembled complex, the NH_2-terminal caspase recruitment domain (CARD) of Apaf-1 form a ring structure that sits above the central hub of the apoptosome[62], and interactions with the CARD in the procaspase-9 prodomain recruit procaspase-9 into the apoptosome. Binding of procaspase-9 to the apoptosome results in its activation, by proteolytic cleavage. Active caspase-9 cleaves and activates the main proteases of the apoptosis execution phase, effectors caspases-3 and -7 [63]. SMAC/Diablo facilitates caspase activation by binding the X-linked inhibitor of apoptosis protein (XIAP)

and promoting apoptosis by inhibiting IAP (inhibitors of apoptosis proteins) activity[64], that specifically inhibit caspases 3, 7, and 9 and thereby prevent apoptosis[65].

Other pro-apoptotic proteins are released from the mitochondria during apoptosis and provoke nuclear condensation and chromatin fragmentation: AIF, endonuclease G and CAD. AIF translocates to the nucleus and causes DNA fragmentation into ~50–300 kb pieces and condensation of peripheral nuclear chromatin[66]. Endonuclease G also translocates to the nucleus where it cleaves nuclear chromatin to produce oligonucleosomal DNA fragments[67]. AIF and endonuclease G both function in a caspase-independent manner. CAD is subsequently released from the mitochondria and translocates to the nucleus where, after cleavage by caspase-3, it leads to oligonucleosomal DNA fragmentation and a more pronounced and advanced chromatin condensation[68,47] .

One example of the "cross-talk" between the death-receptor (extrinsic) pathway and the mitochondrial (intrinsic) pathway[45] happens when mitochondrial damage in the Fas pathway of apoptosis is mediated by the caspase-8 cleavage of pro-apoptotic BID (BH3-family) that translocate to the mitochondria to release cytochrome c [47].

1.1.4 RELEVANCE OF MORTALIN (MThSP70) TO CANCER CELLS

Cancer cells depend heavily on mitochondria, a key organelle for regulation of metabolism, survival and death signaling[69]. Mortalin/mtHsp70 has been shown to be highly expressed in cancer cells and to promote proliferation, metastasis and angiogenesis, and downregulate apoptotic signaling. It has been shown to interact with p53, telomerase and hnRNP-K in cancer cells[70,71]. It was shown to contribute to carcinogenesis by sequestrating the wild type p53, a key tumor suppressor protein, in the cytoplasm resulting in an abrogation of its transcriptional activation function[72]. Whereas p53 is inactivated by mortalin in cancer cells, telomerase and hnRNP-K are activated and were shown to contribute to malignant transformation. Increased mortalin expression was shown to inhibit p53-BAX interactions and activate AKT that are required for apoptotic signaling and to mediate resistance of ovarian cancer cells to cisplatin[73].

1.2 MAGMAS

Magmas (mitochondria-associated protein involved in granulocyte-macrophage colony-stimulating factor signal transduction) was identifies as a GM-CSF inducible gene in PGMD1 murine myeloid cells [74]. 61 Magmas homologs were analyzed in 52 species distributed among animals, plants and fungi and it was seen that all members possess three novel sequence motifs in addition to a conserved leader peptide. Analysis of Magmas gene organization demonstrated incremental intron acquisition in plants and vertebrates[75].

In humans it has been localized on the 16p13.3 chromosome with a genome of 11,16 Kb. It has 5 exons and encodes for the mitochondrial protein Tim16 of 125 aa[76] (Figure 4).

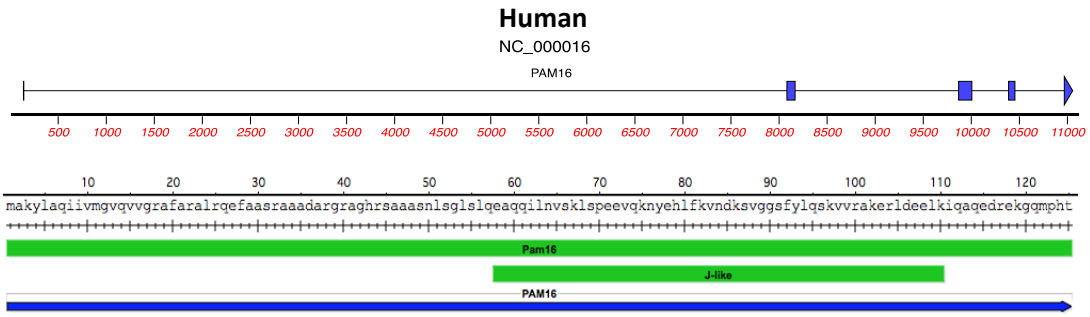

Figure 4: human Magmas genome and protein organization

Tim16 is member of the translocase complex TIM23, located in the mitochondrial inner membrane, that drives proteins from the intermembrane space into the matrix and its expression is both developmentally regulated and tissue specific[77]. The protein is highly conserved, and is required for mitochondria function and cell survival. Immuno-precipitation and immunoaffinity chromatography studies show that Magmas mostly associates with other mitochondrial proteins. Reduction in Magmas expression results in decreased mitochondrial function[75].

The yeast ortholog of Tim16, Pam16, has been shown to functionally interact with another protein Pam18 (Tim14), to regulate the importation of peptides into the mitochondria through the import complex[78]. Studies have also established that the functional Tim14/Tim16 complex is a heterodimer[79,80,81].

Tim16 and Tim14 together with Tim44, mtHsp70 and Mge1 form the PAM (Protein associated Motor) complex of TIM23. The ADP/ATP states of Hsp70 regulate its interactions with client proteins [82,83]. However, the basal ATPase activity of Hsp70 is not sufficient to drive the reactions efficiently and, thus, requires J-proteins as cofactors to stimulate its ATPase activity[84,85,86]. Hence, J-proteins are the critical components of the

Hsp70 chaperone machine and drive the multifunctionality of Hsp70s[84]. In yeast, mitochondrial import motor consists of a single J-protein, Pam18, which stimulates yeast mitochondrial Hsp70 (Ssc1) ATPase activity and forms a heterodimeric subcomplex with Pam16, a J-like protein that inhibits its ATPase stimulatory activity and thereby exerts a regulatory role on the overall activity of import motor and the transport process[33,87,88,89]. Homologs of Pam16 and Pam18-like proteins are found across all eukaryotic species.

In contrast to yeast, which has a single J-protein Pam18, humans involve two J-proteins, Tim15 and Tim14, able to form two distinct subcomplexes with Tim16 at the import channel[90].

1.2.1 J-PROTEINS

J-domain is a general feature of molecular chaperones that are highly conserved throughout evolution. Prokaryotic and eukaryotic Hsp70 proteins, for example, are over 50% identical at the amino acid level. The DnaJ family of molecular chaperones however, share this conservation only within a single 70 amino acid domain called the J-domain, and outside of this region the family is greatly divergent. Members of the J-protein family function as coupling factors to stimulate ATP hydrolysis by a partner Hsp70 when a polypeptide is present in its substrate-binding pocket.

DnaJ family has been classify upon the degree of domain conservation with E. coli DnaJ: type I- full domain conservation with N-terminal J-domain that is linked by a glycine-rich region to a zinc-finger domain followed by a carboxy-terminal domain; type II- N-terminal J-domain and G/F domains; type III- J-domain only[91]. The domain consists of four helices, the second of which has a charged surface that includes at least one pair of basic residues that are essential for interaction with the ATPase domain of Hsp70[92]. Further residues on the same face of this helix show backbone amide-proton chemical shifts in the presence of Hsp70, which indicates that they form an entire surface that is occluded in the transient DnaJ–Hsp70 complex[93]. Flexibility in the isolated J-domain is constrained on docking with the surface of the Hsp70 partner, as the J- domain assumes a fit with a bend induced in helix II[94]. The turn between helix II and III has the sequence triptych HPD, which is essential for the interaction of the protein with Hsp70[93,95].

Although Pam18 and Pam16 have significant sequence similarity, particularly in their J-domain regions, significant differences exist as well. Pam18 has a single transmembrane domain, with 60 N-terminal amino acids extending into the intermembrane space (IMS)[31,96,97]. Pam16 does not extend into the IMS, and it has been classified as a peripheral membrane protein[80,88]. Tim16 is a J-like protein as it contains a domain with sequence

similarity to the J-domain of Tim14 but lacks the invariant tripeptide motif His-Pro-Asp (HPD), a signature of J proteins, having a DKE motif instead. Pam18 and Pam16 form a heterodimeric complex, which is defined here as J-complex, and they strongly interact in a hydrophobic pocket that includes L150 of Pam18 and L97 of Pam16, leaving the conserved HPD motif of Pam18 available for stimulating Hsp70 ATPase activity[33] (Figure 5).

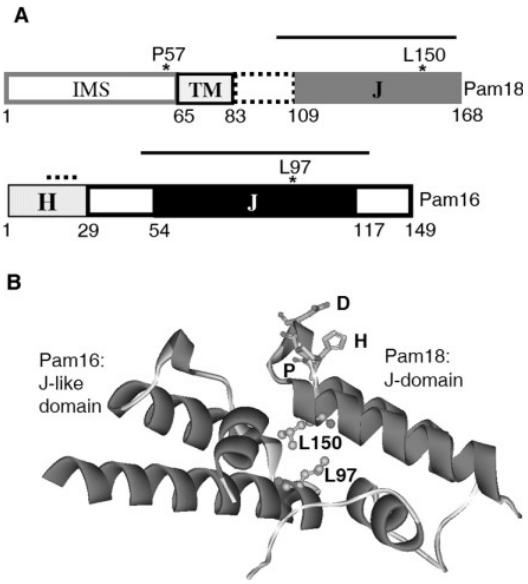

Figure 5: Domain organization of Pam16 and Pam18. (A) Pam18: aa 1-60, intermembrane space (IMS); aa 65-83, transmembrane (TM); aa 101-168, J-domain (J). Pam16: aa 1-29, hydrophobic (H); aa 54-117, J-like domain (J). Amino-acid alterations analyzed in this report are indicated by asterisks or, in the N terminus of Pam16, by a dotted line, indicating K19, E23, R26, and Q27. The segment of Pam18 and Pam16 used in structural determination[33] is indicated by the solid line. (B) Interaction of Pam18 and Pam16 J-domians[88].

Pam16 plays a major role in translocon association, as alterations affecting the stability of the Pam18:Pam16 heterodimer dramatically affect association of Pam18, but not Pam16, with the translocon[88]. The molecular function of Pam16 in the protein import motor remained unknown, but it is known that it inhibits the Pam18-mediated stimulation of the ATPase activity of mtHsp70[98] .

Alterations that destabilized the Pam16:Pam18 heterodimer had deleterious effects on cell growth and mitochondrial protein import[79]. Mutations that destroy the complex seems to be lethal demonstrating that complex formation is an essential requirement for the viability of cells[32].

1.2.2 MAGMAS AND NEOPLASIES

Magmas, that encodes for the 13-kDa mitochondrial protein Tim16, is ubiquitously expressed in eukaryotic cells and it was identified as a granulocyte-macrophage-colony stimulating factor (GM-CSF) inducible gene in hematopoietic cells. Although Magma's role in key cellular processes is still not entirely clear, some studies have highlighted a possible correlation between Tim16's over-expression and key events such as cell growth and apoptosis. Because GM-CSF receptor levels are elevated in prostate cancer, Magmas expression was examined in normal and neoplastic tissue. Magmas was found to be over-expressed in 50% prostate cancer, regardless to changes in mitochondrial content, suggesting a role for this gene in tumor development[99].

Studies conducted in our laboratory demonstrated that Magmas mRNA is over-expressed in 72% human pituitary adenomas as well as in ACTH-secreting mouse pituitary adenoma cell lines (AtT-20 D16v-F2 cells) compared to their respective human and murine normal counterparts (Figure 6). Fluorescence microscopy analysis showed that such over-expression lies in the mitochondria, and RQ-PCR experiments suggest that Magmas over-expression is not parallel to increased expression of other mitochondrial proteins. Magmas silencing determined a reduced rate of DNA synthesis, an accumulation in G0/G1 phase, and a concomitant decrease in S phase in At-T20 D16v-F2 cells, supporting the hypothesis that Magmas may play a role in tumor development by protecting neoplastic cells from apoptosis and by promoting cell proliferation. Moreover, Magmas-silenced cells displayed basal caspase 3/7 activity and DNA fragmentation levels similar to control cells, which both increased under pro-apoptotic stimuli[100].

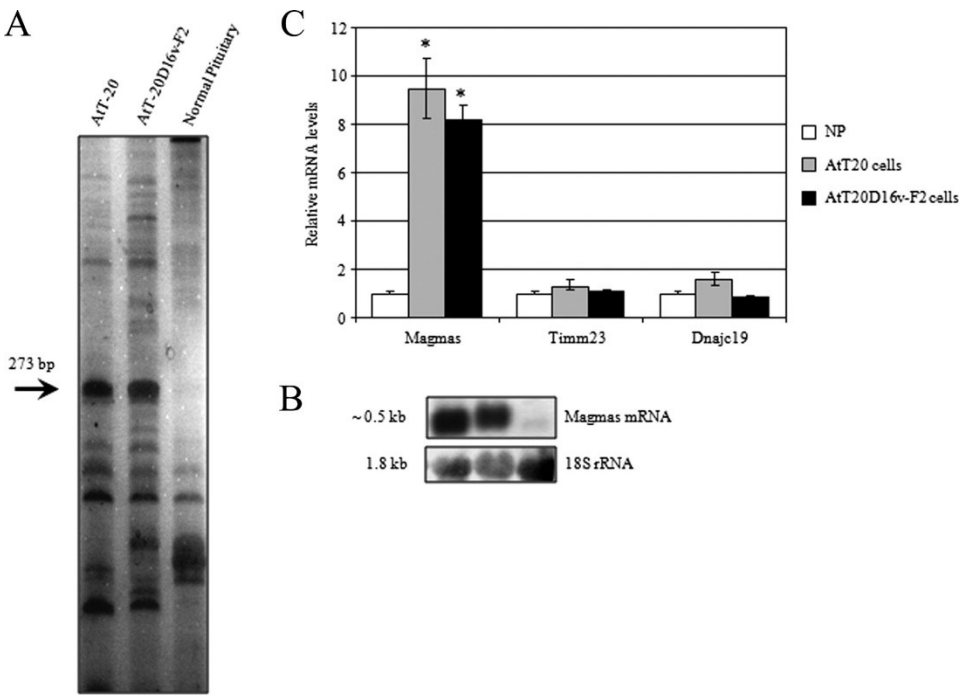

Figure 6: Identification of *Magmas* cDNA by DD-PCR and expression levels of *Magmas*, *Timm23*, and *DNAjc19* genes in AtT-20 and AtT-20 D16v-F2 cell lines. A) The *arrow* indicates *Magmas* cDNA fragments. B) The 273-bp cDNA was used as a probe to confirm the expression of *Magmas* (_0.5 kb) by Northern blot analysis in a pool of mouse normal pituitary mRNAs and in the AtT-20 and AtT-20 D16v-F2 cell lines. Magmas mRNA signal was normalized to mouse 18S RNA (*bottom panel*). C) Expression of mouse *Magmas*, *Timm23*, and *DNAjc19* genes in AtT-20 and AtT-20 D16v-F2 cell lines was determined by RQ-PCR and normalized to L37 as a housekeeping control. RQ-PCRs were run in triplicate, and the data are presented as a fold change of mRNA levels in target gene expression (mean _ SE) in the cell lines relative to the normal pituitary pool (NP). *, P _ 0.05[100].

The protective role of Magmas toward apoptotic stimuli was also confirmed in two GH-secreting rat pituitary adenoma cell lines, where Magmas over-expression protects from apoptosis by inhibiting staurosporine-induced cytochrome c release from mitochondria, influencing BAX and Bcl2 modulation by proapoptotic stimuli[101].

These data point to a role for Magmas in tumor resistance to proapoptotic stimuli (such as chemotherapic drugs), indicating that Magmas inhibition may represent a successful strategy to overcome chemoresistance[102].

Magmas has been also identified as a ‘reactive oxygen species (ROS) regulator’. Over-expression of Magmas led to reduction in ROS and increased cellular tolerance to oxidative stress, whereas its downregulation elevated the cellular ROS level and made the cells more susceptible to ROS-mediated apoptosis. Magmas enhances the activity of electron transport

chain (ETC) complexes, causing reduced ROS production suggesting that J-like domain of Magmas is essential for maintenance of redox balance[103].

Recently a homozygous missense Magmas mutation (pAsn76Asp) was reported in patients from two unrelated Lebanese families, affected with a rare lethal spondylometaphyseal dysplasia: Megarbane– Dagher–Melki type, a Skeletal dysplasias (SD) characterized by pre- and postnatal disproportionate short stature, short limbs, cardiomegaly, bone malformations, and early death[104,105]. The pAsn76Asp mutation lies in the helix II of Magmas J-like domain. The latter domain forms, with the J-domain of DNAJC19 (Tim14), a stable heterodimeric subcomplex. This is the first report linking a mutation in Magmas gene with a human developmental disorder, connecting this mitochondrial protein in the ossification process[106]. A second homozygous mutation (pQ74P) was reported on a 5 years old child[107].

1.2.3 MAGMAS INHIBITORS

Concerning the involvement of Magmas gene in human tumors such as prostate cancer or invasive adenocarcinoma, where a higher amount of Tim16 in the abnormal cells is not due to an increased number of mitochondria, small molecule of Magmas inhibitors (SMMI) have been synthesized. To study if these SMMI could be beneficial for studying mitochondrial function and for diagnosing and treating human disease, the first molecules where tested in *Saccharomyces cerevisiae* and mice, where these molecules were biologically active. This study showed that compound 9 (Figure 7) was predicted to bind at the dimer interface establishing multiple idrophobic contacts with both Tim14 (L100, K111, L114, Q115, T120) and Tim16 (F95) residues, resulting in complex dissociation. In addition, compound 9 likely interfered with the N-terminal arm of Tim14 that interacts with Tim16 helix III, known to be necessary for complex formation and function. Moreover, they shown that an overexpression of Magmas reduces sensitivity to SMMI 9[81].

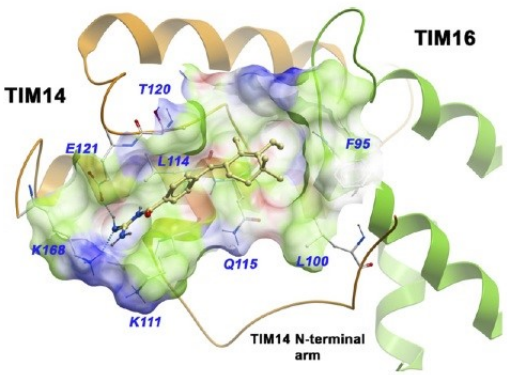

Figure 7: Model of SMMI 9 binding in the Tim14–Tim16 interface pocket. The predicted Tim14–Tim16 binding pocket surface is color coded according to protein binding properties

(white: neutral surface; green: hydrophobic surface; red: hydrogen bonding acceptor potential; blue: hydrogen bond donor potential; brown; SMMI 9)[81] .

Our laboratory together with the Dept. of Chemical and Pharmaceutical Sciences of the University of Ferrara, synthesized 6 compounds, derived from compound 9, challenging their effect toward the proapoptotic effects of staurosporine in TT cell line, deriving from a human medullary thyroid carcinoma (MTC). One of these molecules, the compound 5, turned out to be not cytotoxic but enhanced the proapoptotic effects of staurosporine by reducing mitochondrial membrane potential (MMP) activation[102] (Figure 8).

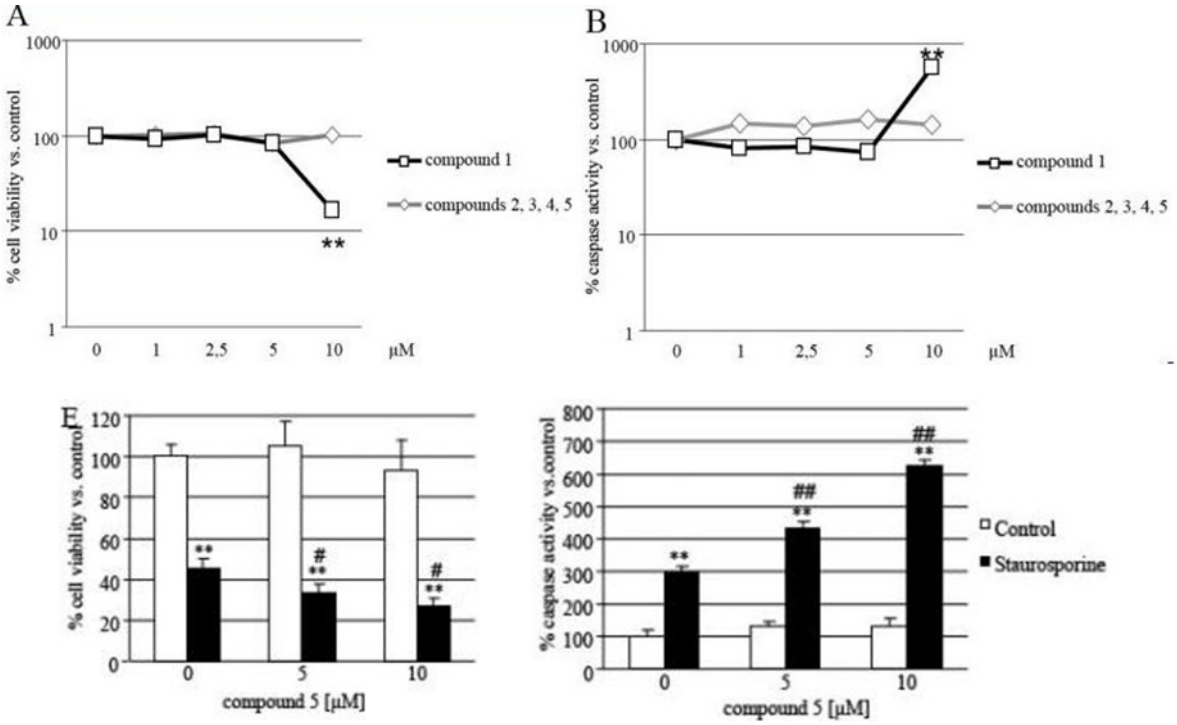

Figure 8: Effects of compounds 1, 2, 3, 4, and 5 on cell viability and apoptosis. TT cells were treated with increasing doses (1−10 μM) of compound 1 (black line) or compound 2, 3, 4, or 5 (gray line), renewing the treatment every 24 h. After 72 h, cell viability was measured by ATPlite assay (A) and apoptosis activation was measured by caspase 3/7 assay (B). ** indicates $P < 0.01$ vs control cells. (E) Effects of compound 5 5 and 10 μM in combination with staurosporine 50 nM on cell viability and apoptosis. ** indicates $P < 0.01$ vs control cells. # indicates $P < 0.05$ and ## indicates $P < 0.01$ vs staurosporine-treated cells[102].

Mass spectrometry studies have demonstrated that compound 5 was entirely present inside mitochondria of TT cell line, while it was absent in the medium.

Furthermore, our lab silenced Magmas in MCF7 cells by specific shRNA and found that compound 5 sensitizes control MCF7 cells to the pro-apoptotic stimuli of doxorubicin and cisplatin, but fails to do so in silenced cells, indicating that compound 5 targets Tim16 and that Tim16 levels modulate the chemosensitizing effects of compound 5 (Figure 9).

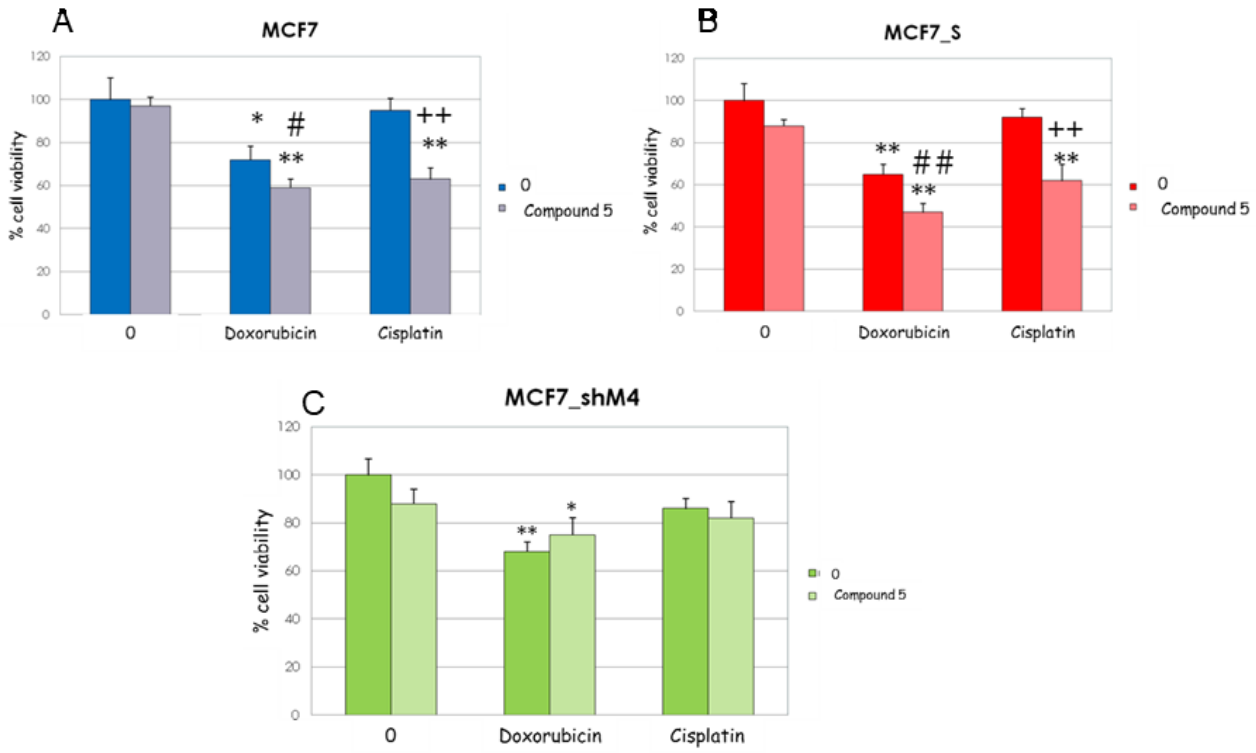

Figure 9: Effects of compound 5, doxorubicin and cisplatin on cell viability in MCF7 cells (A), MCF7_S transfected with the scramble shRNA (B) and MCF7_shM4 silenced with a shRNA (C). (* p< 0,05 vs ct, ** p< 0,01 vs ct, # p < 0,05 vs doxorubicin treated-cells, ## p < 0,01 vs doxorubicin treated-cells, ++ p < 0,01 vs cisplatin treated-cells).

The evidence that Magmas down-regulation sensitizes pituitary cells to proapoptotic stimuli prompted the search for chemical compounds that may be effective in reducing Magmas function. The availability of such compounds may indeed represent a powerful therapeutic tool to enhance tumor sensitivity to drugs inducing apoptosis, thereby contrasting the proliferative tumor potential. These data suggested that these compounds may be useful in association with classical chemotherapeutic drugs for cancer treatment.

This strategy would allow a reduction of the chemotherapeutic agent effective dose, with a consequent decrease in side effect development, overcoming also chemoresistance.

1.3 CHEMORESISTANCE

Chemotherapy is one of the principal modes of treatment for cancer, but the effectiveness of chemotherapy is limited by drug resistance. Resistance to chemotherapeutics can be divided into two broad categories: intrinsic or acquired. Intrinsic resistance indicates that before receiving chemotherapy, resistance-mediating factors pre-exist in the bulk of tumor cells that make the therapy ineffective. Acquired drug resistance can develop during treatment of tumors that were initially sensitive and can be caused by mutations arising during treatment, as well as through various other adaptive responses, such as increased expression of the therapeutic target and activation of alternative compensatory signaling pathways[108]. Moreover, it is increasingly recognized that tumors can contain a high degree of molecular heterogeneity[109], thus drug resistance can arise through therapy-induced selection of a resistant minor subpopulation of cells that was present in the original tumor[110]. Overcoming intrinsic and acquired drug resistance is a major challenge in treating cancer patients because chemoresistance causes recurrence, cancer dissemination and death.

Chemoresistance causes disease relapse and metastasis, challenges the improvement of clinical outcome for the cancer patients, and remains the main obstacle to cancer therapy[111]. Most cancers are intrinsically resistant to chemotherapy or become resistant after an initial partial response[112]. Chemoresistance, whether intrinsic or acquired, is attributable to genetic or epigenetic processes taking place in neoplastic cells[113]. Several explanations for drug resistance have been put forward: (*a*) decreased accumulation of drug within cells because of reduced inward transport or increased drug efflux; (*b*) enhanced inactivation or detoxification of the drug; (*c*) failure to convert the prodrug to its active form; (*d*) altered amounts or activities of target proteins; (*e*) enhanced capacity for DNA repair; and (*f*) increased resistance to apoptosis. Multiple factors in that list appear to coexist in cancer cells. An increased understanding of mechanisms underlying drug resistance may lead to the development of more successful therapeutic protocols[114].

The use of modern genomic, proteomic and functional analytical techniques has resulted in a substantial increase in the ability to identify novel genes and signaling networks that are involved in determining the responsiveness of tumors to a particular drug treatment. Moreover, the use of high-throughput techniques in combination with bioinformatics and systems biology approaches has aided the interrogation of clinical samples and allowed the identification of molecular signatures and genotypes that predict responses to certain drugs. In addition, such approaches can identify novel therapeutic targets for overcoming or bypassing drug resistance. As the understanding of the molecular biology of cancer has

advanced, drug development has shifted towards agents that target specific molecular alterations in tumors. These 'molecularly targeted therapies' have had varying degrees of success because a diverse range of resistance mechanisms have limited patient responses[110].

1.3.1 MEDULLARY THYROID CANCER

Medullary thyroid cancer (MTC) accounts for 3%–4% of all thyroid cancers[115,116]. The clinical course of MTC can be indolent, remaining unchanged for years, or it can be aggressive, associated with high mortality. Although the majority of MTC cases are sporadic (70-80%), approximately 20-30% are hereditary because of a germline mutation in the 'REarranged during Transfection' (RET) proto-oncogene, transmitted as an autosomal dominant trait[117,118,119, 120,121]. Sporadic MTC (sMTC) can arise clinically at any age but its incidence peaks between the fourth and sixth decade of life. Patients with sporadic MTC usually present a palpable thyroid nodule. Clinical neck lymph node metastases are detected in half of patients and may reveal the disease. Metastases outside the neck, in the liver, lungs or bones are present initially in 20% of cases[122]. Hereditary MTC can present in isolation (familial medullary thyroid cancer [FMTC]) or as part of the multiple endocrine neoplasia syndrome type 2 (MEN2; MEN2A or MEN2B).

Genetic abnormalities are present in MTC, and hereditary forms are characterized by germline RET mutations while sporadic MTC showed somatic alterations in 40-60% of patients[123].

MTC arises from the neural crest, specifically the parafollicular C cells of the thyroid gland and for this reason is considered a neuroendocrine tumor. Although the C cells are located throughout the thyroid gland, they are predominant at the junction of the upper third and lower two-thirds, which is where the majority of MTCs are found. C cells secrete a variety of peptides and hormones, and MTC is characterized by the secretion of calcitonin, which is used as a diagnostic and prognostic marker in MTC[124].

1.3.2 MTC AND CHEMORESISTANCE

The only effective MTC treatment is surgical resection of the tumor and the most difficult problem is treatment of unresectable metastatic MTC[125].

Pharmacological cancer therapy for decades was performed with non-targeted mostly DNA-interacting cytostatic drugs. Administration of these so-called conventional cytostatics usually is entailed with severe side-effects[126]. One of the main disadvantages of those substances is that they do not specifically target cancer cells but all (also benign) rapidly

dividing cells. This non-specific mechanism of action was the rationale to develop specifically targeted anti-cancer Tyrosine kinase inhibitors (TKI). Initially, great expectations were associated with these drugs; some were met, others not. TKI are a very worthy additional option for physicians in clinical management of certain types and lines of cancer treatment[127]. Small-molecule inhibitors of RET, including vandetanib[128] and cabozantinib[129], have been demonstrated to extend the PFS of patients with progressive, advanced-stage MTC, and are both now approved in the USA and EU for use in such patients. Interestingly, the available RET TKIs are also potent inhibitors of VEGFR, leaving open questions as to whether RET inhibition in addition to inhibition of VEGFR and/or other kinases might also contribute to the clinical effectiveness of these agents. Other small-molecule multikinase inhibitors that block VEGFR signalling have shown promise in the treatment of radioactive iodine (RAI)-refractory differentiated thyroid cancer (DTC): sorafenib and lenvatinib are approved for use in the metastatic setting[130]. Metastatic MTC responds poorly to conventional treatments with chemotherapy and radiotherapy[131]. Doxorubicin treatment resulted in tumor response rates between 0% and 20% in patients with recurrent MTC. In these trials, all responses were partial and lasted only a few months. Combination therapy with doxorubicin and cisplatin yielded response rates similar to those achieved with doxorubicin alone, but with additional major toxic effects[132]. The aim of the introduction of these targeted therapies is to extend life duration while assuring a good quality of life. Toxicities of many of these new therapies, although less life-threatening than cytotoxic chemotherapies, are common and can be dose limiting, and clinicians should be familiar with recognizing and managing the side effects if they intend to use these agents[133]. Even if PFS of patients treated with TKI therapy is significantly longer, the chemoresistance problem is still existing.

The challenge is to find novel therapeutic approaches in overcoming chemoresistance and the MTC cell line, TT cells, are a good chemoresistent candidate for these studies[134].

1.3.3 BREAST CANCER

Breast cancer is the second most common cancer in the world, but is the most common malignancy in women and it has a high incidence and mortality rate, with 1,384,155 (25% of all cancers) estimated new cases worldwide with nearly 459,000 related deaths.[135,136]. One in eight women in the United States will develop breast cancer in her lifetime and it has been predicted that the worldwide incidence of female breast cancer will reach approximately 3.2 million new cases per year by 2050[137]. The disease is the single commonest cause of death

among women aged 40-50[138]. Only 5–10% of breast cancer cases are hereditary, however, for women with germline BRCA mutations, the breast cancer risk is substantial. Women with BRCA1 and BRCA2 mutation-associated breast cancer also face elevated risk of second malignancies[139]. There are many types of breast cancer and they can be broadly categorized into in situ carcinoma and invasive (infiltrating) carcinoma[140]. Moreover, the type of breast cancer is determined by the specific cells in the breast that are affected. Most breast cancers begin in the cells that line the ducts (ductal cancers). Some begin in the cells that line the lobules (lobular cancers)[141]. However, the most common types are ductal carcinoma in situ, invasive ductal carcinoma, and invasive lobular carcinoma. While the histological classification scheme has been a valuable tool for several decades, it has become necessary to more accurately stratify patients based on relative risk of recurrence or progression[140]. Clinically, this heterogeneous disease is categorized into three basic therapeutic groups. The estrogen receptor (ER) positive group is the most numerous and diverse, with several genomic tests to assist in predicting outcomes for ER^+ patients receiving endocrine therapy[142,143]. The HER2 (also called ERBB2) amplified group[144] is a great clinical success because of effective therapeutic targeting of HER2, which has led to intense efforts to characterize other DNA copy number aberrations[145,146]. Triple-negative breast cancers (TNBCs, lacking expression of ER, progesterone receptor (PR) and HER2), also known as basal-like breast cancers[147], are a group with only chemotherapy options, and have an increased incidence in patients with germline BRCA1 mutations [148,149] or of African ancestry[150].

1.3.4 BREAST CANCER AND CHEMORESISTENCE

Four types of breast cancer, including Basal (also known as, triple negative), HER2 (human epidermal growth factor receptor 2) positive, Luminal A (estrogen-receptor and/or progesterone-receptor positive, HER2 negative), and Luminal B (estrogen-receptor and/or progesterone-receptor positive, HER2 positive or negative)[151] demonstrate phenotypic and genotypic heterogeneity, which is a common feature of breast cancer[152]. Heterogeneity is considered a dilemma for breast cancer therapy[153]. Early detection is key for patients; with a >90% 5-year survival rate for patients diagnosed at stages 0, I or II. Approximately 10% of patients present with stages III and IV, where treatment options are determined on an individual patient basis. For advanced breast cancer, traditional chemotherapy and radiation can be used. Primary breast cancers without distant spread are highly curable with local or regional treatment. However, most women with primary breast cancer have subclinical

metastases and eventually develop distant metastases that complicates the curability of the disease. Over the past several decades, breast cancer survival rates have significantly improved[154]. While many factors are credited, including the development of early detection methods, this improvement can be attributed to the development of new treatment modalities and new drugs. Regimens based on anthracyclines (doxorubicin, daunomycin, and epirubicin)[155] and taxanes (paclitaxel and docetaxel)[156157] are the most frequently used combination therapy for breast cancers. However, the response rates remain suboptimal[158]. Taxane chemotherapy is one of the most common therapeutic options in breast cancer; however, its effectiveness usually decreases progressively until it reaches a point where the treatment must be modified. As seen in clinical practice, after multiple rounds of treatment, triple negative tumors acquired resistance to the drug; this resistance, once present, remained even if the treatment was not supplied[159]. The *MDR1*-encoded Pgp is responsible for multidrug resistance in cultured cells exposed to antitumor agents, including doxorubicin, vincristine, and taxanes, etoposide, teniposide, Actinomycin D. Many of these agents are used to treat breast cancers[160]. It has been seen in previous studies that the human cell line MCF7, deriving from a pleural effusion of a patient with metastatic breast cancer, is able to reproduce this chemoresistance towards doxorubicin, resulting a good model for these studies[161,162].

1.4 ANIMAL MODELS

Animal models can be an essential tool in the delineation of human disease pathophysiology, as well as a test bed for potential therapeutic strategies. Animal models represent a good tool to predict human outcomes and to determine safety margins and toxicity. In the following studies the focus will be on two different models, xenograft mice and zebrafish.

1.4.1 SUBCUTANEOUS XENOGRAFT MICE

Mouse models of cancer have consistently been used to determine the in vivo activity of new anti-cancer therapeutics prior to clinical development and testing in humans. The most common models are xenografts of human tumors and cell lines grown subcutaneously in immunodeficient mice such as athymic (nude) or severe combined immune deficient (SCID) mice. These mouse strains exhibit very high take rates for xenografts, making them ideal hosts for in vivo propagation of human tumor cells. Xenograft tumors are usually established via subcutaneous inoculation of a predetermined number of tumor cells into the flank of nude

mice. Xenograft models are commonly used to determine ideal drug dosing, treatment schedules, and routes of drug administration that maximize anti-tumor efficacy and therapeutic window. To study the *in vivo* effects of the compound 5[102], the Tim16 inhibitor, in combination with the chemotherapeutic drug paclitaxel, nude mice were injected subcutaneously with MTC cells. Previous *in vitro* studies conducted in our lab on TT cell line shown that compound 5 was able to increase the effect of paclitaxel by 14% and to reduce basal and pentagastrin induced calcitonin secretion.

1.4.2 ZEBRAFISH

The zebrafish (*Danio Rerio*) is one of the most important vertebrate model organisms in genetics, developmental biology, neurophysiology and biomedicine[163,164,165]. Since 1970s, the zebrafish has become increasingly important to scientific research as a genetically tractable vertebrate model system. Through the 1980s, the development of zebrafish genetic techniques, such as 'cloning'[166] , mutagenesis [167,168,169,170], transgenesis[171] and mapping approaches[172], underpinned the use of zebrafish to apply invertebrate-style forward genetics to questions of vertebrate development. The zebrafish is a tropical freshwater fish belonging to the family Cyprinidae, native to Southeast Asia[173]. Zebrafish have a number of unique features that have contributed to its attraction, such as its rapid development, easy maintenance in the laboratory, large number of offspring, transparency of embryos and access to experimental manipulation[174]. It is a small (3-5 cm), robust fish, so large numbers can be kept easily and cheaply in the laboratory, where it breeds all year round. Females can spawn every 2-3 days and a single clutch may contain several hundred eggs. Generation time is short, typically 3-4 months, making it suitable for selection experiments. Zebrafish eggs are large relative to other fish (0.7 mm in diameter at fertilisation) and optically transparent, the yolk being sequestered into a separate cell. Furthermore, fertilization is external so live embryos are accessible to manipulation and can be monitored through all developmental stages under a dissecting microscope. Development is rapid, with precursors to all major organs developing within 36 hours and larvae displaying food seeking and active avoidance behaviors within five days post fertilisation, i.e. 2-3 days after hatching [175,176](Figure 10). Zebrafish possess 26,206 protein-coding genes[177] , more than any previously sequenced vertebrate, and they have a higher number of species-specific genes in their genome than do human, mouse or chicken. A direct comparison of the zebrafish and human protein-coding genes reveals a number of interesting features. 71.4% of human genes have at least one

zebrafish orthologue, reciprocally, 69% of zebrafish genes have at least one human orthologue[178].

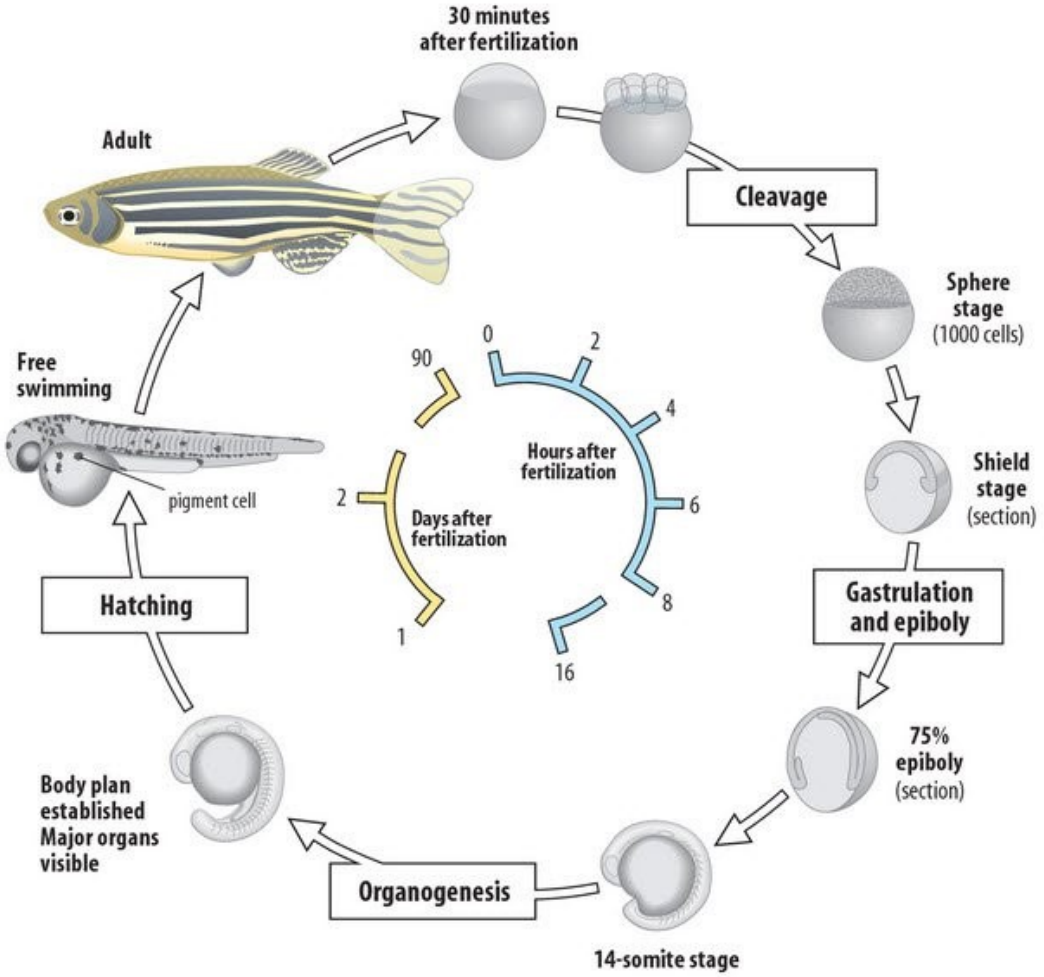

Figure 10: Life cycle of the zebrafish. Zebrafish develop rapidly from one one-cell zygote that sits on top of a large yolk cell. Gastrulation begins approximately 6 h post fertilization, hatching at 2 days as a free-swimming larva. Zebrafish reach sexual matu- rity around 3 months of age and can live for up to 5 years.

1.4.3 TOXICITY TEST IN ZEBRAFISH

Zebrafish embryo (Danio Rerio) has emerged as a useful prototype for investigating vertebrate development and as a promising alternative model for developmental toxicity screening[179]. Their transparency makes them well suitable for embryo-larval toxicity tests which are generally more sensitive than toxicity tests with juvenile and adult fish. Moreover, the high cost and the long-term assessment of developmental toxicity testing in mammals, the vertebrate zebrafish has become a useful alternative model organism for high-throughput developmental toxicity testing[180]. Acute fish toxicity tests are required for the testing of

chemicals, pesticides, biocides and pharmaceuticals for environmental risk assessment (Commission of the European Communities 1967, 1991, 1992, 1993a, b, 1994; CVMP/VICH 2000; EMEA/CHMP 2006; VICH 2004). In a number of countries (OSPAR 2000) they are also used for routine testing of waste water effluents[174]. Acute toxicity in fish embryos correlates very well with acute toxicity in adults. Originally designed as an alternative for the acute fish toxicity test according to, e.g., OECD TG 203[181], the fish embryo test (FET) with the zebrafish has been optimized, standardized, and validated by the Working Group of the National Coordinators (WNT) of the OECD Test Guideline Program in 2013 (OECD 2013)[182] and adopted as OECD TG 236 as a test to assess toxicity of embryonic forms of fish. Given its excellent correlation with the acute fish toxicity test and the fact that non-feeding developmental stages of fish are not categorized as protected stages according to the new European Directive 2010/63/EU on the protection of animals used for scientific purposes, the FET is ready for use not only for range-finding but also as a true alternative for the acute fish toxicity test, as required for a multitude of national and international regulations. If, for ethical reasons, not accepted as a full alternative, the FET represents at least a refinement in the sense of the 3Rs principle[183]. According to the procedure specified by OECD TG 236 (OECD 2013), newly fertilized zebrafish embryos are exposed to the test chemical for a total of 96 h. Every 24 h, up to four apical observations are recorded as indicators of lethality[184,185,186]: (1) coagulation of fertilized eggs, (2) lack of somite formation, (3) lack of detachment of the tail bud from the yolk sac, and (4) lack of heartbeat. In order not to miss the possible very early adverse effects on zebrafish development, particular care has to be taken to initiate exposure as early as possible (at latest 1.5 h after fertilization) (Figure 11).

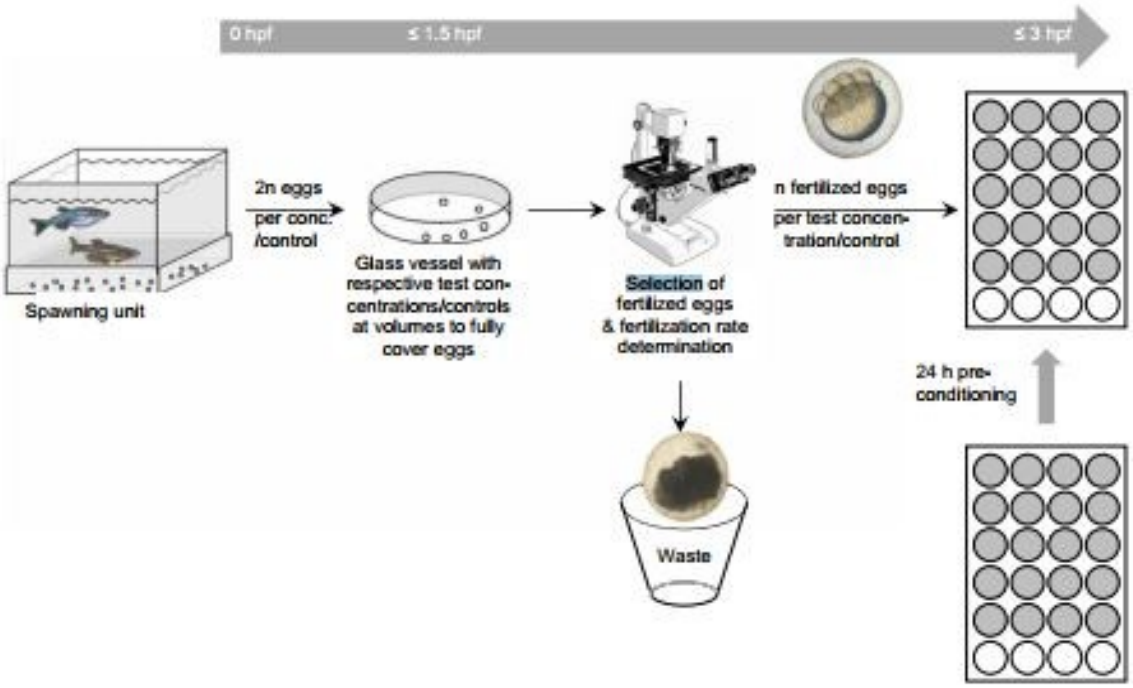

Figure 11: **Scheme of the zebrafish embryo acute toxicity test procedure (from left to right):** production of eggs, collection of the eggs, pre-exposure immediately after fertilization in glass vessels, selection of fertilized eggs with an inverted microscope or binocular and distribution of fertilized eggs into 24-well plates prepared with the respective test concentrations/controls, n = number of eggs required per test concentration/control (here 20), hpf = hours post-fertilization.

1.5 GENOME EDITING

Targeted genome editing has become a powerful genetic tool for studying gene function or for modifying genomes. These advances in the comprehension of the genetic basis of disease have improved the understanding of disease mechanisms and pointed toward potential therapeutic strategies. A rapidly developing alternative technology to manipulate gene expression is genome editing, which, in contrast to gene-transfer approaches, uses programmable DNA nucleases. Four genome-editing platforms currently predominate the field: meganucleases, zinc-finger nucleases (ZFNs), transcription activator-like effector nucleases (TALENs), and the (clustered regularly interspaced short palindromic repeat) CRISPR–Cas9 system[187](Figure 12). All of them can achieve precise genetic modifications by inducing targeted DNA double-strand breaks (DSBs)[188]. Foundational to the field of gene editing was the discovery that targeted DNA double strand breaks (DSBs) could be used to stimulate the endogenous cellular repair machinery. Breaks in the DNA are typically repaired through one of two major pathways—homology-directed repair (HDR) or nonhomologous end-joining (NHEJ)[189]. HDR relies on strand invasion of the broken end into a homologous sequence and subsequent repair of the break in a template-dependent manner[190]. Alternatively, NHEJ functions to repair DSBs without a template through direct relegation of the cleaved ends[191]. This repair pathway is error-prone and often results in insertions and/or deletions (indels) at the site of the break. Stimulation of NHEJ by site-specific DSBs has been used to disrupt target genes in a wide variety of cell types and organisms by taking advantage of these indels to shift the reading frame of a gene[192].

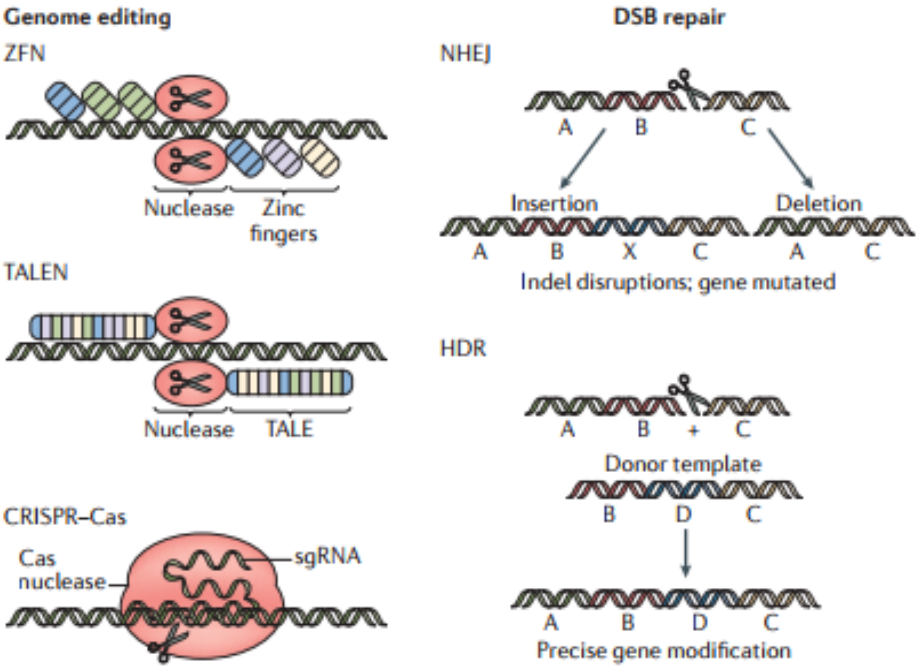

Figure 12: The mechanisms of genome editing and DSB repair. Zinc-finger nuclease (ZFN), transcription activator-like effector nuclease (TALEN) and CRISPR–Cas systems can induce double-strand breaks (DSBs) in DNA. One of two mechanisms repairs the DSB to achieve genome editing: non-homologous end joining (NHEJ) or homology-directed repair (HDR). NHEJ disrupts the target gene through insertions or deletions, whereas HDR inserts donor DNA template into the target genomic region to install insertions, deletions or alterations of genomic sequences. sgRNA, single guide RNA[187].

Programmable nuclease-mediated NHEJ can disrupt disease-causing genes permanently. It is possible to use NHEJ to restore the reading frame of a dysfunctional gene to treat a disease[193]. In the following study the focus will be on the CRISPR/Cas9 system that introduces a DSB at a genomic sequence of interest and the lesion that is generated is repaired via nonhomologous end joining (NHEJ), which is an endogenously equipped pathway in living nuclei to repair DSBs by connecting lesions. NHEJ is an error-prone mechanism; thus, small insertions or deletions can be introduced and can disrupt target genes by shifting the reading frame, resulting in mRNA degradation or the production of nonfunctional proteins[194]. When a gRNA is set within an open reading frame of a gene of interest, a frameshift mutation is expected to be induced by repair error. This method can also be applied to generate double-, triple- or multiple-gene knockouts by introducing a set of gRNAs for target genomic sequences and Cas9[195].

1.5.1 CRISPR/Cas9 TECHNOLOGY

The development of recombinant DNA technology in the 1970s marked the beginning of a new era for biology. For the first time, molecular biologists gained the ability to manipulate DNA molecules, making it possible to study genes and harness them to develop novel medicine and biotechnology. Recent advances in genome engineering technologies are sparking a new revolution in biological research[196]. The field of biology is now experiencing a transformative phase with the advent of facile genome engineering in animals and plants using RNA-programmable CRISPR-Cas9. CRISPRs (clustered regularly interspaced palindromic repeats) had been described in 1987 by Japanese researchers as a series of short direct repeats interspaced with short sequences in the genome of Escherichia coli[197]. In 2007, infection experiments of the lactic acid bacterium Streptococcus thermophilus with lytic phages provided the first experimental evidence of CRISPR/Cas–mediated adaptive immunity[198]. In 2012 the first biochemical characterization of Cas9-mediated cleavage[199,200]. The CRISPR-Cas9 technology originates from type II CRISPR-Cas systems, which provide bacteria with adaptive immunity to viruses and plasmids and requires only a single protein for RNA-guided DNA recognition and cleavage[201]. The RNA-guided Cas9 nucleases from the microbial CRISPR-Cas systems are robust and versatile tools for stimulating targeted double-stranded DNA breaks (DSBs) in eukaryotic cells[202]. Two molecules must be introduced into each target cell, a Cas9 protein and a single guide RNA (sgRNA). The sgRNA is the result of a crRNA (CRISPR-targeting RNA), that provides target specificity, and a tracrRNA (trans-activation crRNA) that acts as a scaffold between the crRNA and Cas9 endonuclease. SgRNA and Cas9 form a complex with genomic DNA (gDNA), specifically targeting DNA sites complementary to an approximately 20-base sequence within the sgRNA and neighboring a protospacer adjacent motif (PAM), the identity of which is dictated by the particular Cas9 protein employed (Figure 13). For the most commonly used Cas9 to date from *Streptococcus pyogenes*, the optimal PAM sequence is NGG (where 'N' is any nucleobase). The protospacer specifies the target sequence for Cas9, and is used by bacteria as a mechanism to remember and defend against foreign pathogens. The wild-type Cas9 (wtCas9) has two endonuclease domains that produce double-stranded breaks (DSBs) in the targeted gDNA sites. DSBs produced by wtCas9 are subsequently repaired through endogenous DNA repair mechanisms, either non-homologous end-joining (NHEJ) or homology-directed repair (HDR)[203].

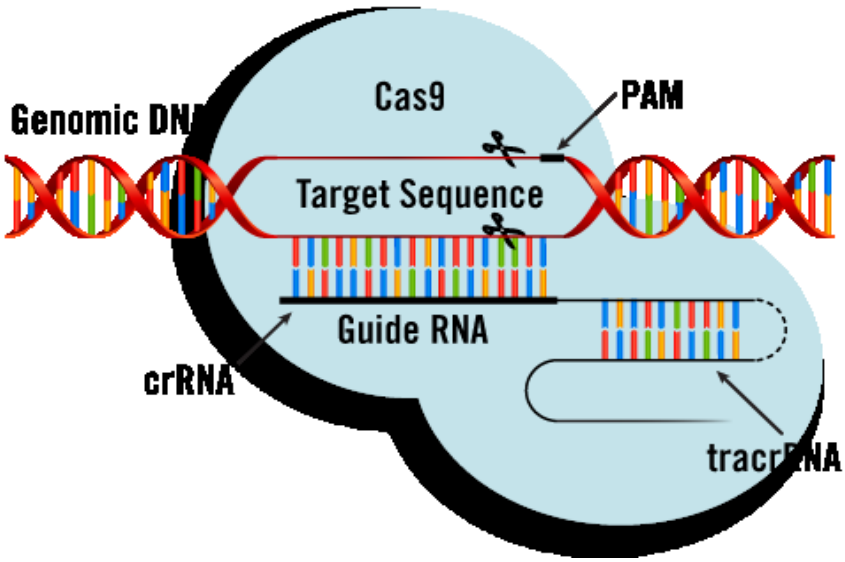

Figure 13: Cas9 is recruited to the DNA target site by the duplex tracrRNA:crRNA (gRNA). The crRNA binds the complementary DNA strand upstream of the PAM sequence. Cas9 domains generate a DS break.

1.5.2 CRISPR/Cas9 IN ZEBRAFISH

CRISPR/Cas9 technology of genome editing has greatly facilitated the targeted inactivation of genes *in vitro* and *in vivo* in a wide range of organisms. In zebrafish it allows the rapid generation of knock-out lines by simply injecting a single guide RNA (sgRNA) and Cas9 mRNA into one-cell stage embryos[204]. Targeting an early exonic sequence frequently leads to gene disruption through frame-shifts or non-sense mutations. Transfection of sgRNAs and Cas9 mRNA or DNA into bacteria, human or mouse cells was shown to efficiently inactivate target genes[205,206,207,208]. The CRISPR/Cas9 technology was subsequently used in mice to observe *in vivo* loss-of-function phenotypes and to generate knock-out strains[209]. In zebrafish, injection of sgRNAs and Cas9 mRNA into one-cell stage embryos similarly yields indels at target sites with relatively high, although variable, frequencies[210,211]. Mutations are inheritable due to mosaic targeting of the germline, allowing rapid establishment of mutant strains. Since gene inactivation by CRISPR/Cas9 is complete and permanent, this technology provides an effective complementary approach to morpholinos for loss-of-function studies in zebrafish, particularly at later stages of development. Mutant lines are invaluable to analyze gene function in both embryos and adults. The global loss of some genes is embryonic lethal, making them challenging to study in adults, and there is a great need in the field to create tissue-specific knockouts[211]. The Magmas gene in zebrafish is located on

the chromosome 3 and, as in humans, it has 5 exons. Its genome consists in 7,5 Kb and encodes for the Protein Pam16 of 129 aa[212] (Figure 14).

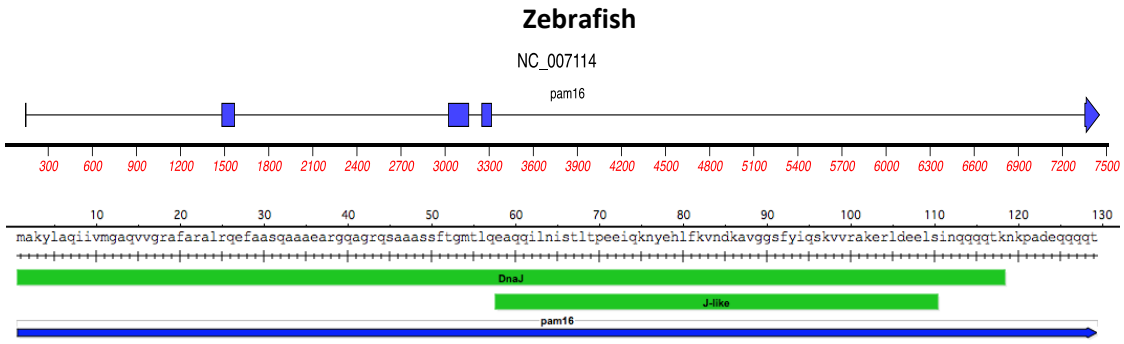

Figure 14: zebrafish Magmas genome and protein organization.

The Pam16 protein in zebrafish is highly conserved and it counts the same number of amino acid of the human ortholog. It has the J-like domain, but instead have the DKS moitif it has the DKA.

To study the Tim16 gene in zebrafish, 3 *in vitro* transcribed sgRNA were synthesized (Figure 15) and micro-injected into the yolk of one-cell stage embryos with the CRISPR/Cas9 technology.

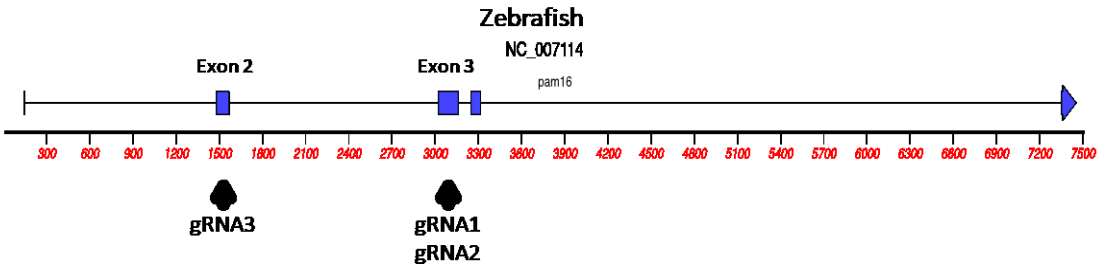

Figure 15: Complementary site of sgRNA1, sgRNA2 AND sgRNA3.

In this study the focus will be on the gRNA2, through which 6 founders have been identified. These fish have been outcrossed with wildtype AB fish, which generated 5 different F1 family. Actually, we are in a F2 situation (Figure 16).

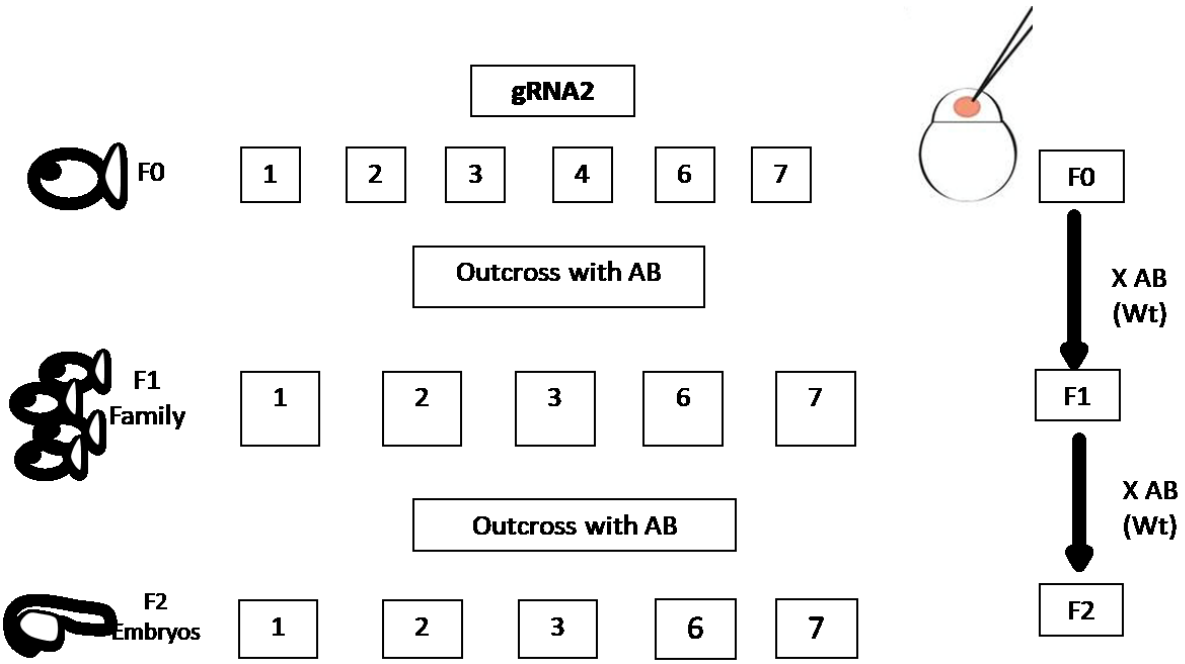

Figure 16: CRISPR/Cas9 experimental study with sgRNA2.

2. AIM OF THE STUDY

Magmas gene (mitochondria-associated protein involved in granulocyte-macrophage colony-stimulating factor signal transduction) encodes for the mitochondrial protein Tim16 that is a member of the TIM23 translocase, located in the mitochondrial inner membrane. Tim16 is a highly conserved protein, developmentally regulated and tissue specific[77]. Tim16 is a J-like protein that forms a heterodimer with the J-protein Tim14 and they are both co-chaperones of the mtHsp70[88]. Both proteins participate in the PAM complex that pulls protein precursors from the intermembrane space into the mitochondrial matrix[32].

An over-expression of Tim16 has been demonstrated in prostate cancer[99] and in 72% of human pituitary adenomas, as well as in ACTH-secreting mouse pituitary adenoma cell lines[100] and in two GH-secreting rat pituitary adenoma cell lines[101]. These studies showed that Magmas may play a role in tumor development by protecting neoplastic cells from apoptosis and by promoting cell proliferation. It was also observed that its over-expression protects from apoptosis by inhibiting staurosporine-induced cytochrome c release from mitochondria, influencing Bax and Bcl2 modulation by proapoptotic stimuli.

Our lab together with the Dept. of Chemical and Pharmaceutical Sciences of the University of Ferrara, synthesized a Tim16 inhibitor, named "compound 5" and challenged its effects towards the proapoptotic effects of staurosporine in TT cells, deriving from a human medullary thyroid carcinoma (MTC). Compound 5 turned out not to be cytotoxic but was capable of enhancing the proapoptotic effects of staurosporine by reducing mitochondrial membrane potential (MMP) activation[102].

Considering that an over-expression of Tim16 seems to play a consistent role in neoplastic cells and that its inhibitor, compound 5, seems to modulate Tim16 activity by enhancing the proapoptotic effects of an apoptosis inductor, such as staurosporine, the aim of this study is to better understand the effects of Tim16 in cancer chemoresistance.

For this purpose, chemotherapeutic drugs and different *in vitro* and *in vivo* models were used.

Experiments have been performed on:

1. MCF7 cells deriving from human breast cancer, in order to understand the possible role of Tim16 in the chemoresistance to doxorubicin.
2. Xenograft mice injected with TT cell lines, deriving from human MTC, to understand the *in vivo* role of Tim16.
3. Zebrafish model to study compound 5 toxicity *in vivo* and to create a mutated model for the Magmas gene.

3. MATERIAL AND METHODS

3.1 DRUGS AND CHEMICALS:

Doxorubicin (Adriamycin) was provided by Cell Signalling Technology (Danvers, Massachusetts, USA); the compound was dissolved in dimethyl sulfoxide (DMSO) and stored at -20 °C as a 10mM stock solution. Dilution to the final concentration was made in culture medium immediately before use.

Paclitaxel was provided by Accord (Milano, IT); the compound was dissolved in physiological salt solution (PSS) and stored at t -20 °C as a 1mM stock solution. Dilution to the final concentration was made in culture medium immediately before use.

Compound 5 (N-carbamidoyl-4-((3-ethyl-2,4,4-trimethylcyclohexyl)methyl)benzamide (Figure 17) was synthesized by the Department of Chemical and Pharmaceutical Sciences of the University of Ferrara (Italy); the compound was dissolved in in dimethyl sulfoxide (DMSO) and stored at -80°C as a 10 or 5 mM stock solution. Dilution to the final concentration was made in culture medium immediately before use.

All other reagents, if not otherwise specified were purchased from Sigma (Milano, IT).

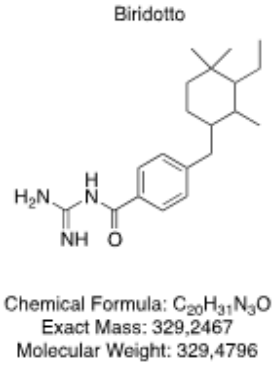

Figure 17: Chemical formula of compound 5

3.2 IN VITRO IMMORTALIZED HUMAN CELL LINES:

The TT cell line, deriving from a 77 years old female with thyroid medullary carcinoma, was purchased from ATCC (American Type Culture Collection, Manassas, VA, USA; ATCC CRL-1803) and grown in F12 medium (Euroclone, Milano, Italy), supplemented with 10% fetal bovine serum, 10 U/ml Penicillin/Streptomycin, 0.025 µg/ml antimycotic. The

nontumorigenic breast epithelial MCF-12A cell line and the adenocarcinoma MCF-7 cell line, deriving from a 69 years old female with breast cancer, were purchased from the ATCC and both grown in DMEM-High Glucose (Euroclone, Milano, Italy) supplemented with 10% fetal bovine serum, 10 U/ml Penicillin/Streptomycin, 0.025 µg/ml antimycotic. All the cell lines were maintained at 37 °C in a humidified atmosphere with 5% CO_2.

3.3 CELL VIABILITY ASSAY:

Cell viability was assessed by ATPlite assay (Perkin-Elmer, Monza, IT) and luminescence was measured with the EnVisionTM 2104 Multilabel Reader (Perkin-Elmer). The CellTiter-Glo® Luminescent Cell Viability Assay is a homogeneous method to determine the number of viable cells in culture based on quantitation of the ATP present, which signals the presence of metabolically active cells and is directly proportional to the cells number present in the culture. The Assay relies on the properties of a proprietary thermostable luciferase (Ultra-GloTM Recombinant Luciferase), which generates a stable "glow-type" luminescent signal after a specific reaction, as shown in Figure 18, with a consequent light emission.

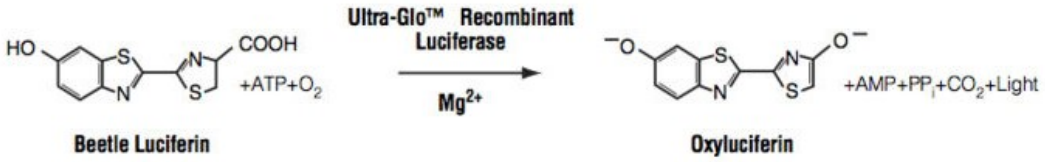

Figure 18: Mono-oxygenation of luciferin is catalyzed by luciferase in the presence of Mg2+, ATP and molecular oxygen.

Briefly, MCF12A and MCF7 cells were seeded 2 x 10^4/well in 96-well black plates in complete medium (10% FBS). Cells were synchronized by overnight incubation in 0.5 % FBS medium. The day after, cells were treated with 5 µM Compound 5 and/or 200 nM doxorubicin in complete medium. Control cells were treated with the vehicle alone (0.1% DMSO); treatments were renewed every 24 h. After incubation time of 48 hours, cell viability assay was assessed adding substrate solution directly to cell culture plates. Results are expressed as mean value ± standard error of the mean (S.E.M) percent RLU vs. untreated control cells in tree replicates.

3.4 CASPASE ASSAY:

Caspase activity was performed by using Caspase-Glo 3/7 assay (Promega, Milano, IT) according to the manufacturer's instructions. Luminescence was measured with the EnVision^{TM} 2104 Multilabel Reader Multilabel Counter (Perkin-Elmer) and expressed as relative light units (RLU). The Caspase-Glo® 3/7 Assay is a homogeneous, luminescent assay that measures caspase-3 and -7 activities. These members of the cysteine aspartic acid-specific protease (caspase) family play key effector roles in apoptosis in mammalian cells. The Caspase-Glo® 3/7 Assay relies on the properties of a proprietary thermostable luciferase (Ultra-GloTM Recombinant Luciferase), which is formulated to generate a stable "glow-type" luminescent signal, after cell lysis and caspase cleavage of the substrate, Figure 19; luminescence is proportional to the amount of caspase activity present.

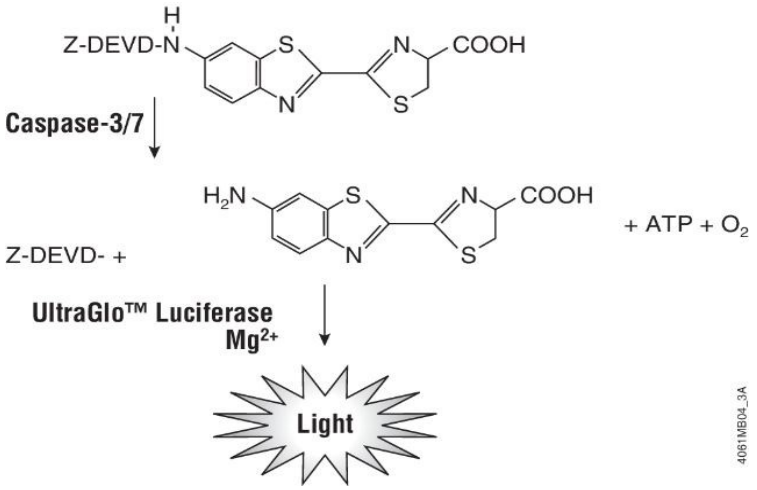

Figure 19: Caspase-3/7 cleavage of the luminogenic substrate containing the DEVD sequence. Following caspase cleavage, a substrate for luciferase (aminoluciferin) is released, resulting in the luciferase reaction and the production of light.

Briefly, MCF12A and MCF7 cells were seeded at 2 x 10^4 cells per well in 96-well white plates and treated as previously described for the CellTiter-Glo® Luminescent Cell Viability Assay. Results are expressed as mean value ± SEM percent RLU vs. control cells in three replicates.

3.5 ELISA:

BAX production was used as antigen recognition assay. As target we used MCF12A and MCF7 cells. 10^4 cells/well were seeded in 96-well plates, synchronized by a 24 h incubation in 0.5 % FBS medium and then treated with 5 μM compound 5 and/or 200 nM doxorubicin. After 48 hours supernatants were collected and BAX secretion was measured by using Human BAX ELISA kit (DRG diagnostics, Marburg, Germany) and the EnVisionTM 2104 Multilabel Reader (Perkin-Elmer). All the samples were measured in triplicates.

3.6 PROTEIN ISOLATION:

The cells were seeded at a cell density of 10^6 cells/ml in 100-mm dishes (Corning) in complete medium (10% FBS). Cells were synchronized by overnight incubation in 0.5 % FBS medium, and the day after, cells were treated with compound 5 and/or doxorubicin in complete medium and then after 3-6-48 hours cell pellets were collected. For protein isolation from mice tumours, total cell lysates were obtained by using Tissue Raptor (Qiagen, Hilden, Germany), according to the manufacturer's instructions. Human cell lines and mice tissues were dissolved in RIPA buffer (Pierce Biotechnology, Inc, Rockford, Illinois, USA) (25 mM Tris-HCl pH 7.6, 150 mM NaCl, 1% NP-40, 1% sodium deoxycholate, 0.1% SDS), kept in ice for 30 min, and then centrifuged at 13,000 rpm for 20 min at 4°C. The supernatant, containing the proteins, was then transferred to a new tube and protein concentration was measured by using the BCA Protein Assay Reagent Kit (Pierce Biotechnology).

3.7 WESTERN BLOT ANALYSIS:

For protein evaluation, proteins were mixed with 2X Laemmli buffer[213] (62,5 mM Tris-HCl (pH 6.8), 25% glycerol, 2.1% sodium dodecyl sulphate, 0.01% bromophenol blue, DTT) and denaturized at 95°C for 5 min. 20 μg or 30 μg of protein, deriving from mice tissues or Human cell lines respectively, were fractionated on a precast 4-10% SDS-PAGE gel (Perkin Elmer) and transferred by electrophoresis to polyvinylidene difluoride (PVDF) membranes (PerkinElmer) by using the Lightning BlotterTM (PerkinElmer).

Protein panel profile was performed by using protein extracts and the following primary antibodies: 1:10000 rabbit anti-PAM16 antibody (Abcam, Cambridge, MA, USA), 1:1000 rabbit cytochrome c antibody (Cell Signalling, Beverly, MA, USA), 1:1000 rabbit BNIP3L/Nix antibody (Cell Signalling, Beverly, MA, USA), 1:1000 rabbit RIP antibody

(Cell Signalling, Beverly, MA, USA), 1:1000 mouse anti-DNAJC19 antibody (Abcam, Cambridge, MA, USA), 1:500 mouse anti-Grp75 antibody (Abcam, Cambridge, MA, USA), 1:500 mouse anti-DNAJC15 antibody (Abcam, Cambridge, MA, USA), 1:1000 mouse Caspase-9 antibody (Cell Signalling, Beverly, MA, USA), 1:1000 rabbit anti-GAPDH antibody (Cell Signalling, Beverly, MA, USA), 1:1000 rabbit anti-p53 antibody (Cell Signalling, Beverly, MA, USA), 1:1000 rabbit anti-VDAC1 antibody (Abcam, Cambridge, MA, USA).

Anti-rabbit or anti-mouse HRP IgG antibodies (Dako Italia, Milano, Italy) were used at a dilution from 1:2000 to 1:5000 and proteins were revealed by enhanced chemiluminescence using the Azure c300 (Azure Biosystems, Dublin, CA, USA). Quantification of the band intensity was performed using the open source image processing program ImageJ. Three independent experiments were performed; data are expressed as the ratio between protein of interest and GAPDH/VDAC1 signal intensity, expressed as a ratio protein/housekeeping.

3.8 IMMUNOPRECIPITATION:

Approximately $5x10^6$ MCF7 cells were seeded in 100 mm-dishes (Corning) and cultivated overnight. Cells were treated for 3 and 6 hours with 5 µM Compound 5 and then collected with 400 µl of IP Lysis Buffer for 20 minutes on ice. The lysate was centrifuged (13000 x g for 10 minutes) and 1 mg of the supernatant was incubated with 10 µg anti-PAM16 antibody overnight at 4°C, after a pre-clearing of the lysate using the Control Agarose Resin, following the Pierce Co-Immunoprecipitation (Co-IP) kit (Thermo Scientific, Waltham, Massachusetts, USA). The precipitates were washed three times with 200 µl of IP Lysis/Wash Buffer, eluted in 20 µl of Elution Buffer, added with the 5X sample buffer and boiled for 5 minutes at 95°C. Proteins were then separated by 4-10% SDS-Page (PerkinElmer) and analyzed by immunoblot analysis.

3.9 MITOCHONDRIA ISOLATION

In order to submit mitochondria to mass spectrometry, 5 x 10^6 MCF7 cells were seeded 100 mm-dishes (Corning) and cultivated overnight. Cells were treated for 3 and 6 hours with Compound 5 5 µM and then collected with 1 ml of Lysis Buffer using the Qproteome Mitochondria Isolation Kit (QIAgen). The mitochondrial pellet was submitted to mass spectrometry.

3.10 MASS SPECTROMETRY

Each sample was treated with 1 mL of a mixture of CH_3CN and H_2O (6:4) with CF_3COOH (0.1 %). Cell membrane disruption was induced by ultrasonication for 10 min. After filtration (0.2 µm), the obtained solutions were analysed through LC-HRMS analysis performed by a ESI-Q-TOF Nano HPLC-CHIP Cube® Agilent 6520 instrument (Agilent Technologies USA) using a linear gradient (0.4µL/min) from 100% solvent A (97% water/3% acetonitrile/0.1% formic acid) to 90% solvent B (97% acetonitrile/3% water/0.1% formic acid) in 5 minutes and from 90% solvent B to 0% solvent B in 5 minutes, using a Zorbax C18 Coloumn (43mmX75µm, 5µm) equipped with enrichment coloumn (4mm 40nL). In Figure 20 there is the compound 5 mass spectra profile.

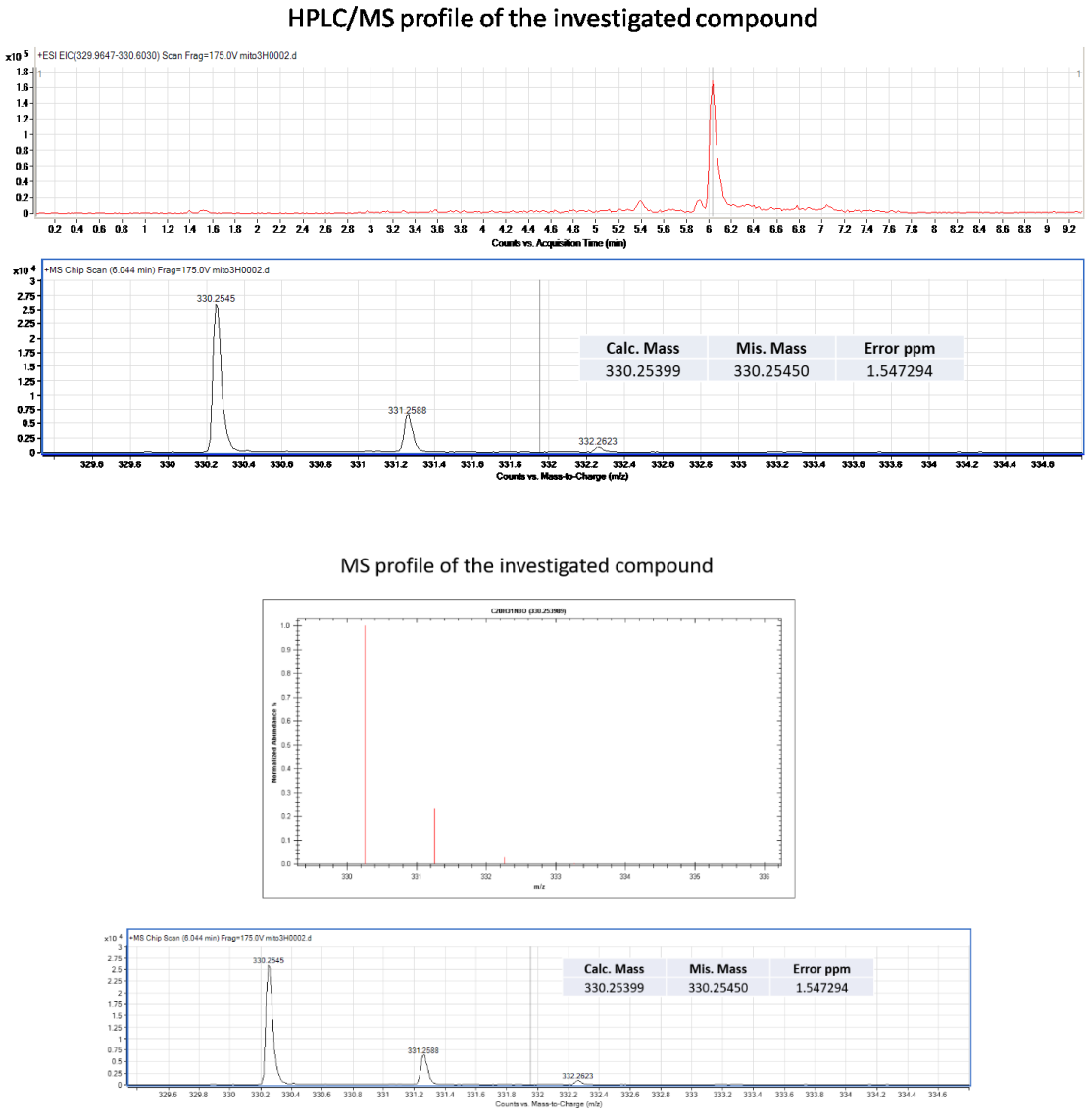

Figure 20: Mass spectra profile of compound 5. This compound is characterized by three abundant isotopic peaks at 330,331 and 332 m/z.

3.11 FISH EMBRYO ACUTE TOXICITY (FET) TEST:

To evaluate the toxicity of compound 5 the FET Test was performed on Zebrafish (*Danio Rerio*) using the OECD 2013 guidelines for the testing of chemicals[182].

Eggs were collected immediately after fertilization, washed several times with the E3 (5 mM NaCl, 0.17 mM KCl, 0.33 mM CaCl2, 0.33 mM MgSO4) and only the fertilized embryos were transferred to a 96-well cell culture plate with 1 embryo per well in 200 ul of E3 with different concentrations of compound 5 (0; 5uM; 10uM; 25uM; 30uM). Doxorubicin was used as positive control (50mg/L) and DMSO was used as vehicle control. 35-48 embryos were used for each concentration. Every treatment was performed twice.

The survival of zebrafish embryos from blastula stage to early larval stage where observed after 96 hours. The number of surviving embryos of each treatment at this time point were recorded.

3.12 CRISPR/Cas9 EDITING IN ZEBRAFISH:

3.12.1 gRNAs IN VITRO SYNTHESIS

sgRNA Scorer 1.0[214215] was used to generate a list of input sequences with a defined spacer length and a PAM sequence (Tab 1- 2).

	gRNA sequence (PAM sequence in red)	Score	Location
sgRNA 1	AACGCCAGAGGAGATCCAGAAGG	98,79	End of exon 3
sgRNA 2	AGCGGGCAGACAGTCTGCGGCGG	92,99	exon 3
sgRNA 3	CATTGTAATGGGGGCTCAGGTGG	86,28	exon 2

Tab 1. Tim16 sgRNA sequences with the PAM (-NGG) sequences

	Oligo sequence ordered (5'>3')
sgRNA 1	TAATACGACTCACTATAGG**AACGCCAGAGGAGATCCAGA**GTTTTAGAGCTAGAAATAGCAAG
sgRNA 2	TAATACGACTCACTATAGG**AGCGGGCAGACAGTCTGCGG**GTTTTAGAGCTAGAAATAGCAAG
sgRNA 3	TAATACGACTCACTATAGG**CATTGTAATGGGGGCTCAGG**GTTTTAGAGCTAGAAATAGCAAG

Tab 2. Tim16 gRNA sequences, preceded by the specific T7 polymerase template and followed by a common tracer sequence.

Oligos were purchased by IDT (Coralville, Iowa, USA) and resuspended as a 250 µM stock solution.

PCR primers were also designed to amplify a product size of ~ 400 bp flanking the targeted mutation site (IDT).

	5'	**3'**
Exon 3	ATGCACACACATTGGCCAG	AGCGTCATCTCTTACCTTCGA
Exon 2	TGGGCTGGATAAAAACCAAT	GTGAACATTTCCTCGCACTGT

Tab 3. Primers 5' and 3' to amplify ~400bp of exon 2 and 3

The follow reaction was used to generate the new sgRNA:

HF Phusion Buffer	4 µl
10 mM dNTPs	0,4 µl
Phusion DNA pol.	0,2 µl
Scaffold oligo (10µM)	5 µl
gRNA oligo (10 µM)	5 µl
ddH_2O	5,4 µl
Total volume	**20 µl**

Tab 4. PCR reaction.

The tubes were placed in the thermal cycler (Mastercycler® pro, Eppendorf, Hamburg, Germany) and run with the following program:

Temperature	**Time**	**Cycles**
95°C	30sec	**1**
95°C	10sec	**40**
60°C	10sec	
72°C	10sec	
72°C	5 min	**1**
4 °C	**hold**	**1**

Tab 5. PCR setting.

1 µl of the reaction was run on a 2% agarose gel electrophoresis and the image was taken with the Chemidoc (Biorad, Hercules, California, USA).

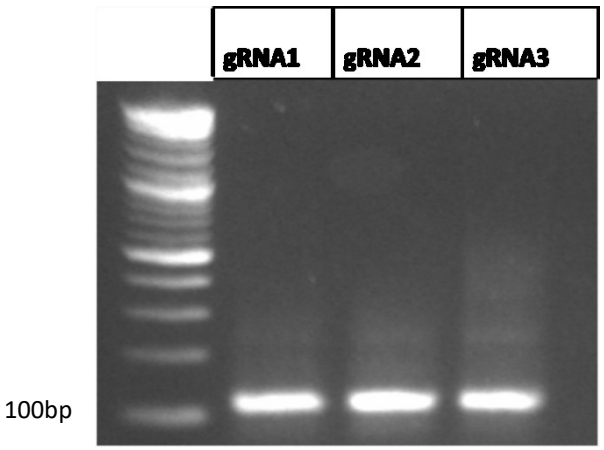

Figure 21: 2% agarose gel to verify PCR product, the amplicon is 125bp.

The PCR products were purified with the QIAquick PCR Purification Kit (Qiagen, Hilden, Germany), eluted in 30 µl of water and quantified with the Invitrogen Qubit® 2.0 Fluorometer (Thermo Fisher, Waltham, Massachusetts, USA).

To transcribe the three sgRNAs from the DNA template was used the SureGuide gRNA Synthesis Kit (Agilent Genomics, Santa Clara, CA, USA) following the table 6.

DEPC Water	3,75 µl
5X Transcription Buffer	2,5 µl
rATP	0,5 µl
rCTP	0,5 µl
rGTP	0,5 µl
rUTP	0,5 µl
0.75M DTT	0,5 µl
Yeast Pyrophosphatase	0,25 µl
RNase Block	0,25 µl
T7 RNA Polymerase	0,5 µl
DNA input	2,5 µl
Total	**12,25 µl**

Tab 6. SureGuide sgRNA Synthesis reaction.

The three sgRNAs were purified following the same SureGuide kit (Agilent), eluted in 30 µl of water and quantified with the Qubit (Thermo Fisher).

160 ng of the sgRNAs were run on a 2% agarose gel electrophoresis (Figure 2).

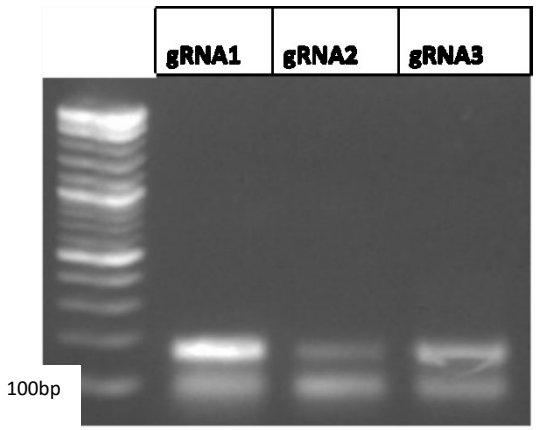

Figure 22: 2% agarose gel to verify PCR product.

3.12.2 ZEBRAFISH EMBRYOS MICROINJECTION

Gene editing of Tim16 was performed by microinjection of 500 pg recombinant S. pyogenes Cas9 (PNA Bio, Thousand Oaks, CA, USA) complexed with 250 pg of sgRNA (1,2 or 3) into a 1-cell-stage embryo, to ensure a high efficiency delivery of injected mRNA to the embryo as well as to reduce mosaicism. The injected volume was ~1 nl of solution, which was measured with a millimetric ruler, in mineral oil. The injected embryos were maintained in E3 medium at 28.5°C and phenotyped for morphological abnormalities under a Zeiss Discovery V8 stereomicro-scope (Zeiss, Oberkochen, Germany) over the first 5 days of development. When analysed, embryos and larvae were anesthetized by placing them in water with 0.003% tricaine methanesulfonate (Sigma, St. Louis, MO, USA). Embryos that had a putative phenotype were removed and lysed for further genotyping analysis. Embryos/larvae were raised to adulthood.

3.12.3 GENOMIC DNA EXTRACTION

To extract the genomic DNA of embryos and larvae, they were incubated with 100 µl DirectPCR Lysis Reagent (Viagen Biotech, Los Angeles, CA, USA) added with Proteinase K 1:1000 (Qiagen, Hilden, Germany) with the following genotyping condition: 55°C, 60 min; 85°C, 45 min; 4°C, hold in the thermal cycler (Eppendorf).

3.12.4 DETECTION OF CRISPR/Cas9 INDUCED MUTATIONS

The target locus of Tim16 was PCR amplified using the Platinum Blue PCR Supermix (Fisher Scientific, Hampton, New Hampshire, USA) and the primers listed before (Tab 3): 18 µl Platinum Blue mix, 0,5 µl 10 µM 5' primer, 0,5 µl 10 µM 3' primer, 1 µl gDNA at this conditions: 94°C, 3 min; 42 cycles of 94°C, 30 sec; 55°C, 30 sec; 72°C, 30 sec; 72°C, 10 min. 2-3 µl of the sample was run on an 1% agarose gel to verify the size of the product. 8 µl of the amplified product was than hybridized using 1,6 µl of NEB buffer 2 (BioLabs, Ipswich, Massachusetts, USA) and 6,4 µl of ddH_20 following this protocol: 95°C, 2 min; -1C/s to 85°C; -0,1 C/s to 25°C; hold at 4°C. The effectiveness of editing was confirmed with restriction enzyme digestion assay, using the T7 endonuclease assay (BioLabs): 0,4 µl of NEB buffer 2, 0,2 µl of T7El, 3,4 µl of ddH_20 added directly to the hybridized mix and incubated at 37°C for 1 hour.
Half the reaction was run directly on a 2% agarose gel electrophoresis.

3.12.5 CLONING, SEQUENCING AND TIDE ASSAYS

F1 embryos, obtained out-crossing F0 microinjected with wild-type fish, positive to the T7 assay, were sent to sequence at Genewiz (South Plainfield, NJ, USA). The PCR product was purified with the QIAquick PCR Purification Kit (Qiagen), eluted in 15 µl of water, quantified with Qubit (Thermo Fisher) and 10 ng of each sample was sent to sequence with the 5' or 3' primer 5 µM.
To rapidly assess genome editing by CRISPR/Cas9 of a target locus, the TIDE (Tracking of Indels by Decomposition) software [216] was use. It is based on the quantitative sequence trace data from two standard capillary sequencing reactions, quantifies the editing efficacy and identifies the predominant types of insertion and deletions (indels) in the DNA of a targeted cell pool[217] (Figure 23).

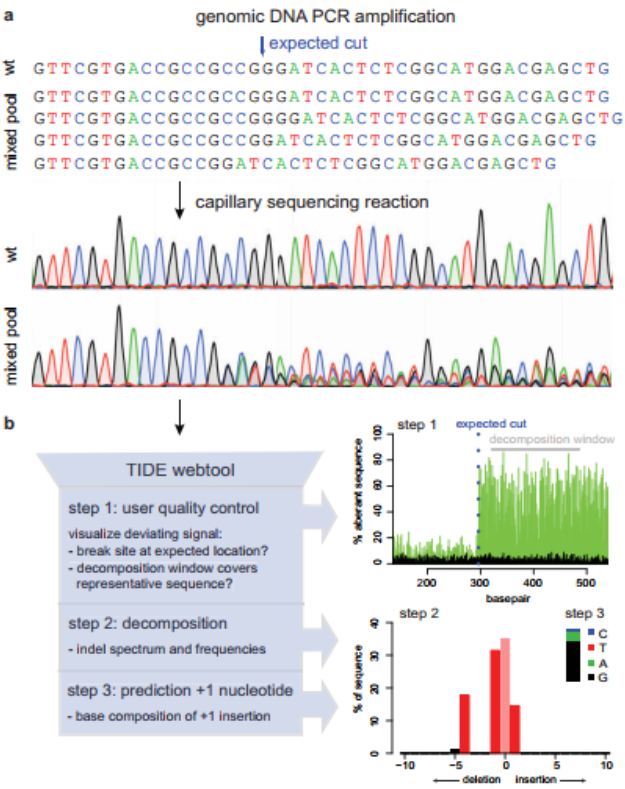

Figure 23: Assessment of genome editing by sequence trace decomposition. (a) Due to imperfect repair after cutting by a targeted nuclease, the DNA in the cell pool consists of a mixture of indels, which yields a composite sequence trace after the break site. (b) Overview of TIDE algorithm and output, which consists of three main steps: (1) Visualization of aberrant sequence signal in control (black) and treated sample (green), the expected break site (vertical dotted line) and the region used for decomposition (gray bar); (2) Decomposition yielding the spectrum of indels and their frequencies; (3) Inference of the base composition of +1 insertions[216].

To determine the frequency of the desired editing event in the pool of cells, one can amplify the targeted genomic region by polymerase chain reaction (PCR), clone individual DNA molecules in a bacterial vector and analyze 50–100 clones by sequencing. This approach is labor-intensive, time-consuming and relatively costly. This approach was used to verify the type of editing once the F1 were grown up. A fresh PCR product was cloned into a pCR II-TOPO vector using the TOPO TA Cloning Kit (Thermo Fisher) using 1 µl of fresh PCR, 0,5 µl of Salt Solution, 1 µl of ddH_2O and 0,5 µl of pCR II-TOPO. The mix was then transformed in 25 µl TOP10 competent cells adding ~10 ng of plasmid DNA directly to the cells; the tubes were incubated for 5 minutes on ice, heated for 30s in a 42°C water bath, placed in ice 2 minutes, added of 125 µl of SOC medium and incubated at 37°C while shacking at 250 rpm for 60 minutes. 30 µl of transformation were spread on the LB/agar/antibiotic plates and incubated overnight at 37°C. The day after 5 colonies were taken and cultured overnight in LB medium containing 50 ng/ml ampicillin. The plasmid DNA was isolate using the

QIAprep MiniPrep Kit (Qiagen), quantified using the NanoDrop™ One Microvolume UV-Vis Spectrophotometers (Thermo Fisher Scientific) and submitted for sequencing using SP6 primer to Genewiz.

3.13 ZEBRAFISH HUSBANDRY

Zebrafish (*Danio Rerio*) were bred and reared according to established guidelines[218]. They grow in the fish facility with a 14 hours light/10 hours dark cycle. Zebrafish embryos were obtained from natural spawning of two lines, wild-type AB and Tim16 mutants. For the Toxicity Assay were use wild-type AB.

3.14 EXPERIMENTAL MICE

7 weeks-old nude female mice were injected with 1,5 x 10^7 TT cells in 200 µl of Matrigel (BD Bioscences)/F12 1:1 dilution, a human tumor-forming cell line, in order to obtain measurable masses[219,220]. Cells were established via subcutaneous inoculation into the flank of mice. Tumor growth was monitored daily and tumor volumes were measured every two days. When tumor mass became palpable in successfully engrafted mice, after 7 weeks, animals were randomly divided into 4 groups according to the delivered treatments[221]: control solution, intra-tumoral 5µM Compound 5, intra-peritoneal 10 mg/Kg Paclitaxel, and intra-tumoral Compound 5 + intra-peritoneal Paclitaxel. They were treated twice (day 0 and day 2) and tumor volumes were measured after 2 and 4 days of treatments. Mice were sacrificed, tumors were excised and protein expression was evaluated by Western Blot[222].

3.15 STATISTICAL ANALYSIS

Results are expressed as the mean value ± standard error of the mean (SEM). A preliminary analysis was carried out in order to determine whether the data sets conformed to a normal distribution using both D'Agostino-Pearson omnibus and Shapiro-Wilk normality tests. Student's paired t test and/or MannWhitney test were used to evaluate individual differences between means (GraphPad PRISM6 Software). Differences were considered significant at $P < 0.05$.

4. RESULTS

4.1 PAM COMPLEX PROTEIN BASAL LEVELS IN MCF7 AND MCF12A CELL LINES

Since Tim16, the mitochondrial protein encoded by Magmas gene, results to be over-expressed in different cell lines (ACTH-secreting mouse and GH-secreting rat pituitary adenoma cell lines) as well as human tissues (prostate, pituitary adenomas)[99,100,101], we investigated its expression in different cell lines. We previously found that MCF7 cells express higher level of Tim16 as compared to the normal cell line, the MCF12A cells. Therefore, we investigated Tim16 expression pattern concurrently with other proteins involved in the PAM complex, such as mtHsp70, Tim14 and Tim15 in these cell lines.

Total proteins were extracted and quantified from MCF7 and MCF12A cell lines and a Western blot for Tim14, Tim15, Tim16 and mtHsp70 was performed with 30 µg of protein (Figure 24 A). Protein level quantification was performed by densitometry analysis; results represent the mean of 3 different experiments and are expressed as the ratio between the protein of interest and the housekeeping protein, GAPDH (p/GAPDH) (Figure 24 B).

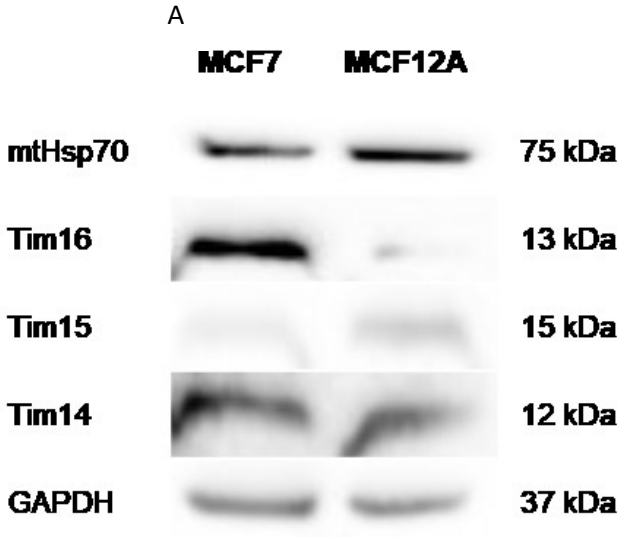

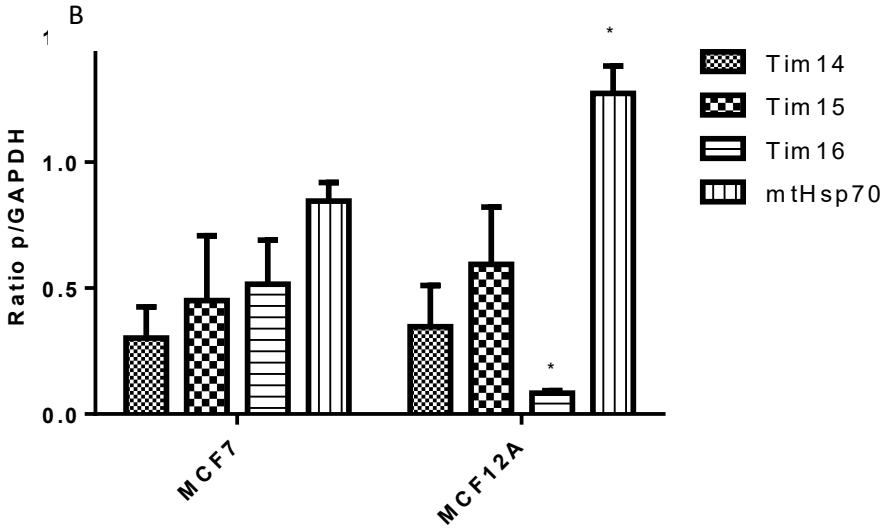

Figure 24: A) Western blot analysis of Tim14, Tim15, Tim16 and mtHsp70 in MCF7 and MCF12A cells. A representative blot of three independent experiments is shown. B) Protein expression in both cell lines expressed as the ratio between total protein and GAPDH. (*p<0.05 vs MCF7).

MCF7 cell line displayed ~6- fold higher Tim16 levels as compared to MCF12A. On the contrary, MCF12A cells displayed ~1,5-fold higher mtHsp70 levels as compared to MCF7 cells (Figure 24 B). Tim14 and Tim15 expression levels were not significantly different in the two cell lines. We found that MCF7 cells display a significantly higher level of Tim16 and a lower level of mtHSP70 as compared to MCF12A cells.

4.2 EVALUATION OF CELL VIABILITY AND CASPASE 9 ACTIVATION IN MCF7 AND MCF12A CELLS AFTER TREATMENT WITH COMPOUND 5 OR/AND DOXORUBICIN

Our group previously demonstrated that Magmas silencing increased cell sensitivity to apoptotic stimuli (represented by staurosporine), while its over-expression increased cell viability and apoptosis reduction[100,101]. Considering that MCF7 cells express high Tim16 levels, we investigated compound 5 effects on cell viability and caspase 9 activation, in combination with a chemotherapeutic drug commonly used to treat breast cancer, such as doxorubicin.

MCF7 and MCF12A cells were incubated for 48h in a cultured medium with 5 µM compound 5 and/or 200 nM doxorubicin. The effects have been evaluated in terms of cell viability reduction (Figure 25 A-B) and caspase 9 activation (Figure 25 C-D).

As shown in Figure 25 A-B, compound 5 does not affect cell viability in both MCF7 and MCF12A cell lines; doxorubicin significantly reduces cell viability by 30% vs. control in

MCF7 cells and by 20% vs. control in MCF12A cells. In addition, compound 5 enhances doxorubicin effect by 15-20% in MCF7 cells, while it does not alter doxorubicin action in MCF12A cells.

To verify whether compound 5 and doxorubicin influence apoptotic process, we evaluated caspase 9 activity. As shown in Figure 25 C-D, the combined treatment with compound 5 and doxorubicin results in a significant increase in caspase 9 activation only in MCF7 cell line and not in MCF12A cells.

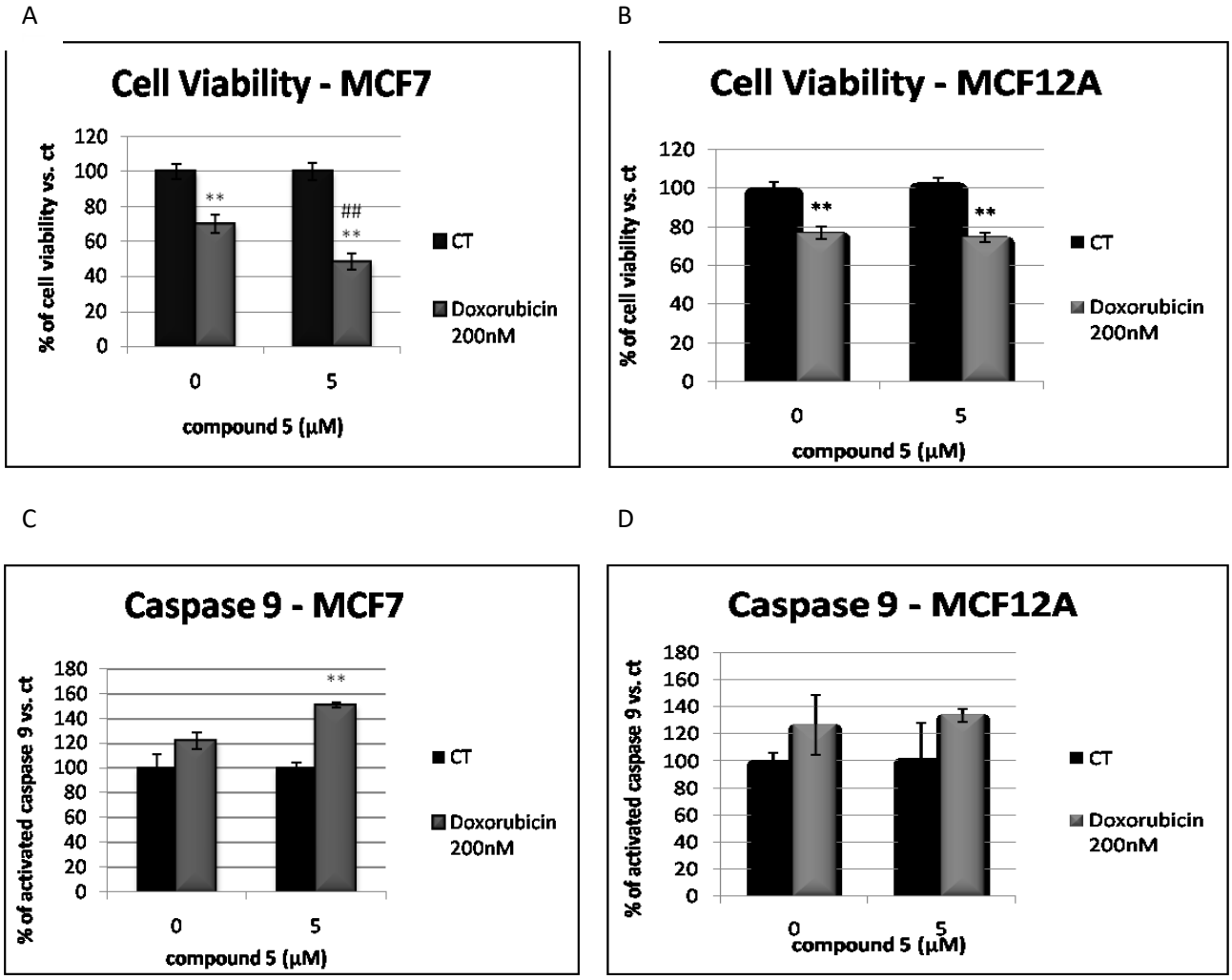

Figure 25: MCF7 and MCF12A cells ATPlite Assays (A-B) and Caspase 9 activation Assays (C-D) assessed after 48h of treatment with 5 µM compound 5 and/or 200 nM doxorubicin. (**p<0,01 vs control, ##p<0.01 vs. doxorubicin treatment).

4.3 EVALUATION OF BAX LEVELS

Upon cellular stress, the functional balance of proapoptotic BCL-2 (B-cell lymphoma 2) family members, such as BAX, BAK or BOK and anti-apoptotic Bcl-2 family members, such as BCL-2 or BCL-XL, is shifted in favor of the pro-apoptotic proteins[50,51,52]. As a consequence, mitochondrial transmembrane potential ($\Delta\Psi m$) is altered with the formation of mitochondrial permeability transition (MPT) pores[53] and the release into the cytosol of pro-apoptotic proteins, normally sequestered from the intermembrane space[50]. The BCL2-family members BAX, normally localized in the cytosol as a monomer, and BAK, normally localized in the mitochondria[54], directly activated by the tumor suppressor p53[55], form pores in the outer mitochondrial membrane (OMM), which releases several proteins, including cytochrome c and SMAC/Diablo, from the intermembrane space into the cytosol[56]. To verify whether compound 5 and/or doxorubicin activate the apoptotic process, BAX level was evaluated.

MCF7 and MCF12A were treated for 48h with 5 µM compound 5 and/or 200 nM doxorubicin and the cellular lysate has been submitted to BAX ELISA Assay. As shown in Figure 26, MCF7 cells show significantly higher BAX levels, as compared to control, after compound 5 and/or doxorubicin treatment. Doxorubicin induces BAX expression by 25%, compound 5 by 8% and the co-treatment increases BAX level to a greater extent as compared to the individual treatments. In MCF12A cells, BAX levels seem not to be influenced by the indicated compounds.

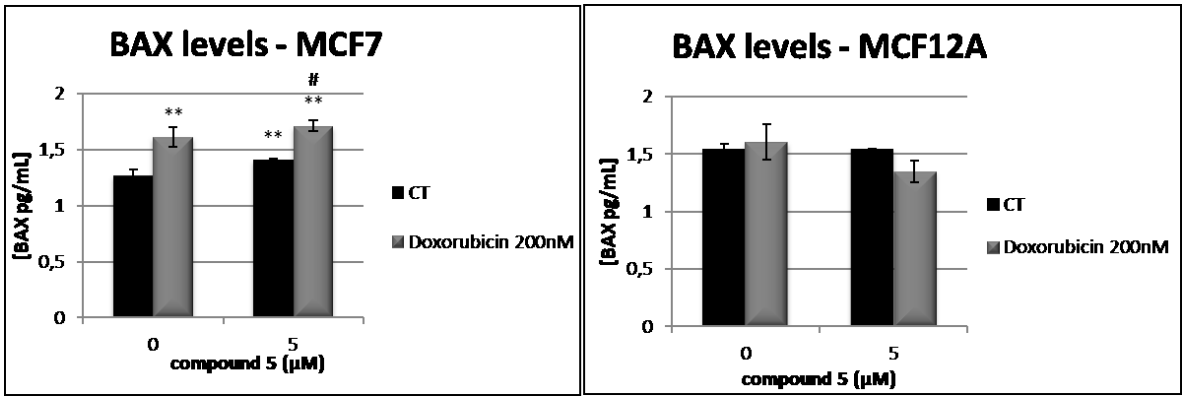

Figure 26: BAX levels in MCF7 and MCF12A cells evaluated by ELISA Assay, assessed after 48h of treatment with 5 µM compound 5 and/or 200 nM doxorubicin. (**p<0,01 vs ct, #p<0,05 vs doxorubicin treatment).

4.4 PROTEIN PROFILE IN MCF7 CELLS AFTER TREATMENT WITH COMPOUND 5 AND/OR DOXORUBICIN

We previously showed that compound 5 enhances doxorubicin effect mainly in MCF7 cells, that show higher levels of Tim16, by decreasing cell viability and increasing caspase 9 activation.

In order to further understand the effects of these molecules on expression levels of proteins such as Tim16, Tim14 or cytochrome c, we performed a Western blot analysis on MCF7 cells.

MCF7 were treated for 48h with 5 µM compound 5 and/or 200 nM doxorubicin; total proteins were extracted, quantified and 30 µg of protein were analyzed (Figure 27).

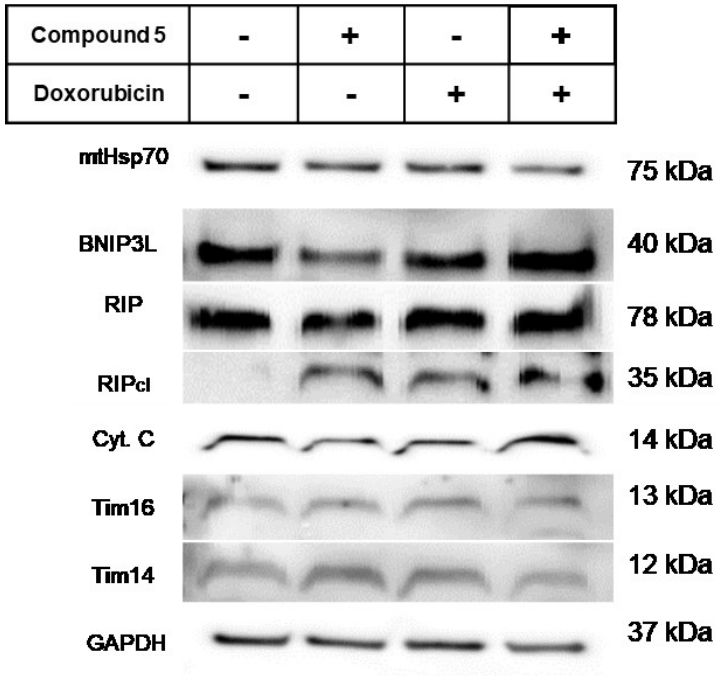

Figure 27: Western blot analysis of Tim14, Tim16, mtHsp70, BNIP3L, RIP and cytochrome c in MCF7 cells treated with 5 µM compound 5 and/or 200 nM doxorubicin. GAPDH was used as housekeeping. A representative blot of three independent experiments is shown.

As shown in Figure 27 Tim16 levels are not affected by the indicated compounds, since protein levels remain stable, similarly to what observed for Tim14 and mtHsp70.

The death domain kinase RIP, a key component of the TNF signaling complex, is cleaved by Caspase-8 in TNF-induced apoptosis[223]. Here, compound 5 and doxorubicin induce an increase in cleaved RIP levels, which increase even more with co-treatment.

BNIP3L/Nix is a "BH3-only protein" belonging to the Bcl-2 family, that can stimulate apoptotic or necrotic cell death[49]. The levels of this protein are not modified by treatment with compound 5, but are enhanced by co-treatment with doxorubicin.
Doxorubicin and compound 5 together induce cytochrome c levels, an effect not detected for the single treatments.

4.5 EFFECTS OF COMPOUND 5 ON Tim16-Tim14 BINDING

It is already known that Tim16 forms a heterodimer with Tim14 and that its inhibitors, such as SMMI9, interfere with this binding[811]. Compound 5 has never been tested in this context and its effect on Tim16-Tim14 binding is unknown. To better understand the effects of compound 5, the interaction of these proteins, including also mtHsp70, was investigated by co-immunoprecipitation (CoIP). This experiment was performed using the MCF7 cells, that display higher levels of Tim16, treated with the inhibitor at 5 μM for 3 and 6 hours. Proteins were co-immunoprecipitated with the Tim16 antibody (Figure 28 A). Protein level quantification was performed by densitometry analysis and the results of each protein densitometry are represented in a graph (Figure 28 B), and expressed as a ratio between the protein of interest and Tim16 (p/Tim16).

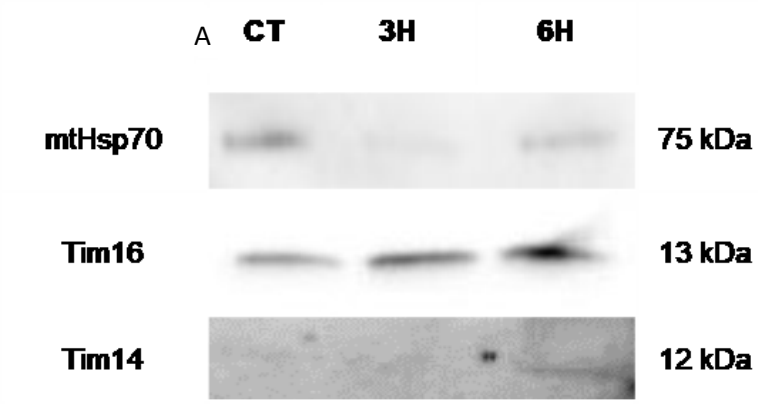

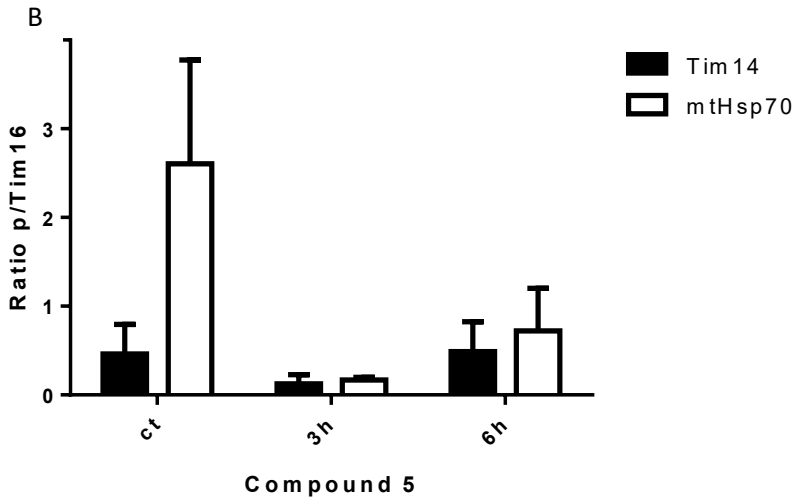

Figure 28: Co-immunoprecipitation of Tim16, Tim14 and mtHsp70 after 3 or 6h of treatment with compound 5. A) MCF7 cells were collected, immunoprecipitated and analysed with immunoblotting. A representative blot of three independent experiments is shown. B) Protein expression in the untreated and the treated cells expressed as the ratio between total protein and Tim16.

These findings suggest that compound 5 acts mainly at 3h, interfering in the binding between Tim16 and both Tim14 and mtHsp70. Compound 5 seems to bind Tim16 in a reversible manner, since after 6 h the binding between Tim16 and both Tim14 and mtHsp70 is partially restored.

4.6 EVALUATION OF COMPOUND 5 PRESENCE IN MITOCHONDRIA

To verify the actual presence of compound 5 into the mitochondrial compartment, mitochondrial cell extracts mass spectrometry was performed after 3 or 6 hours of treatment with the Tim16 inhibitor. MCF7 cells were treated with compound 5 and collected; mitochondria were isolated and submitted to mass spectrometry. By comparing mass spectra results we found that compound 5 is present in the mitochondria of treated MCF7 cells (Figure 29 B-C) and not in the mitochondria of untreated MCF7 cells (Figure 29 A). The 3 characteristic mass spectrometry peaks of compound 5 can be recognized in the mitochondrial extracts of cells treated for 3 and 6 hours. These peaks are not visible in the spectrum of control untreated cells. The evidence that compound 5 is present in the mitochondria further supports our previous results, showing that Tim16-Tim14-mtHsp70 binding is modulated by compound 5.

A

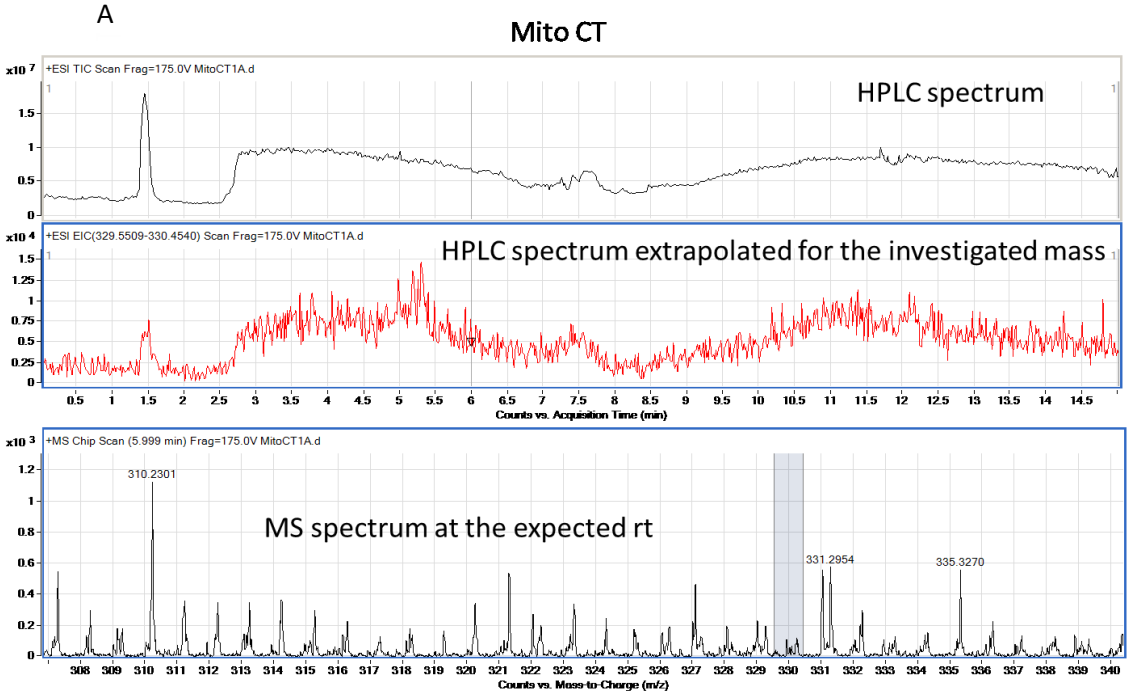
Mito CT
+ESI TIC Scan Frag=175.0V MitoCT1A.d
HPLC spectrum
+ESI EIC(329.5509-330.4540) Scan Frag=175.0V MitoCT1A.d
HPLC spectrum extrapolated for the investigated mass
Counts vs. Acquisition Time (min)
+MS Chip Scan (5.999 min) Frag=175.0V MitoCT1A.d
310.2301
MS spectrum at the expected rt
331.2954
335.3270
Counts vs. Mass-to-Charge (m/z)

B

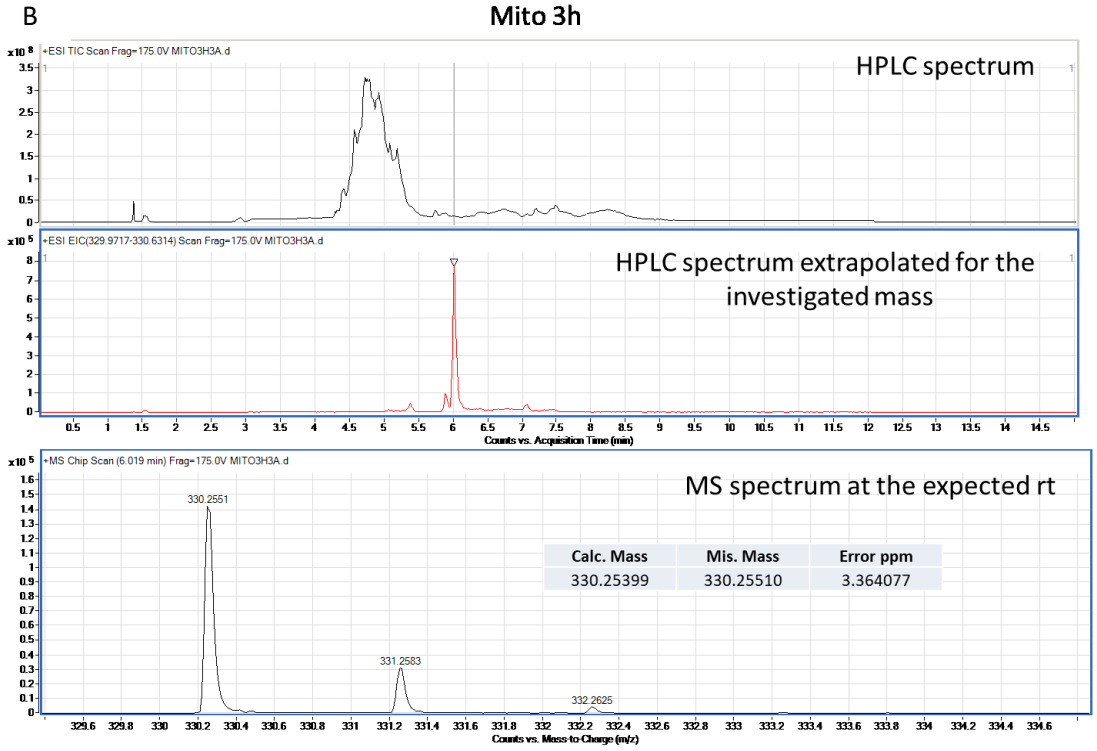
Mito 3h
+ESI TIC Scan Frag=175.0V MITO3H3A.d
HPLC spectrum
+ESI EIC(329.9717-330.6314) Scan Frag=175.0V MITO3H3A.d
HPLC spectrum extrapolated for the investigated mass
Counts vs. Acquisition Time (min)
+MS Chip Scan (6.019 min) Frag=175.0V MITO3H3A.d
330.2551
MS spectrum at the expected rt
Calc. Mass
Mis. Mass
Error ppm
330.25399
330.25510
3.364077
331.2583
332.2625
Counts vs. Mass-to-Charge (m/z)

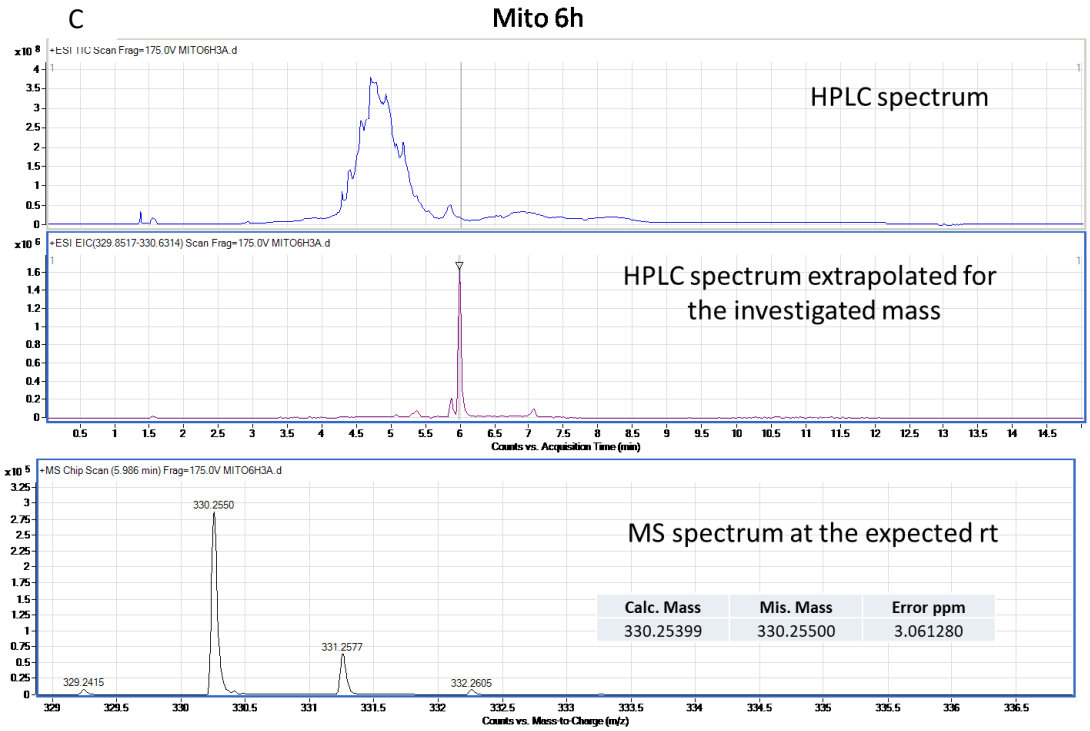

Figure 29: Mass spectra of untreated (A) and compound 5 treated MCF7 cells for 3 hours (B) and 6 hours (C).

4.7 PROTEIN PROFILE IN MCF7 CELLS AFTER 3 AND 6 HOURS OF TREATMENT WITH COMPOUND 5

Once it was established that compound 5 was inside the mitochondria and that the effect that we observed after 3 and 6 hours was indeed due to this molecule, we investigated the cell protein profile.

In order to evaluate the effects of compound 5 on MCF7 cells we performed a Western blot analysis after the isolation of both cytosolic and mitochondrial fractions, to better understand if there was an activation of the apoptotic process.

We investigated the mitochondrial PAM-complex proteins, Tim16 and mtHsp70 and proteins involved in the apoptotic pathway as p53, cytochrome c, BNIP3L and RIP. As housekeeping we used the GAPDH for the cytosolic fraction and VDCA1 for the mitochondrial one.

As shown in figure 30, p53 and cytochrome c are highly expressed in the mitochondrial compartment after 3 hours, but not so after 6 hours. This evidence may indicate that the action of compound 5 on the Tim16-Tim14 binding at 3 hours influences p53 protein that is in part in the cytosolic fraction but mostly in the mitochondrial one. It is known that p53

translocates to the mitochondria and initiates a first wave of MOMP, interacting with BCL2 protein family, in response to death stimuli[224]. This could be the case, but the effect, however, seems transient and there is no evidence of a cytochrome c release in the cytosol.

BNIP3L protein levels increase after 6 hours and RIP is slightly cleaved already after 3h, but much more after 6 hours.

On the contrary proteins belonging to the PAM complex do not display significant changes in the three conditions.

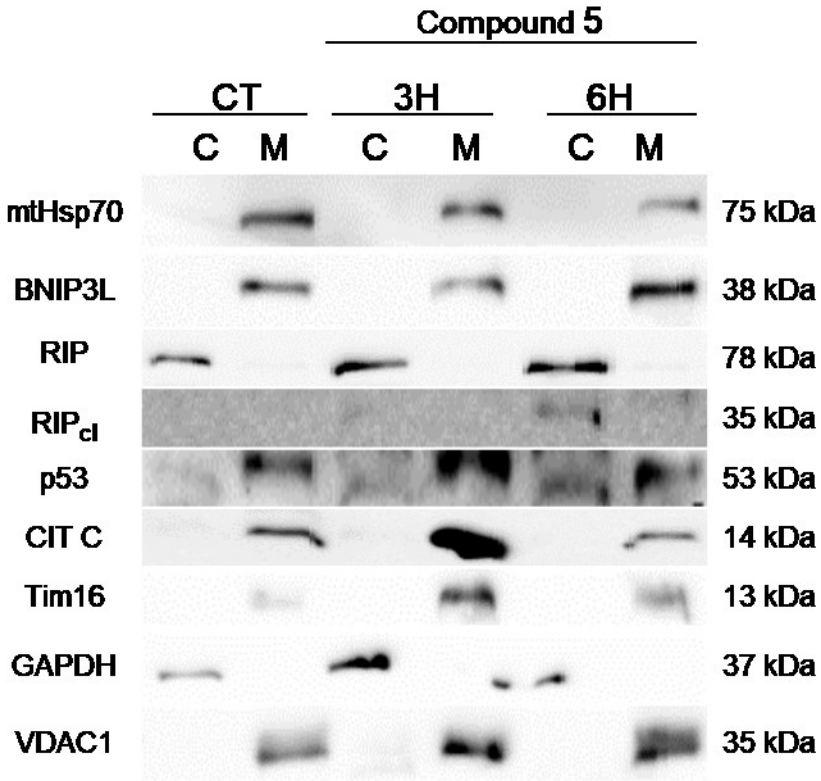

Figure 30: Western blot analysis of Tim16, mtHsp70, BNIP3L, RIP, P53 and cytochrome c in MCF7 cells treated for 3 and 6 hours with 5 µM compound 5 and separated for the cytosolic (C) and the mitochondrial (M) fractions. GAPDH was used as housekeeping for the cytosolic fraction, VDAC1 for the mitochondrial fraction. A representative blot of three independent experiments is shown.

Protein signal densitometry was performed for each protein and Figure 31 shows p53 levels (A) with the cytosolic and mitochondrial protein expression normalized against GAPDH and VDAC1 respectively; cytochrome c (B) and BNIP3L graphs (C) are normalized against VDAC1.

The figure shows that mitochondrial levels of p53 at 3 hours is ~2-fold higher as compared to the mitochondrial levels in the untreated cells, that show the same p53 expression level as cells treated for 6 hours. cytochrome c levels are ~6,5-fold higher at 3 hours vs. control and ~2,5- fold higher at 6 hours vs. control. BNIP3L display similar levels in the untreated cells and at 3 hours, but at 6 hours its levels are ~2,5-fold higher than the untreated cells.

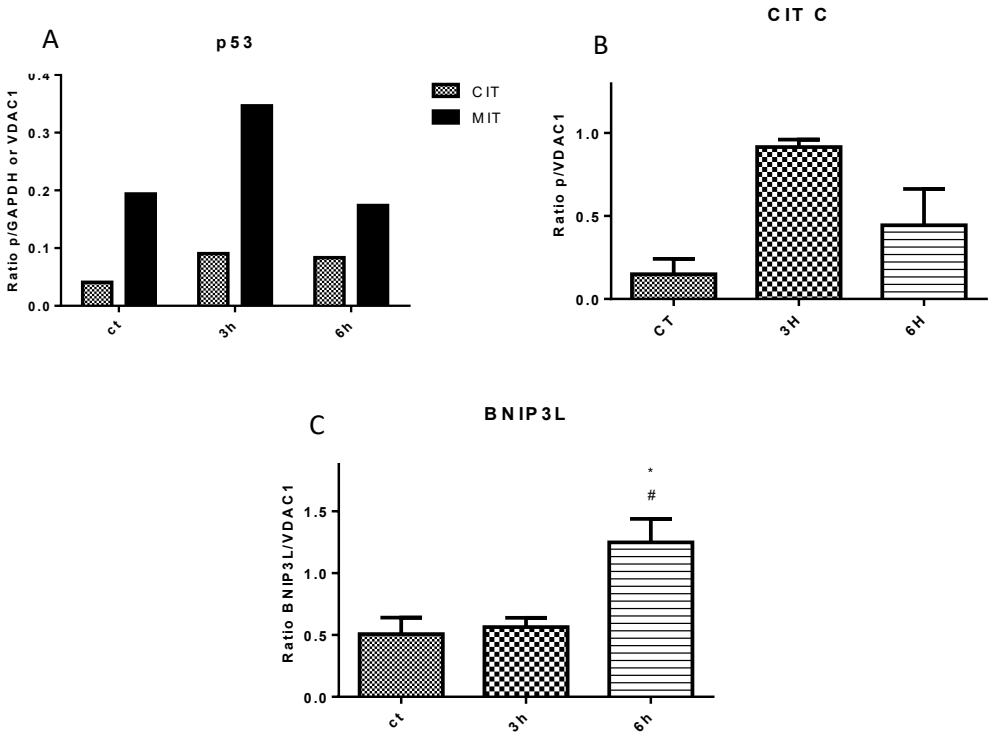

Figure 31: p53, cyt. C, BNIP3L expression after densitometry analysis. of MCF7 cells treated for 3 and 6 hours with 5 µM compound 5. A) p53 expression in the cytosolic fraction (grey bars) and mitochondrial fraction (black bars). They are express as a ratio between p53 and the cytosolic housekeeping (GAPDH) or the mitochondrial housekeeping (VDAC1). B) Cyt. C express as a ratio between the protein and the mitochondrial housekeeping VDAC1; C) BNIP3L express as a ratio between the protein and the mitochondrial housekeeping VDAC1. (*p<0,05 vs ct; #p< 0,05 vs 3h).

4.8 PROTEIN PROFILE IN MCF7 CELLS AFTER 3 AND 6 HOURS OF TREATMENT WITH COMPOUND 5 AND/OR DOXORUBICIN

To evaluate the influence that a chemotherapeutic drug, such as doxorubicin, could have on the effects induced by compound 5, we performed the experiment described above by using both molecules.

MCF7 cells were treated with 5 µM compound 5 and/or 200 nM doxorubicin for 3 and 6 hours and a Western blot analysis was performed with 30 µg of protein, evaluating mtHsp70 and Caspase 9 activation, as shown in Figure 32.

As shown, mtHsp70 levels do not change, while the levels of cleaved Caspase 9 increase after treatment with doxorubicin treatment for 6 hours and after treatment with doxorubicin + compound 5 for 3 and 6 hours. Treatment with compound 5 alone for 3 and 6 hours does not seem to modify basal cleaved Caspase 9 levels.

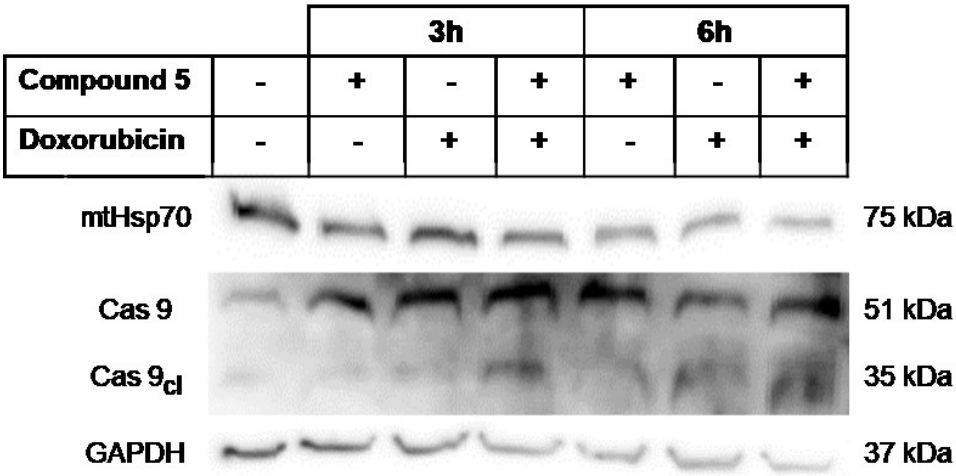

Figure 32: Western blot analysis of mtHsp70 and Caspase 9 in MCF7 cells treated for 3 and 6 hours with 5 µM compound 5 and/or 200nM doxorubicin. GAPDH was used as housekeeping. A representative blot of three independent experiments is shown.

4.9 TOXICITY TEST OF COMPOUND 5 IN ZEBRAFISH

In order to understand the *in vivo* toxicity of Compound 5, we performed a Fish Embryo Acute Toxicity (FET) Test in zebrafish using the OECD 2013 guidelines for the testing of chemicals[182].

Newly fertilized zebrafish embryos were exposed to different concentrations of compound 5 (0, 5, 10, 25, and 30 µM), within the first 3 hours post fertilization (hpf), for a total of 96 hours. After 4 days the number of surviving embryos after each treatment was recorded.

As shown in Figure 33, compound 5 at the concentration of 5 µM (the concentration used to perform *in vitro* experiments with cell lines) does not affect embryos survival as compared to control. The number of surviving embryos decreases at higher concentrations of compound 5 in a dose-response manner: a concentration of 25-30 µM is toxic for

embryos. The graph represents surviving embryos as % of total number of incubated embryos.

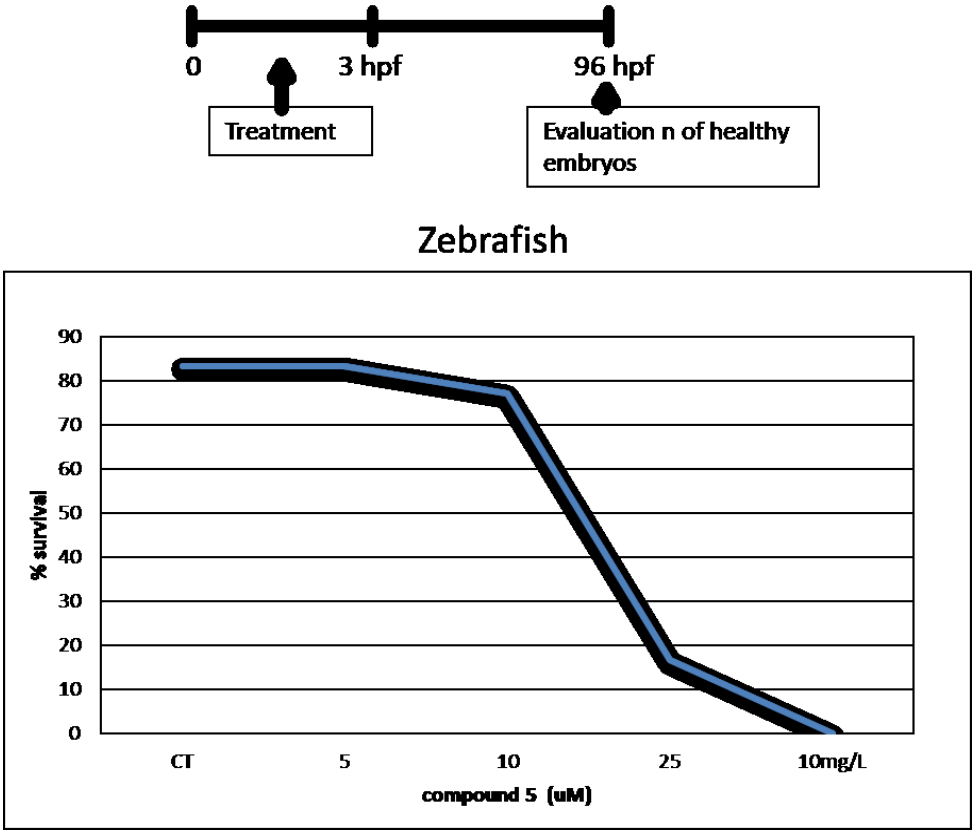

Figure 33: % survival at 4 days post fertilization of zebrafish embryos treated with 5 different concentrations of compound 5 (0-5-10-25-30 µM). This experiment was performed twice.

4.10 *IN VIVO* EFFECTS OF COMPOUND 5 AND PACLITAXEL IN XENOGRAFT MICE

Previous *in vitro* studies conducted in our lab on TT cells shown that compound 5 is able to increase the cytotoxic effect of paclitaxel by 14% and to reduce basal and pentagastrin induced calcitonin secretion. Furthermore, in TT cells we tested a library of Tim16 inhibitors, identifying compound 5 as not cytotoxic but able to enhance the proapoptotic effects of staurosporine by reducing mitochondrial membrane potential (MMP) activation[102]. After the *in vivo* evaluation of compound 5 toxicity in zebrafish embryos, we wanted to investigate the *in vivo* action of compound 5, in combination with paclitaxel, a chemotherapeutic drug, commonly used to treat MTC, in mice.

To perform this experiment, mice were injected subcutaneously with TT cells into the flank. After 3 weeks, a tumor mass could be detected and mice were divided in 4 groups and started treatment with: control solution, intra-tumoral 5 µM compound 5, intra-peritoneal 10 mg/Kg Paclitaxel, and intra-tumoral Compound 5 + intra-peritoneal Paclitaxel. Mice were treated twice (day 0 and day 2) and data were collected after 2 and 4 days of treatment (Figure 34). Results were plotted as tumor volume (mm^3) and expressed as % vs. day 0.

As shown in Figure 34, at day 4, tumors in control mice increased in volume by ~80% vs. day 0; in mice treated with compound 5 tumor volumes increased by ~40% vs. day 0; tumors treated with paclitaxel increased by ~30% vs. day 0; in mice treated with both Compound 5 and paclitaxel tumor volume decreased by ~10%.

Compoun5 and paclitaxel as single treatments induced a decrease in tumor volume by ~50% and ~150%, respectively. The combination resulted in a 10-fold increase in mass volume reduction. Mice weight was similar, between 20 and 25 gr.

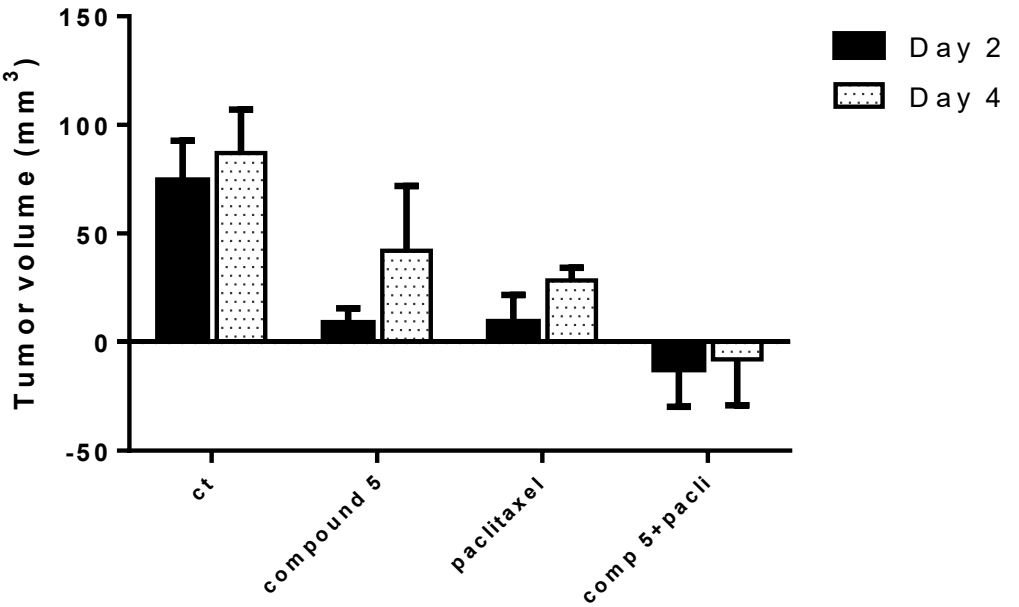

Figure 34: Tumor volume, express in mm^3, measured in xenograft mice after 2 and 4 days of treatment with control solution, 5µM compound 5, 10mg/Kg paclitaxel and the combination of both, compared to day 0 (first treatment).

4.11 PROTEIN PROFILE IN TUMORS EXTRACTED FROM XENOGRAFT MICE

In order to evaluate protein expression in mice tumors treated with compound 5 and paclitaxel, tumors were isolated and protein expression of Tim16, RIP and BNIP31 was evaluated by Western blot, using 20 µg of protein. Western blot was normalized for the housekeeping GAPDH and the densitometry analysis is expressed as a ratio between Tim16 and the housekeeping.

As shown in Figure 35 A-B Tim16 levels do not change between treated and untreated mice.

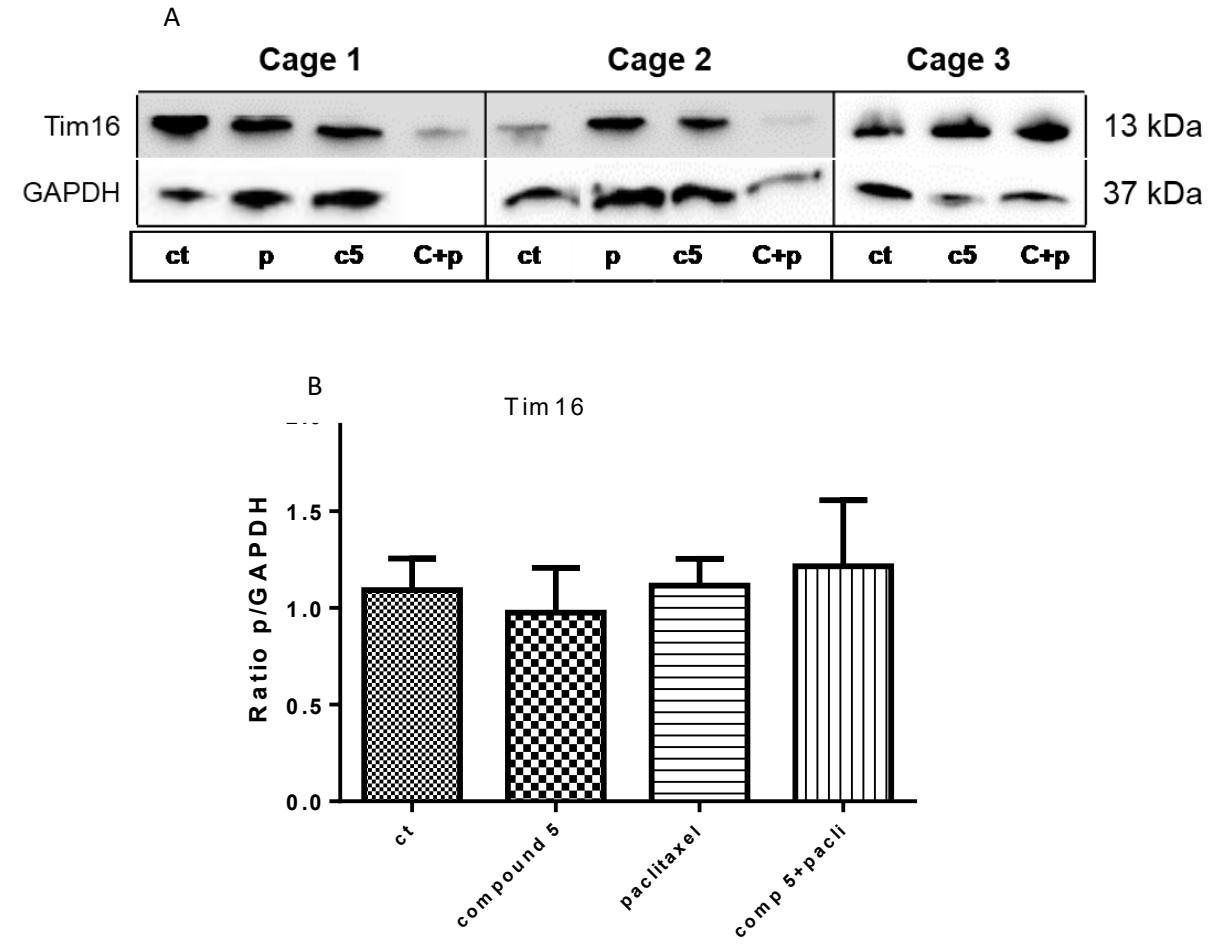

Figure 35: A) Western blot analysis of Tim16 in tumoral masses, isolated from xenograft mice, treated with 5 µM compound 5 and/or 10mg/kg paclitaxel. GAPDH was used as housekeeping. The three different cages are shown (ct:control, p:paclitaxel, c5:compound 5, c+p:compound5 +paclitaxel) B) Tim16 expression after combined densitometry analysis, express as a ratio between Tim16 and the housekeeping GAPDH.

We evaluated also RIP expression, involved in the apoptotic pathway (Figure 36). Densitometry analysis is expressed as a ratio between cleaved RIP and total RIP, after

normalization with the housekeeping GAPDH. No difference was detected after treatment with compound 5 or paclitaxel alone, but co-treatment with compound 5 and paclitaxel increased RIP activation by ~3-fold.

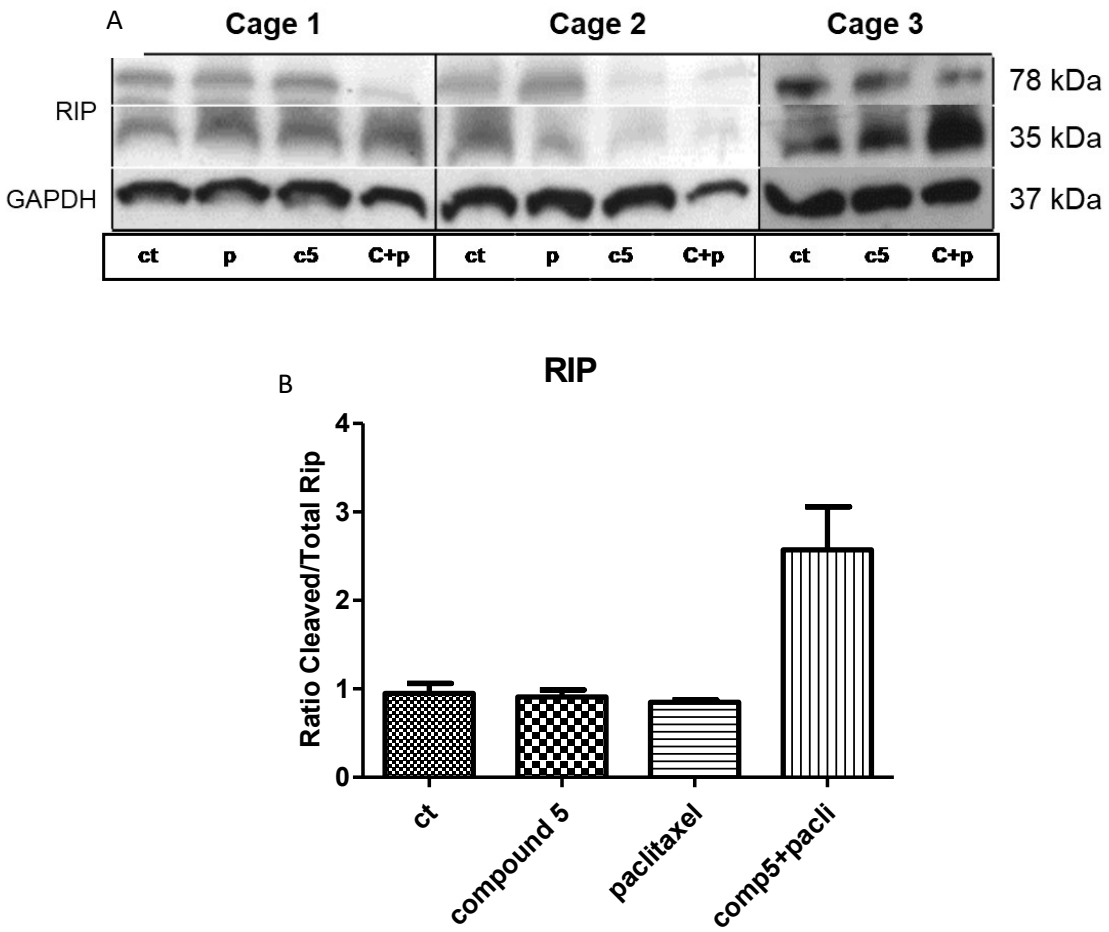

Figure 36: A) Western blot analysis of RIP in tumoral masses, isolated from xenograft mice, treated with 5 µM compound 5 and/or 10mg/kg paclitaxel. GAPDH was used as housekeeping. The three different cages are shown. (ct:control, p:paclitaxel, c5:compound 5, c+p:compound5 +paclitaxel) B) RIP expression after combined densitometry analysis, express as a ratio between cleaved RIP and total RIP, after normalization for the housekeeping GAPDH.

Furthermore, we investigated BNIP3L protein expression, a BCL-2 family protein (Figure 37 A-B). Similarly to what observed for RIP, compound 5 and paclitaxel alone do not influence BNIP3L expression, while the combination of compound 5 and paclitaxel induce higher protein levels.

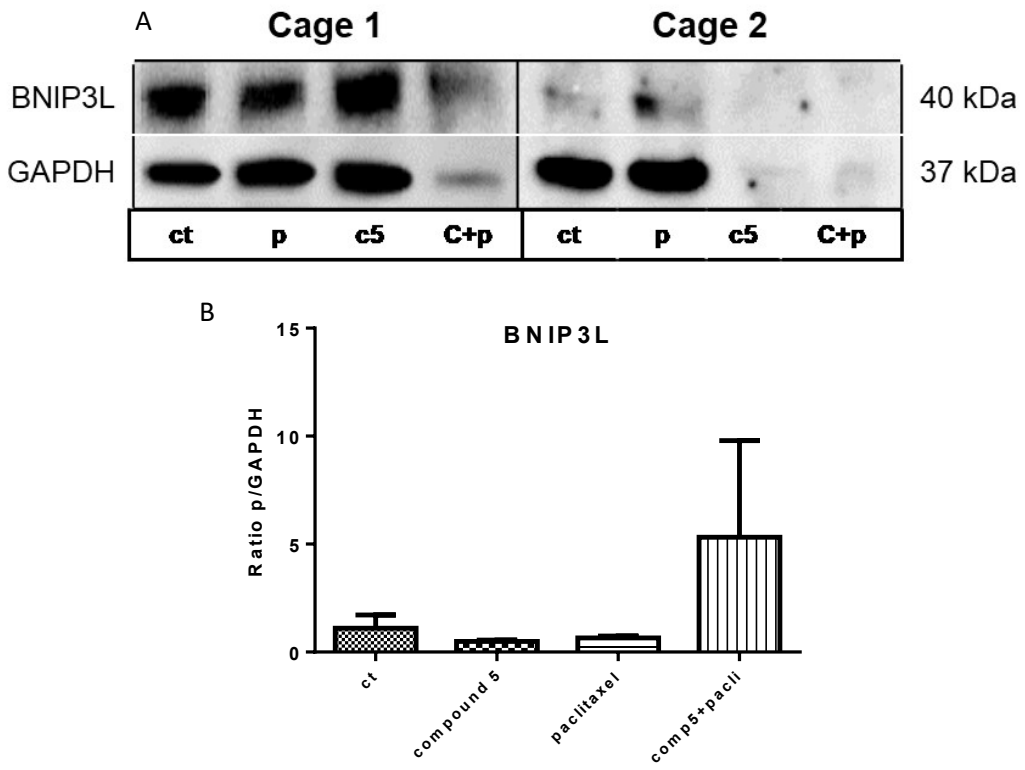

Figure 37: A) Western blot analysis of BNIP3L in tumoral masses, isolated from xenograft mice, treated with 5 µM compound 5 and/or 10mg/kg paclitaxel. GAPDH was used as housekeeping. Two different cages are shown. . (ct:control, p:paclitaxel, c5:compound 5, c+p:compound5 +paclitaxel) B) RBNIP3L expression after combined densitometry analysis, express as a ratio between BNIP3L and the housekeeping GAPDH.

4.12 GENERATION OF A ZEBRAFISH Tim16 MUTANT LINE

In order to better understand the role of Magmas gene, that encodes for the mitochondrial protein Tim16, we have considered to investigate a *in vivo* model, such as zebrafish, by creating a zebrafish mutant line for the Magmas gene, using the CRISPR/Cas9 Technology. It is well known that this technology enables to generate double-stranded DNA breaks (DSBs) in eukaryotic cells[202] using a single guide RNA (sgRNA) and the Cas9 protein. They form a complex with genomic DNA (gDNA), sspecifically targeting DNA sites complementary to an approximately 20-base sequence within the sgRNA and neighboring a protospacer adjacent motif (PAM), the identity of which is dictated by the particular Cas9 protein employed[203].

To generate this mutant line, we identified 3 hypothetical sgRNA that targeted different exons in the Magmas gene. We then acquired the complimentary oligos and then synthesized the desired sgRNAs in vitro, by using the t7 polymerase.

We injected 1 ng of each of the three sgRNAs (alone or in combination sgRNA1+ sgRNA2) with the recombinant S. pyogenes Cas9 into a 1-cell stage embryo to ensure a high efficient delivery of injected mRNA to the embryo, as well as to reduce mosaicism. To verify the editing, 5 days embryos were genotyped and DNA was sequenced. Embryos of the same positive editing strand were raised to adulthood. Once they grew up, we out-crossed the fish with wild type ABs fish and analyzed F1 embryos (first filial generation). After extraction of gDNA from these embryos, we performed a PCR amplification, followed by the T7 assay to verify the presence of editing, and sent to sequence the positively amplified DNAs. We amplified the targeted genomic region by PCR. As shown in figure 38 several fish from 6 different F1 families injected with gRNA2, at first, were analysed.

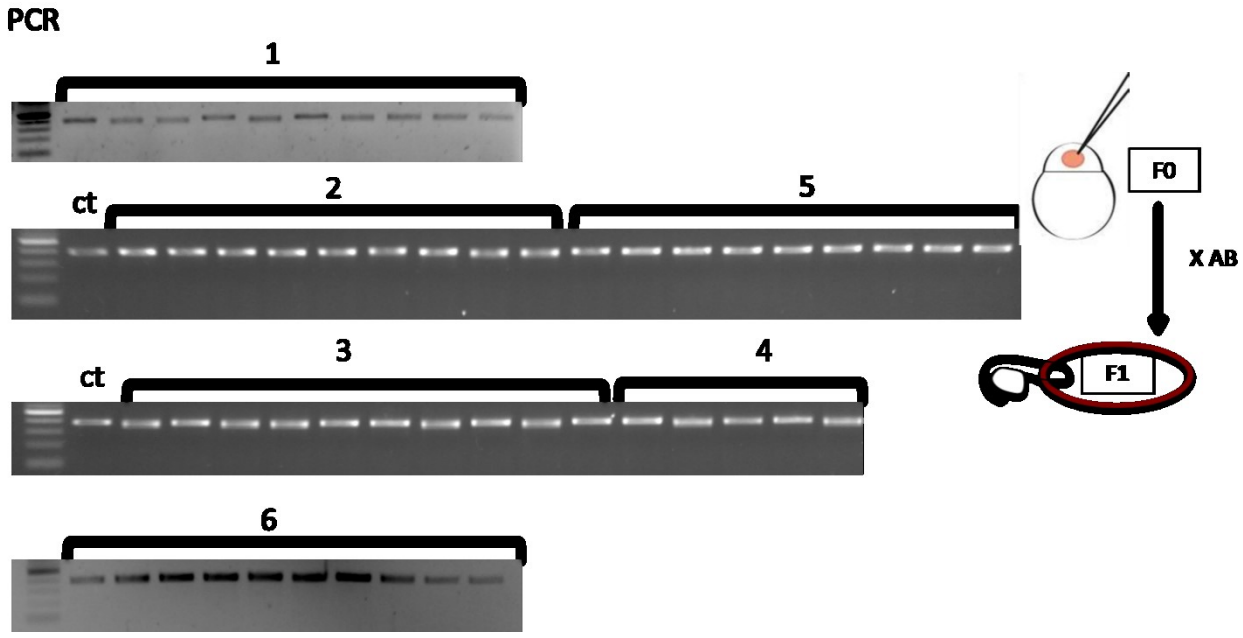

Figure 38: Examples of 2% agarose gel after PCR that amplified the genomic region of Magmas probably edited by sgRNA2 in 6 different families. To each band correspond a F1 embryos.

To evaluate the presence of editing we performed a T7 Endonuclease I Assay. This technique allows to rapidly identify the editing presence. The endonuclease recognizes and cleaves non-perfectly matched DNA. The cleavage site is at the first, second or third phosphodiester bond that is 5′ to the mismatch (Figure 39).

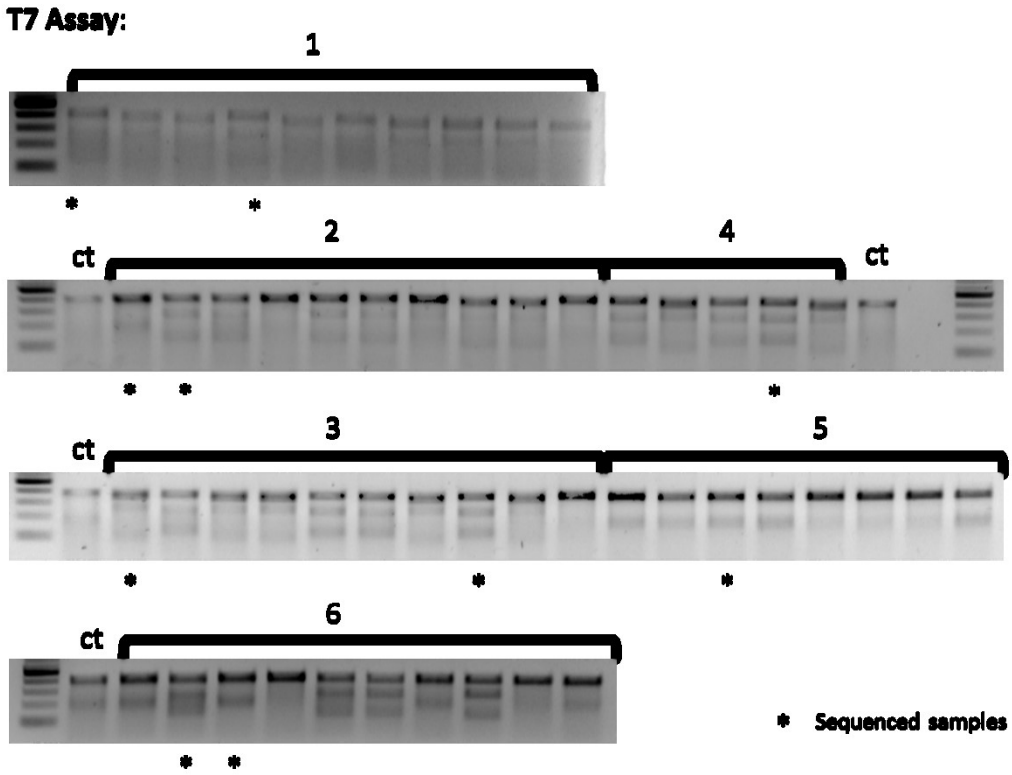

Figure 39: T7 endonuclease Assay to rapidly determine editing. PCR amplificated product has been submitted to T7 endonuclease I. Some fish show a double band, sign of editing. Some samples were sent to sequence (*) to better understand the type of Indels.

DNA from fish positive to the T7 were sent to sequence and a TIDE (Tracking of Indels by Decomposition) assay was than performed to rapidly assess genome editing (Figure 40).
We identified 6 founders F0 injected with gRNA2, 3 founders F0 injected with gRNA1 and 4 founders F0 injected with gRNA1+gRNA2. gRNA3 did not work from the beginning.
F1 embryos of the same family of those positive to T7 and TIDE analysis were raised to adulthood.

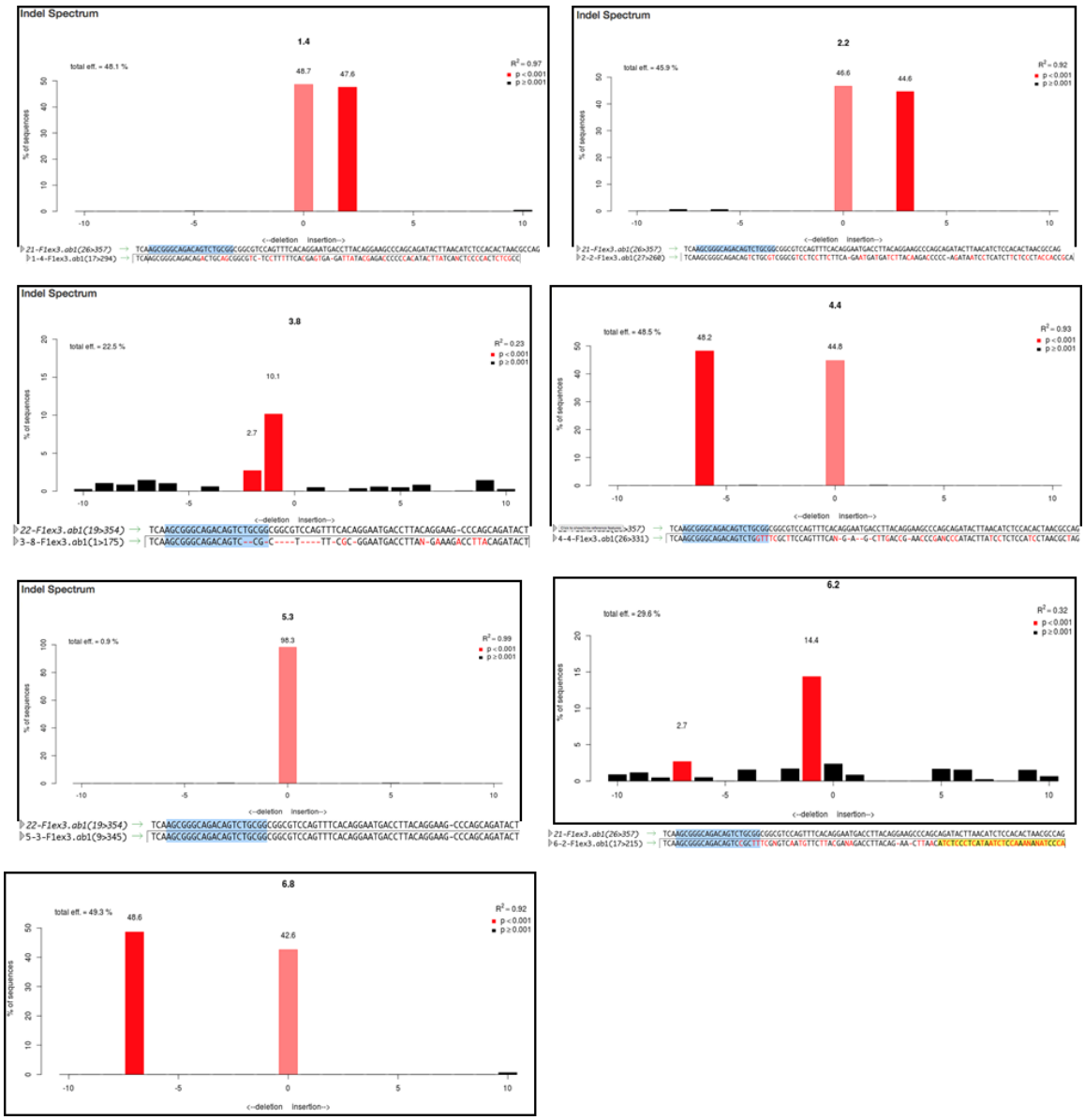

Figure 40: Examples of Indel spectrum determined by TIDE (Tracking of Indels by Decomposition)[216] of some F1 embryos. The method is effective for tracing INDELs in heterozygotes. TIDE uses these peak heights to determine the relative abundance of every possible indel within a chosen size range. R2 is calculated to assess the goodness of fit. The P-value associated with the estimated abundance of each indel is calculated by a two-tailed t-test of the variance–covariance matrix of the standard errors (black $p \geq 0{,}001$, red $p < 0{,}01$).

Once F1 reached adulthood, a fin clipping was performed to identify hypothetical interesting founders. The target genomic region was amplified by PCR (Figure 41 A) and the T7 endonuclease I assay was performed (Figure 41 B).

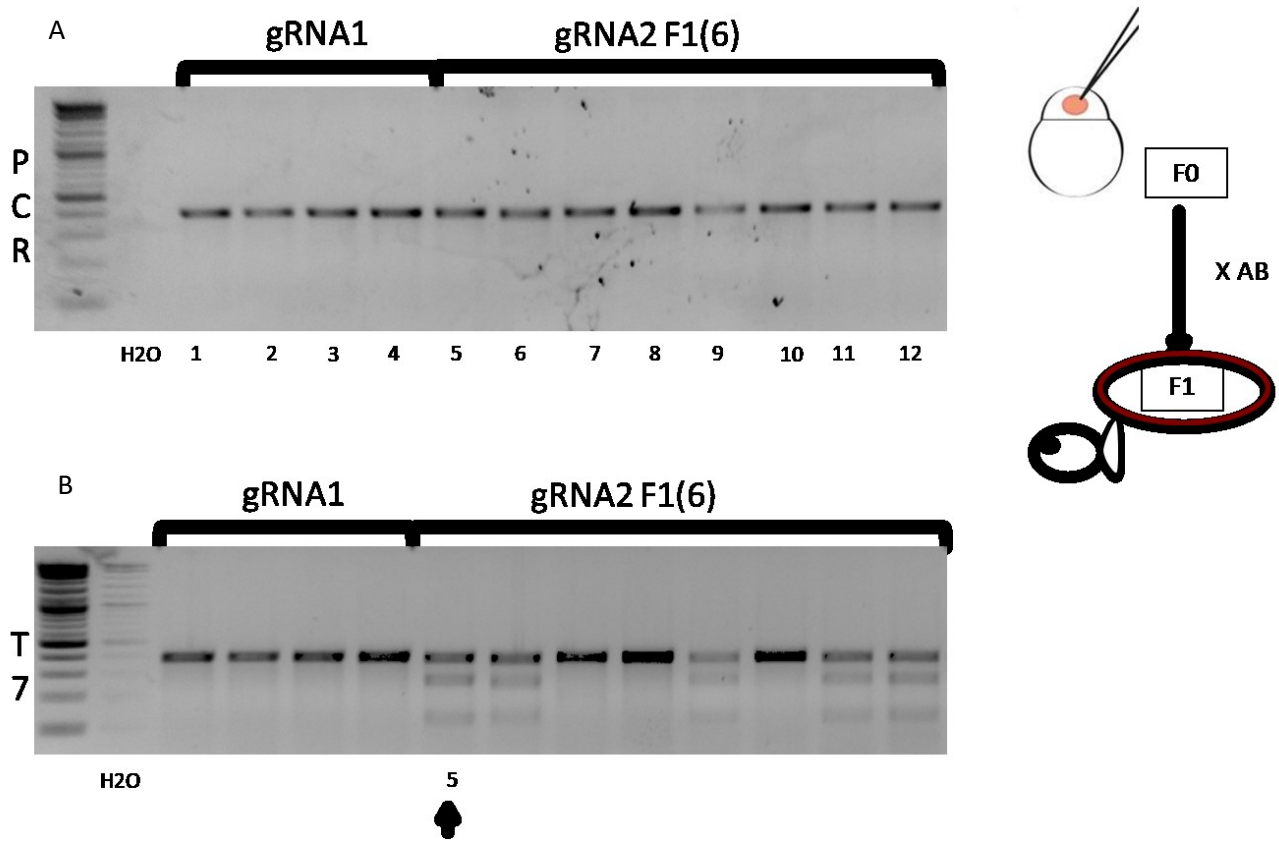

Figure 41: PCR and T7 2% agarose gel. A) PCR amplified of some F1 fin clipped fish injected, at first, with gRNA1 an gRNA2. B) T7 assay to evaluate the presence of editing. In gRNA2 F1 fish, deriving from family 6, we identified 1 edited fish (arrow).

We outcrossed the edited fish (n 5), a male, with a wild type AB female. We genotyped F2 (second filial generation) embryos deriving from this outcross, selecting those that had an abnormal phenotype as well as those with a normal phenotype.

As shown in Figure 42 A, we selected embryos deriving from 3 different fish, of 2 different families, and performed a PCR amplification (Figure 42 B) followed by a T7 assay (Figure 42 C).

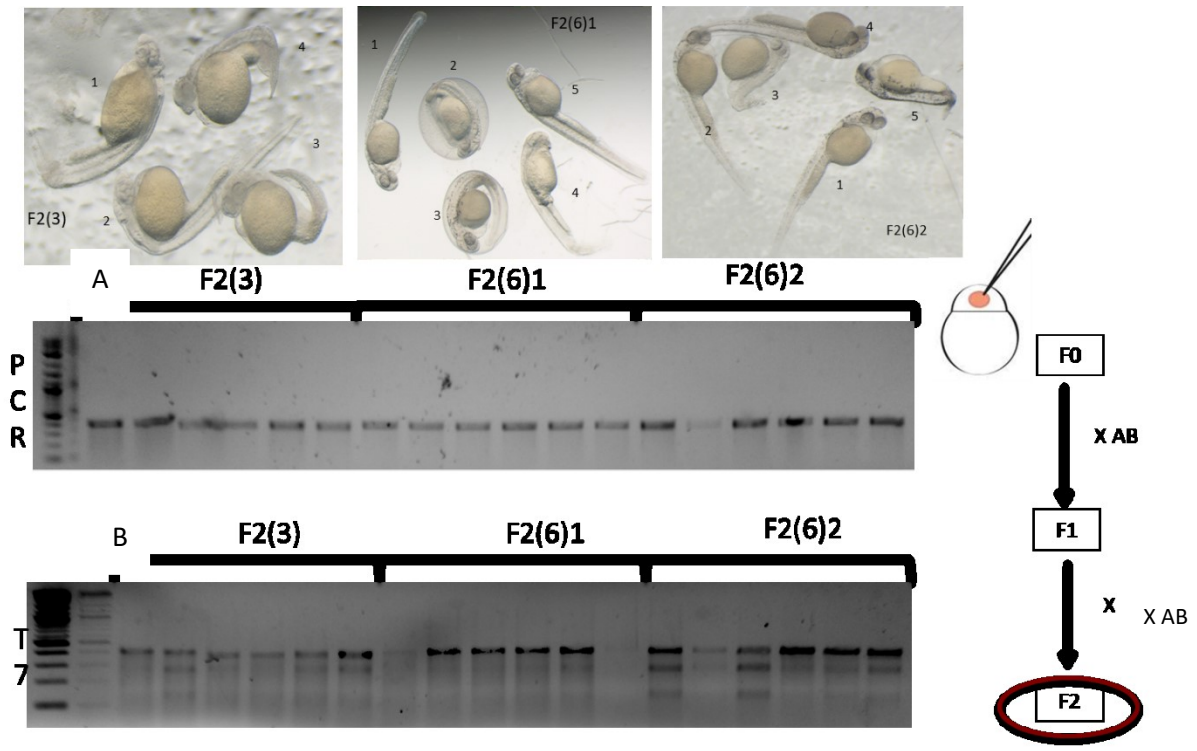

Figure 42: F2 embryos selection, PCR and T7 assay. A) different phenotypes were observed and weird/normal embryos were selected, from 3 different fish deriving from founders injected initially with gRNA2; B) 2% agarose gel after PCR; C) 2% agarose gel after T7 assay.

To determine the type of mutation that occurred in F2(6)2 embryos, we cloned individual DNA molecules in a bacterial vector and analyzed 4 clones each by sequencing embryos 1 and 3, positive to the T7 test.

We found that these F2 embryos has a 7bp deletion, as the father, that may cause a truncated protein (Figure 43).

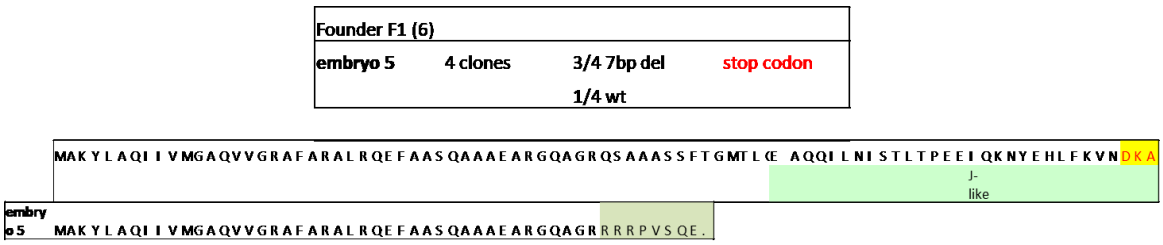

Figure 43: embryo 5, of family 6, injected initially with gRNA2, shows a 7bp deletion that bring to a premature stop codon. It is also represented the hypothetical protein with this stop codon.

Many fish at different filial generations (F0, F1 and F2) injected with gRNA1, gRNA2 and

both, were analyzed. We found lots of small (3-12bp) or big (33-42bp) in-frame mutations with all of these sgRNAs (Figure 44).

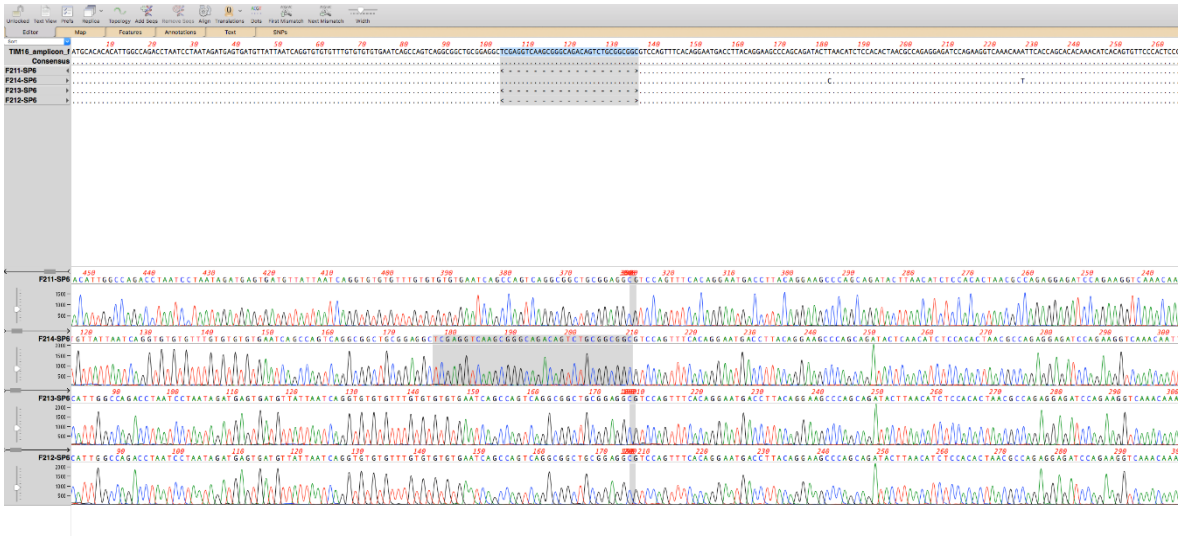

Figure 44: Example of a 33bp in-frame deletion in 3/4 clones of a F2 embryo of family 1, injected with gRNA2, at first.

We focused on fish identified as displaying a 7pb deletion (not in frame). Actually, we are in a F2 generation stage, with fish that are wild-type or heterozygous, so we are not yet aware of what might happen in a homozygous situation.

The most common phenotype observed in this heterozygous fish relates mainly to cardiac edema, or to body malformations such as a shorter and curved tail (Figure 45). The scoring of observed phenotype and a statistical analysis will be performed in future, when more data will be available.

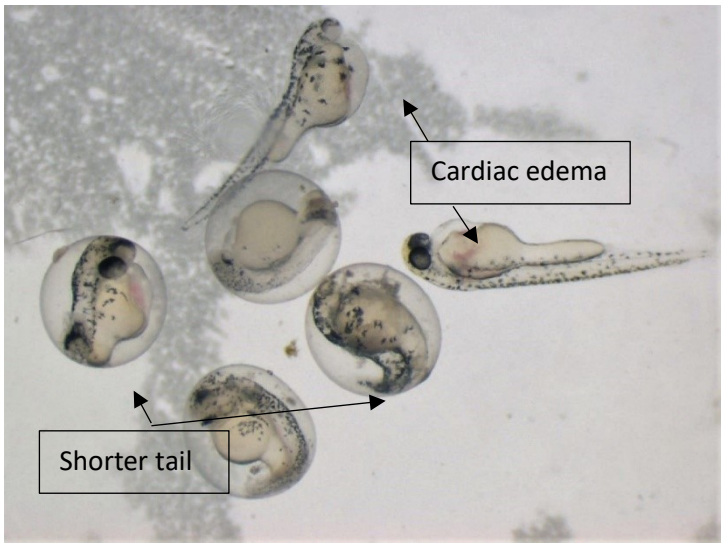

Figure 45: F2(6)2 embryos at ~3dpf showing some phenotypic anomalies.

5. DISCUSSION AND CONCLUSIONS

Magmas (mitochondria-associated protein involved in granulocyte-macrophage colony-stimulating factor signal transduction) was identified as a GM-CSF inducible gene in PGMD1 murine myeloid cells and encodes for the mitochondrial protein Tim16[74].

Tim16 is member of the translocase complex TIM23, located in the mitochondrial inner membrane, that drives proteins from the intermembrane space into the matrix and its expression is both developmentally regulated and tissue specific[77].

It has been widely studied in yeast as Pam16 and has been shown to functionally interact with another protein, Pam18 (Tim14 in humans), to regulate the importation of peptides into the mitochondria through the import complex[78]. Homologs of Pam16 and Pam18 proteins are found across all eukaryotic species. Tim16/Pam16 is a J-like protein as it contains a domain with sequence similarity to the J domain of Tim14/Pam18 but lacks the invariant tripeptide motif His-Pro-Asp (HPD), a signature of J proteins, having a DKE motif instead. They form a heterodimeric complex, which is defined here as J-complex, and they strongly interact in a hydrophobic pocket that includes L150 of Pam18 and L97 of Pam16, leaving the conserved HPD motif of Pam18 available for stimulating Hsp70 ATPase activity[33]. Members of the J-protein family, in fact, function as coupling factors to stimulate ATP hydrolysis by a partner Hsp70 when a polypeptide is present in its substrate-binding pocket. Tim16 and Tim14 together with Tim44, mtHsp70 and Mge1 form the PAM (Protein associated Motor) complex of TIM23. The ADP/ATP states of Hsp70 regulate its interactions with client proteins[8283].

Tim16 was found overexpressed for the first time in prostate cancer and studies conducted in our laboratory demonstrated that Magmas mRNA is overexpressed in 72% human pituitary adenomas as well as in ACTH-secreting mouse pituitary adenoma cell lines (AtT-20 D16v-F2 cells) compared to their respective human and murine normal counterparts.

It was observed that an overexpression of Tim16 protects cells from apoptosis by inhibiting staurosporine-induced cytochrome c release from mitochondria, influencing Bax and Bcl2 modulation by proapoptotic stimuli[101]. Moreover, Magmas-silenced cells displayed basal caspase 3/7 activity and DNA fragmentation levels similar to control cells, which both increased under pro-apoptotic stimuli[100] .

Since Tim16 seems to be involved in cancers, small molecule of Magmas inhibitors (SMMI) have been synthetized[81]. Our laboratory together with the Dept. of Chemical and Pharmaceutical Sciences of the University of Ferrara, synthesized 6 compounds, identifying the compound 5 as not cytotoxic but able to enhance the proapoptotic effects of staurosporine

in TT cell lines, that express Tim16 high levels, by reducing mitochondrial membrane potential (MMP) activation[102]. We found that MCF7 cells, deriving from a human breast cancer, express higher levels of Tim16 as compared to the normal immortalized breast cell line, MCF12A. We found that MCF7 cells displayed 6-fold higher Tim16 levels as compared to MCF12A and, analysing also other protein of the PAM complex, we discovered that mtHsp70 was 1,5-fold higher in MCF12A as compared to MCF7. Therefore, MCF7 cells are a good model to test Magmas inhibitors. Since compound 5 effects were tested only in combination with pro-apoptotic stimuli, such as staurosporine, to better understand if compound 5 could modulate also the response of MCF7 cells to chemotherapeutic drug, such as doxorubicin, commonly used for breast cancers chemotherapy, we tested Tim16 inhibitor in combination with doxorubicin evaluating cell viability and caspase activation in both MCF7 and MCF12A cells. We found that compound 5 modulate the response to the chemotherapic drug in MCF7 cells and not in the normal control MCF12A, further enhancing doxorubicin cytotoxic action and caspase 9 activation. Similarly to previous results, in this study we did not observe a cytotoxic effect of compound 5. To better evaluated whether Tim16 plays a role in cell protection from apoptosis, we evaluated proteins involved in apoptosis and we found that compound 5 enhances doxorubicin action, inducing higher BAX levels in MCF7 cells, with no appreciable effects in MCF12A cells. Moreover, we observed that the combination of compound 5 and doxorubicin obtained a further induction of other apoptotic proteins, such as cytochrome c, BNIP3L and RIP. Therefore, compound 5 sensitises MCF7 cells to the cytotoxic action of doxorubicin by involving apoptosis.

Other studies conducted in our lab have shown that Compound 5 enhanced the pro-apoptotic stimuli of doxorubicin and cisplatin in MCF7 cells and mock-silenced MCF7 cells, but fails to do so in silenced MCF7 cells with a shRNA targeting Magmas. These results indicate that compound 5 targets Tim16 and that Tim16 levels modulate the chemosensitizing effects of compound 5.

Magmas inhibitors are predicted to bind at the Tim 16/Tim 14 dimer interface establishing multiple idrophobic contacts with both Tim14 and Tim16, resulting in complex dissociation. In addition, a Magmas inhibitor named compound 9 likely interfered with the N-terminal portion of Tim14 that interacts with Tim16 helix III, known to be necessary for complex formation and function. Moreover, it has been previously shown that Magmas overexpression reduces sensitivity to SMMI 9[81]. In order to better understand the effects of compound 5 on Tim16-Tim14 interaction, we evaluated its effect in MCF7 cells after treatment for 3 and 6 hours. We observed that compound 5 acted mainly at 3h, as there is a reduction in protein interaction. Both Tim14 and mtHsp70 were less associated to Tim16,

although this effect seemed transient and partially reversed at 6 hours. We also confirmed that the observed effect is due to the presence of compound 5 in the mitochondrial compartment by mass spectrometry. Therefore, our findings support the hypothesis that compound 5 disrupts Tim16-Tim14 interaction in a reversible manner.

Evaluating protein expression at the two different time points, we found that while Tim16-Tim14 and Tim16-mtHsp70 complexes decreased at 3 hours, p53 and cytochrome c levels simultaneously increased, returning almost normal at 6 hours. It is known that p53 is activated by many stress signals through mechanisms that result in stabilization and accumulation of the p53 protein[225]. Moreover, mortalin (mtHsp70) was found to interact with p53 and this interaction was suggested to promote sequestration of p53 in the cytoplasm, thereby inhibiting its nuclear activity[226,227,228] and inducing the resistance of some tumors to radiotherapy and chemotherapy[229]. Inhibition of mortalin increases translocation of p53 to the nucleus[230]. Therefore, our data suggest that compound 5 at 3 hours induces a stress signal that results in a p53 and cytochrome c mitochondrial accumulation, that is partially restored after 6 hours. On the contrary, BNIP3L and RIP expression is higher at 6 hours. On the basis of our results, we hypothesize that after 3 hours compound 5 targets Tim16, disrupting its interaction with both mtHsp70 and Tim14, triggering a signal cascade that involves BNIP3L and RIP after 6h, without influencing Tim16, Tim14 or mtHsp70 expression levels.

We also evaluated the effects of doxorubicin after 3 and 6 hours alone or in combination with compound 5 on Caspase 9 activation. As expected doxorubicin, induced Caspase 9 activation, and this effect was enhanced by co-treatment with compound 5. Therefore, these data support the idea that compound 5 might be used as a chemosensitizing agent.

In order to understand the *in vivo* toxicity of compound 5, we performed a Fish Embryo Acute Toxicity (FET) Test in zebrafish using the OECD 2013 guidelines. As expected, we obtained a dose-response curve. However, we found that compound 5 at the lowest concentrations (5 μM), which we used *in vitro*, was not toxic for embryos. Therefore, we can postulate that the employed concentration might not be toxic in vivo.

Previous *in vitro* studies conducted in our lab on TT cells showed that compound 5 was able to increase the cytotoxic effect of paclitaxel and to reduce basal and pentagastrin induced calcitonin secretion. Furthermore, in TT cells compound 5 is not cytotoxic but able to enhance the proapoptotic effects of staurosporine by reducing mitochondrial membrane potential (MMP) activation[102]. After the *in vivo* evaluation of the compound 5 toxicity in zebrafish embryos, we wanted to investigate the *in vivo* action of compound 5, in combination with paclitaxel, a chemotherapeutic drug commonly used to treat cancer, in

mice. After 2 days of treatment, we found that tumors in control mice increased in volume by a ~ 80%, while the increase in tumor volume was reduced in mice treated with compound 5 (~ 40%) or with paclitaxel (~ 30%). In mice treated with both compound 5 and paclitaxel tumor volume decreased by ~10%. These results indicate that the combinations of compound 5 and the chemotherapeutic drug indices a strong cytotoxic effect also *in vivo.*

We analyzed the protein profiles in tumors extracted from these xenograft mice. Tim16 levels did not change between treated and untreated tumors, while the levels of the pro-apoptotic proteins RIP and BNIP3L were ~3-fold higher in tumors treated with both compound 5 and paclitaxel as compared to the control and the single treatments. These data indicate that compound 5 *in vivo* exerted a similar effect to that observed *in vitro*: if used alone it does not affect apoptosis but can enhance the pro-apoptotic effects of a chemotherapeutic drug, either doxorubicin or paclitaxel.

One of the aims of our study was to create a mutant animal in order to better understand the role of Magmas. Therefore, we tried to create a zebrafish mutant line for the Magmas gene, using the CRISPR/Cas9 Technology.

We started with the injection of 3 different gRNAs and the recombinant Cas9 into a 1-cell stage embryos, and identified 6 founders F0 injected with gRNA2, 3 founders F0 injected with gRNA1 and 4 founders F0 injected with gRNA1+gRNA2. Over time we focused on gRNA2-injected offspring, as it was the one that worked best, and we identified a F1 fish of family 6 as an interesting founder with a 7bp deletion that probably results in a truncated protein.

Unfortunately, our results are too preliminary soon to predict what exactly happens in homozygous condition. We are now in a wild-type/heterozygous situation and we observed some phenotypes as cardiac edema, or body malformations, but at this stage it is difficult to discriminate between casual events and Magmas disruption effects.

However, previous evidence showed that both Tim14 and Tim16 are involved in diseases including cardiac problems. A mutation of Tim14 causes the dilated cardiomyopathy with ataxia (DCMA) syndrome[231,232] . In addition, Magmas mutations were reported in patients affected with a rare lethal spondylometaphyseal dysplasia, the Megarbane– Dagher–Melki type, a skeletal dysplasia (SD) characterized by pre and postnatal disproportionate short stature, short limbs, cardiomegaly, bone malformations, and early death[104,105]. It will definitely be interesting to deepen this study.

To conclude, the aim of this study was to investigate Tim16 effects in cancer chemoresistance. We knew that overexpression of Tim16 protects cells from apoptotic stimuli, therefore using the compound 5, a Tim16 inhibitor, we investigated its *in vitro* and

in vivo action in combination with chemotherapeutic drugs. We found that compound 5 was not cytotoxic but enhanced doxorubicin or paclitaxel effects, and we observed that Tim16 over-expression seems to play a relevant role in the apoptotic pathway, because its inhibition sensitizes the cells to chemotherapeutic drugs, with a concomitant release of pro-apoptotic proteins. Moreover, compound 5 acts only when Tim16 protein is expressed at high levels, because it did not affect the normal cell line MCF12A, which expresses low Tim16 protein levels.

These experiments suggest that compound 5 could be a good candidate to overcome doxorubicin and paclitaxel chemoresistance in cancer expressing high levels of Tim16 protein.

Considering that compound 5 sensitizes chemoresistant cancer cells to the cytotoxic action of chemotherapeutic drugs, without significantly affecting normal cells, it may represent a new therapeutic strategy, with important clinical application, through compound 5 modulates Tim16 activity only in those tumors with a high expression of the protein. Tim16 expression could have a potential role in tumors as a predictor of response to chemotherapy. The use of compound 5 could restore efficacy in chemoresistant cancers and allow a reduction in chemotherapeutic dose and in patients' side effects.

Further studies are necessary to further strengthen our hypothesis, as well to investigate the role of Magmas in the zebrafish model.

6. REFERENCES

[1] Wallace DC. *Mitochondria and cancer*. 2012, Nat Rev Cancer. 12(10):685-98.

[2] Margulis LS. *Origin of Eukaryotic Cells*. 1970, Yale University Press XXII u. 349 S., 89 Abb., 49 Tab.

[3]Gray MW, Burger G, Lang BF. *Mitochondrial evolution*. 1999, Science. 5;283(5407):1476-81.

[4] Cole LW. *The Evolution of Per-cell Organelle Number.* 2016, Frontiers in Cell and Developmental Biology. 2016; 4:85.

[5] Zong WX, Rabinowitz JD, White E. *Mitochondria and Cancer*. 2016, Mol Cell. 3;61(5):667-676.

[6] Duchen MR. *Mitochondria and calcium: from cell signalling to cell death.* 2000, Journal of Physiology 529(Pt 1): 57–68

[7] Susin SA, Lorenzo HK, Zamzami N et al. *Molecular characterization of mitochondrial apoptosis-inducing factor.* 1999, Nature 397: 441–446.

[8]Osellame LD, Blacker TS, Duchen MR. *Cellular and molecular mechanisms of mitochondrial function.* 2012, Best Pract Res Clin Endocrinol Metab. 26(6):711-23.

[9] Friedman JR, Nunnari J. *Mitochondrial form and function*. 2014, Nature 505(7483):335-343.

[10]Amigo I, Traba J, Satrústegui J, del Arco A. *SCaMC-1Like a Member of the Mitochondrial Carrier (MC) Family Preferentially Expressed in Testis and Localized in Mitochondria and Chromatoid Body.* 2012, *PLoS ONE* 7(7):e40470.

[11]Jornayvaz FR, Shulman GI. *Regulation of mitochondrial biogenesis*. 2010, Essays Biochem. 47:69-84.

[12] Prokisch H, Scharfe C, Camp DG 2nd, Xiao W, David L, Andreoli C, Monroe ME, Moore RJ, Gritsenko MA, Kozany C, Hixson KK, Mottaz HM, Zischka H, Ueffing M, Herman ZS, Davis RW, Meitinger T, Oefner PJ, Smith RD, Steinmetz LM. *Integrative analysis of the mitochondrial proteome in yeast.* 2004, PLoS Biol. 2(6):e160.

[13] Sickmann A, Reinders J, Wagner Y, Joppich C, Zahedi R, Meyer HE, Schönfisch B, Perschil I, Chacinska A, Guiard B, Rehling P, Pfanner N, Meisinger C. *The proteome of Saccharomyces cerevisiae mitochondria*. 2003, Proc Natl Acad Sci. 11;100(23):13207-12.

[14] Taylor SW, Fahy E, Zhang B, Glenn GM, Warnock DE, Wiley S, Murphy AN, Gaucher SP, Capaldi RA, Gibson BW, Ghosh SS. *Characterization of the human heart mitochondrial proteome*. 2003, Nat Biotechnol. 21(3):281-6.

[15] Van der Laan M, Chacinska A, Lind M, Perschil I, Sickmann A, Meyer HE, Guiard B, Meisinger C, Pfanner N, Rehling P. *Pam17 is required for architecture and translocation activity of the mitochondrial protein import motor.* 2005, Mol Cell Biol. 25(17):7449-58.

[16] McBride HM, Neuspiel M, Wasiak S. *Mitochondria: more than just a powerhouse*. 2006, Curr Biol. 25;16(14): R551-60.

[17] Shimoda-Matsubayashi S, Matsumine H, Kobayashi T, Nakagawa-Hattori Y, Shimizu Y, Mizuno Y. *Structural dimorphism in the mitochondrial targeting sequence in the human manganese superoxide dismutase gene. A predictive evidence for conformational change to influence mitochondrial transport and a study of allelic association in Parkinson's disease.* 1996, Biochem Biophys Res Commun. 13;226(2):561-5.

[18] Omura T. *Mitochondria-targeting sequence, a multi-role sorting sequence recognized at all steps of protein import into mitochondria*. 1998, J Biochem. 123(6):1010-6.

[19] Mokranjac D, Neupert W. *Protein import into mitochondria*. 2005, Biochem Soc Trans. 33(Pt 5):1019-23.

[20] Roise, D. and Schatz, G. *Mitochondrial presequences*. 1988, J. Biol. Chem. 263, 4509-4511.

[21] Amaya, Y., Arakawa, H., Takiguchi, M., Ebina, Y., Yokota, S., and Mori, M. *A noncleavable signal for mitochondrial import of 3-oxoacyl-CoA thiolase*. 1988, J. Biol. Chem. 263, 14463- 14470

[22] Duhl, D.M., Powell, T., and Poyton, R.O. *Mitochondrial import of cytochrome c oxidase subunit VIIa in Saccharomyces cerevisiae. Identification of sequences required for mitochondrial localization in vivo*. 1990, J. Biol. Chem. 265, 7273-7277

[23] Rehling P, Wiedemann N, Pfanner N, Truscott KN. *The mitochondrial import machinery for preproteins.* 2001, Crit Rev Biochem Mol Biol.36(3):291-336.

[24] Chacinska A, Koehler CM, Milenkovic D, Lithgow T, Pfanner N. *Importing mitochondrial proteins: machineries and mechanisms.* 2009, Cell. 21;138(4):628-44.

[25] Bolender N, Sickmann A, Wagner R, Meisinger C, Pfanner N. *Multiple pathways for sorting mitochondrial precursor proteins*. 2008, EMBO Rep. 9(1):42-9.

[26] Rapaport D, Neupert W. *Biogenesis of Tom40, Core Component of the Tom Complex of Mitochondria*. 1999, The Journal of Cell Biology. 146(2):321-332.

[27] Paschen SA, Waizenegger T, Stan T, Preuss M, Cyrklaff M, Hell K, Rapaport D, Neupert W. *Evolutionary conservation of biogenesis of beta-barrel membrane proteins.* 2003, Nature. 18;426(6968):862-6.

[28]Pfanner, N., Wiedemann, N., Meisinger, C., and Lithgow, T. *Assembling the mitochondrial outer membrane*. 2004, Nat. Struct. Mol. Biol. 11, 1044–1048.

[29] Mokranjac D, Paschen SA, Kozany C, Prokisch H, Hoppins SC, Nargang FE, Neupert W, Hell K. *Tim50, a novel component of the TIM23 preprotein translocase of mitochondria*. 2003, EMBO J. 17;22(4):816-25.

[30] Alder NN, Jensen RE, and Johnson AE. *Fluorescence mapping of mitochondrial TIM23 complex reveals a water-facing, substrate-interacting helix surface.* 2008, Cell 134, 439-450

[31] Chacinska A, Lind M, Frazier AE, Dudek J, Meisinger C, Geissler A, Sickmann A, Meyer HE, Truscott KN, Guiard B, Pfanner N, Rehling P. *Mitochondrial presequence translocase: switching between TOM tethering and motor recruitment involves Tim21 and Tim17.* 2005, Cell. 25;120(6):817-29.

[32] Bukau B, Horwich AL. *The Hsp70 and Hsp60 chaperone machines*. 1998, Cell. 6;92(3):351-66.

[33] Mokranjac D, Bourenkov G, Hell K, Neupert W, Groll M. *Structure and function of Tim14 and Tim16, the J and J-like components of the mitochondrial protein import motor*. 2006, EMBO J. 4;25(19):4675-85. Epub 2006 Sep 14

[34] Neupert, W., and Herrmann, J. M. *Translocation of proteins into mitochondria.* 2007, Annu. Rev. Biochem. 76, 723-749

[35] Miyata N, Tang Z, Conti MA, Johnson ME, Douglas CJ, Hasson SA, Damoiseaux R, Chang CA, Koehler CM. *Adaptation of a Genetic Screen Reveals an Inhibitor for Mitochondrial Protein Import Component Tim44.* 2017, J Biol Chem. 31;292(13):5429-5442.

[36] Gakh O, Cavadini P, Isaya G. *Mitochondrial processing peptidases.* 2002, Biochim Biophys Acta. 2;1592(1):63-77.

[37] Mignotte B, Vayssiere JL. *Mitochondria and apoptosis.* 1998, Eur J Biochem. 15;252(1):1-15.

[38] Vaux DL, Korsmeyer SJ. *Cell death in development*. 1999, Cell. 22;96(2):245-54.

[39] Hengartner MO. *The biochemistry of apoptosis*. 2000, Nature. 12;407(6805):770-6.

[40] Ichim G, Tait SW. A fate worse than death: apoptosis as an oncogenic process. 2016, Nat Rev Cancer. 16(8):539-48.

[41] Locksley RM, Killeen N, Lenardo MJ. *The TNF and TNF receptor superfamilies: integrating mammalian biology.* 2001, Cell. 23;104(4):487-501.

[42] Hsu H, Xiong J, Goeddel DV. *The TNF receptor 1-associated protein TRADD signals cell death and NF-kappa B activation*. 1995, Cell. 19;81(4):495-504.

[43] Wajant H. The *Fas signaling pathway: more than a paradigm.* 2002, Science. 31;296(5573):1635-6.

[44] Scaffidi C, Fulda S, Srinivasan A, Friesen C, Li F, Tomaselli KJ, Debatin KM, Krammer PH, Peter ME. *Two CD95 (APO-1/Fas) signaling pathways*. 1998, EMBO J. 16;17(6):1675-87.

[45] Igney FH, Krammer PH. Death and anti-death: tumour resistance to apoptosis. 2002, Nat Rev Cancer. 2(4):277-88.

[46] Kischkel FC, Hellbardt S, Behrmann I, Germer M, Pawlita M, Krammer PH, Peter ME. *Cytotoxicity-dependent APO-1 (Fas/CD95)-associated proteins form a death-inducing signaling complex (DISC) with the receptor.* 1995, EMBO J. 15;14(22):5579-88.

[47] Elmore S. *Apoptosis: A Review of Programmed Cell Death*. Toxicologic pathology. 2007;35(4):495-516.

[48] Kroemer G, Galluzzi L, Brenner C. *Mitochondrial membrane permeabilization in cell death.* 2007, Physiol Rev. 87(1):99-163.

[49] Chinnadurai G, Vijayalingam S, Gibson SB. *BNIP3 subfamily BH3-only proteins: mitochondrial stress sensors in normal and pathological functions*. 2008, Oncogene. 27 Suppl 1: S114-27.

[50]Saelens X, Festjens N, Vande Walle L, van Gurp M, van Loo G, Vandenabeele P. *Toxic proteins released from mitochondria in cell death*. 2004, Oncogene. 12;23(16):2861-74.

[51] Youle RJ, Strasser A. *The BCL-2 protein family: opposing activities that mediate cell death*. 2008, Nat Rev Mol Cell Biol. 9(1):47-59.

[52] Gross A, McDonnell JM, Korsmeyer SJ. *BCL-2 family members and the mitochondria in apoptosis*. 1999, Genes Dev. 1;13(15):1899-911.

[53] Krippner A, Matsuno-Yagi A, Gottlieb RA, Babior BM. *Loss of function of cytochrome c in Jurkat cells undergoing fas-mediated apoptosis.* 1996, J Biol Chem. 30;271(35):21629-36.

[54] Wang C, Youle RJ. *The Role of Mitochondria in Apoptosis*. 2009, Annual review of genetics. 43:95-118.

[55] Chipuk JE, Kuwana T, Bouchier-Hayes L, Droin NM, Newmeyer DD, Schuler M, Green DR. *Direct activation of Bax by p53 mediates mitochondrial membrane permeabilization and apoptosis*. 2004, Science. 13;303(5660):1010-4.

[56] Kuwana T, Mackey MR, Perkins G, Ellisman MH, Latterich M, Schneiter R, Green DR, Newmeyer DD. *Bid, Bax, and lipids cooperate to form supramolecular openings in the outer mitochondrial membrane*. 2002, Cell. 1;111(3):331-42.

[57] Youle RJ, Karbowski M. Mitochondrial fission in apoptosis. 2005, Nat Rev Mol Cell Biol. 6(8):657-63.

[58] Adrain C, Slee EA, Harte MT, Martin SJ. *Regulation of apoptotic protease activating factor-1 oligomerization and apoptosis by the WD-40 repeat region*. 1999, J Biol Chem. 23;274(30):20855-60.

[59] Zou H, Li Y, Liu X, Wang X. *An APAF-1. cytochrome c multimeric complex is a functional apoptosome that activates procaspase-9.* 1999, J Biol Chem. 23;274(17):11549-56.

[60] Jiang X, Wang X. *Cytochrome c promotes caspase-9 activation by inducing nucleotide binding to Apaf-1*. 2000, J Biol Chem. 6;275(40):31199-203.

[61] Hill MM, Adrain C, Duriez PJ, Creagh EM, Martin SJ. *Analysis of the composition, assembly kinetics and activity of native Apaf-1 apoptosomes*. 2004, The EMBO Journal. 23(10):2134-2145.

[62] Yuan S, Yu X, Topf M, Ludtke SJ, Wang X, Akey CW. *Structure of an apoptosome-procaspase-9 CARD complex*. 2010, Structure. 12;18(5):571-83.

[63] Slee EA, Harte MT, Kluck RM, Wolf BB, Casiano CA, Newmeyer DD, Wang HG, Reed JC, Nicholson DW, Alnemri ES, Green DR, Martin SJ. *Ordering the cytochrome*

c-initiated caspase cascade: hierarchical activation of caspases-2, -3, -6, -7, -8, and -10 in a caspase-9-dependent manner. 1999, J Cell Biol. 25;144(2):281-92.

[64] Schimmer AD. *Inhibitor of apoptosis proteins: translating basic knowledge into clinical practice.* 2004, Cancer Res. 15;64(20):7183-90.

[65] Crook NE, Clem RJ, Miller LK. *An apoptosis-inhibiting baculovirus gene with a zinc finger-like motif.* 1993, *J Virol* 67: 2168-74.

[66] Joza N, Susin SA, Daugas E, Stanford WL, Cho SK, Li CY, Sasaki T, Elia AJ, Cheng HY, Ravagnan L, Ferri KF, Zamzami N, Wakeham A, Hakem R, Yoshida H, Kong YY, Mak

TW, Zúñiga-Pflücker JC, Kroemer G, Penninger JM. *Essential role of the mitochondrial apoptosis-inducing factor in programmed cell death.* 2001, Nature. 29;410(6828):549-54.

[67] Li LY, Luo X, Wang X. Endonuclease G is an apoptotic DNase when released from mitochondria. 2001, Nature. 5;412(6842):95-9.

[68] Enari M, Sakahira H, Yokoyama H, Okawa K, Iwamatsu A, Nagata S. *A caspase-activated DNase that degrades DNA during apoptosis, and its inhibitor ICAD.* 1998, Nature. 1;391(6662):43-50.

[69] Loureiro, R., Mesquita, K. A., Oliveira, P. J. & Vega-Naredo, I. *Mitochondria in cancer stem cells: a target for therapy*. Recent Pat. 2013, Endocr. Metab. Immune Drug Discov. 7, 102–114.

[70] Wadhwa R, Takano S, Kaur K, Deocaris CC, Pereira-Smith OM, Reddel RR, Kaul SC. *Upregulation of mortalin/mthsp70/Grp75 contributes to human carcinogenesis*. 2006, Int J Cancer. 15;118(12):2973-80.

[71] Ma Z, Izumi H, Kanai M, Kabuyama Y, Ahn NG, Fukasawa K. *Mortalin controls centrosome duplication via modulating centrosomal localization of p53*. 2006, Oncogene. 31;25(39):5377-90.

[72] Lu WJ, Lee NP, Kaul SC, Lan F, Poon RT, Wadhwa R, Luk JM. *Induction of mutant p53-dependent apoptosis in human hepatocellular carcinoma by targeting stress protein mortalin*. 2011, Int J Cancer. 15;129(8):1806-14.

[73] Yun CO, Bhargava P, Na Y, Lee JS, Ryu J, Kaul SC, Wadhwa R. *Relevance of mortalin to cancer cell stemness and cancer therapy*. 2017, Sci Rep. 6;7:42016.

[74] Jubinsky PT, Messer A, Bender J, Morris RE, Ciraolo GM, Witte DP, Hawley RG, Short MK. *Identification and characterization of Magmas, a novel mitochondria-associated protein involved in granulocyte-macrophage colony-stimulating factor signal transduction.* 2001, Exp Hematol. 29(12):1392-402.

[75] Peng J, Huang CH, Short MK, Jubinsky PT. *Magmas gene structure and evolution.* 2005, *In Silico Bio*l. 5(3):251-63. Epub

[76] Genatlas, gene database. http://genatlas.medecine.univ-paris5.fr/fiche.php?n=30564

[77] Jubinsky PT, Short MK, Mutema G, Witte DP. *Developmental expression of Magmas in murine tissues and its co-expression with the GM-CSF receptor*. 2003, J Histochem Cytochem. 51(5):585-96.

[78] Li Y, Dudek J, Guiard B, Pfanner N, Rehling P, Voos W. *The presequence translocase-associated protein import motor of mitochondria. Pam16 functions in an antagonistic manner to Pam18*. 2004, J Biol Chem. 3;279(36):38047-54.

[79] D'Silva PR, Schilke B, Walter W, Craig EA. *Role of Pam16's degenerate J domain in protein import across the mitochondrial inner membrane.* 2005, Proc Natl Acad Sci U S A. 30;102(35):12419-24.

[80] Frazier AE, Dudek J, Guiard B, Voos W, Li Y, Lind M, Meisinger C, Geissler A, Sickmann A, Meyer HE, Bilanchone V, Cumsky MG, Truscott KN, Pfanner N, Rehling P. *Pam16 has an essential role in the mitochondrial protein import motor*. 2004, Nat Struct Mol Biol. 11(3):226-33.

[81] Jubinsky PT, Short MK, Ghanem M, Das BC. *Design, synthesis, and biological activity of novel Magmas inhibitors*. 2011, Bioorg Med Chem Lett. 1;21(11):3479-82.

[82] Liu Q, D'Silva P, Walter W, Marszalek J, Craig EA. *Regulated cycling of mitochondrial Hsp70 at the protein import channel*. 2003, Science. 4;300(5616):139-41.

[83] Bukau B, Weissman J, Horwich A. *Molecular chaperones and protein quality control*. 2006, Cell. 5;125(3):443-51.

[84] Kampinga HH, Craig EA. *The HSP70 chaperone machinery: J proteins as drivers of functional specificity*. 2010, Nat Rev Mol Cell Biol. 11(8):579-92.

[85] Laufen T, Mayer MP, Beisel C, Klostermeier D, Mogk A, Reinstein J, Bukau B. *Mechanism of regulation of hsp70 chaperones by DnaJ cochaperones*. 1999, Proc Natl Acad Sci U S A. 11;96(10):5452-7.

[86] Misselwitz B, Staeck O, Rapoport TA. J proteins catalytically activate Hsp70 molecules to trap a wide range of peptide sequences. 1998, Mol Cell. 2(5):593-603.

[87] Mokranjac D, Sichting M, Popov-Celeketić D, Berg A, Hell K, Neupert W. *The import motor of the yeast mitochondrial TIM23 preprotein translocase contains two different J proteins, Tim14 and Mdj2*. 2005, J Biol Chem. 9;280(36):31608-14.

[88] D'Silva PR, Schilke B, Hayashi M, Craig EA. *Interaction of the J-protein heterodimer Pam18/Pam16 of the mitochondrial import motor with the translocon of the inner membrane*. 2008, Mol Biol Cell. 19(1):424-32.

[89] Kozany C, Mokranjac D, Sichting M, Neupert W, Hell K. The J domain-related cochaperone Tim16 is a constituent of the mitochondrial TIM23 preprotein translocase. 2004, Nat Struct Mol Biol. 11(3):234-41.

[90] Sinha D, Srivastava S, D'Silva P. Functional Diversity of Human Mitochondrial *J-proteins Is Independent of Their Association with the Inner Membrane Presequence Translocase*. 2016, J Biol Chem. 12;291(33):17345-59.

[91] Cheetham ME, Caplan AJ. *Structure, function and evolution of DnaJ: conservation and adaptation of chaperone function*. 1998, Cell Stress Chaperones. 3(1):28-36.

[92] Genevaux P, Schwager F, Georgopoulos C, Kelley WL. *Scanning mutagenesis identifies amino acid residues essential for the in vivo activity of the Escherichia coli DnaJ (Hsp40) J-domain*. 2002, Genetics. 162(3):1045-53.

[93] Greene MK, Maskos K, Landry SJ. *Role of the J-domain in the cooperation of Hsp40 with Hsp70.* 1998, Proc Natl Acad Sci U S A. 26;95(11):6108-13.

[94] Landry SJ. *Swivels and stators in the Hsp40-Hsp70 chaperone machine*. 2003, Structure. 11(12):1465-6.

[95]Walsh P, Bursać D, Law YC, Cyr D, Lithgow T. *The J-protein family: modulating protein assembly, disassembly and translocation.* 2004, BO Rep. 5(6):567-71.

[96] D'Silva PD, Schilke B, Walter W, Andrew A, Craig EA. *J protein cochaperone of the mitochondrial inner membrane required for protein import into the mitochondrial matrix.* 2003, Proc Natl Acad Sci U S A. 25;100(24):13839-44.

[97] Truscott KN, Voos W, Frazier AE, Lind M, Li Y, Geissler A, Dudek J, Müller H, Sickmann A, Meyer HE, Meisinger C, Guiard B, Rehling P, Pfanner N. *A J-protein is an*

essential subunit of the presequence translocase-associated protein import motor of mitochondria. 2003, J Cell Biol. 24;163(4):707-13.

[98] Li Y, Dudek J, Guiard B, Pfanner N, Rehling P, Voos W. *The presequence translocase-associated protein import motor of mitochondria. Pam16 functions in an antagonistic manner to Pam18*. 2004, J Biol Chem. 3;279(36):38047-54.

[99] Jubinsky PT, Short MK, Mutema G, Morris RE, Ciraolo GM, Li M. *Magmas expression in neoplastic human prostate*. 2005, J Mol Histol. 36(1-2):69-75.

[100] Tagliati F, Gentilin E, Buratto M, Molè D, degli Uberti EC, Zatelli MC. *Magmas, a gene newly identified as overexpressed in human and mouse ACTH-secreting pituitary adenomas, protects pituitary cells from apoptotic stimuli*. 2010, Endocrinology. 151(10):4635-42.

[101] Tagliati F, Gagliano T, Gentilin E, Minoia M, Molè D, Delgi Uberti EC, Zatelli MC. *Magmas Overexpression Inhibits Staurosporine Induced Apoptosis in Rat Pituitary Adenoma Cell Lines*. 2013, PLoS One. 27;8(9).

[102] Zatelli MC, Gagliano T, Pelà M, Bianco S, Bertolasi V, Tagliati F, Guerrini R, degli Uberti E, Salvadori S, Trapella C. *N-carbamidoyl-4-((3-ethyl-2,4,4-trimethylcyclohexyl) methyl) benzamide enhances staurosporine cytotoxic effects likely inhibiting the protective action of Magmas toward cell apoptosis*. 2014, J Med Chem. 12;57(11):4606-14.

[103] Srivastava S, Sinha D, Saha PP, Marthala H, D'Silva P. *Magmas functions as a ROS regulator and provides cytoprotection against oxidative stress-mediated damages*. 2014, Cell Death Dis. 28;5: e1394.

[104] Mégarbané A, Dagher R, Melki I. *Sib pair with previously unreported skeletal dysplasia.* 2008, Am J Med Genet A. 15;146A (22):2916-9.

[105] Mégarbané A, Mehawej C, El Zahr A, Haddad S, Cormier-Daire V. *A second family with autosomal recessive spondylometaphyseal dysplasia and early death*. 2014, Am J Med Genet A. 164A(4):1010-4.

[106] Mehawej C, Delahodde A, Legeai-Mallet L, Delague V, Kaci N, Desvignes JP, Kibar Z, Capo-Chichi JM, Chouery E, Munnich A, Cormier-Daire V, Mégarbané *A. The impairment of MAGMAS function in human is responsible for a severe skeletal dysplasia.* 2014, PLoS Genet. 1;10(5):e1004311.

[107] Moosa S, Fano V, Obregon MG, Altmüller J, Thiele H, Nürnberg P, Nishimura G, Wollnik B. *A novel homozygous PAM16 mutation in a patient with a milder phenotype and longer survival*. 2016, Am J Med Genet A. 170(9):2436-9.

[108] Longley DB, Johnston PG. Molecular mechanisms of drug resistance. 2005, J Pathol. 205(2):275-92.

[109] Swanton C. *Intratumor heterogeneity: evolution through space and time*. 2012, Cancer Res. 1;72(19):4875-82.

[110] Holohan C, Van Schaeybroeck S, Longley DB, Johnston PG. *Cancer drug resistance: an evolving paradigm*. 2013, Nat Rev Cancer. 13(10):714-26.

[111] Zheng H-C. *The molecular mechanisms of chemoresistance in cancer*s. 2017, *Oncotarget*. 8(35):59950-59964.

[112] Harrison DJ. Molecular mechanisms of drug resistance in tumours. 1995, J Pathol. 175(1):7-12.

[113] Tomida A., Tsuruo T. Drug resistance pathways as targets. 2001, *Anticancer Drug Development*, 77-90,

[114] Yasui K, Mihara S, Zhao C, Okamoto H, Saito-Ohara F, Tomida A, Funato T, Yokomizo A, Naito S, Imoto I, Tsuruo T, Inazawa J. Alteration in copy numbers of genes as a mechanism for acquired drug resistance. 2004, Cancer Res. 15;64(4):1403-10.

[115] Hundahl SA, Cady B, Cunningham MP, Mazzaferri E, McKee RF, Rosai J, Shah JP, Fremgen AM, Stewart AK, Hölzer S. *Initial results from a prospective cohort study of 5583 cases of thyroid carcinoma treated in the united states during 1996. U.S. and German Thyroid Cancer Study Group. An American College of Surgeons Commission on Cancer Patient Care Evaluation study*. 2000, Cancer. 1;89(1):202-17.

[116] Thyroid Cancer Treatment (PDQ®) Medullary Thyroid Cancer. [Accessed July 29, 2013]. Available at http://www.cancer.gov/cancertopics/pdq/treatment/thyroid/HealthProfessional/page7.

[117] Eng C, Clayton D, Schuffenecker I, Lenoir G, Cote G, Gagel RF, van Amstel HK, Lips CJ, Nishisho I, Takai SI, Marsh DJ, Robinson BG, Frank-Raue K, Raue F, Xue F, Noll WW, Romei C, Pacini F, Fink M, Niederle B, Zedenius J, Nordenskjöld M, Komminoth P, Hendy GN, Mulligan LM, et al. *The relationship between specific RET proto-oncogene mutations and disease phenotype in multiple endocrine neoplasia type 2. International RET mutation consortium analysis.* 1996, JAMA. 276:1575–1579.

[118] Moline J, Eng C. Multiple endocrine neoplasia type 2: an overview. 2011, Genet Med. 13(9):755-64.

[119] Mulligan LM, Eng C, Healey CS, et al. *Specific mutations of the RET proto-oncogene are related to disease phenotype in MEN 2A and FMTC*. 1994, Nat Genet. 6:70–74.

[120] Hofstra RM, Landsvater RM, Ceccherini I, Stulp RP, Stelwagen T, Luo Y, Pasini B, Höppener JW, van Amstel HK, Romeo G, et al. *A mutation in the RET proto-oncogene associated with multiple endocrine neoplasia type 2B and sporadic medullary thyroid carcinoma*. 1994, Nature. 27;367(6461):375-6.

[121] Hazard JB, Hawk WA, Crile G Jr. *Medullary (solid) carcinoma of the thyroid; a clinicopathologic entity*. 1959, J Clin Endocrinol Metab. 19(1):152-61.

[122] Figlioli G, Landi S, Romei C, Elisei R, Gemignani F. *Medullary thyroid carcinoma (MTC) and RET proto-oncogene: mutation spectrum in the familial cases and a meta-analysis of studies on the sporadic form*. 2013, Mutat Res. 752(1):36-44.

[123] Taccaliti A, Silvetti F, Palmonella G, Boscaro M. *Genetic alterations in medullary thyroid cancer: diagnostic and prognostic markers*. 2011, Curr Genomics. 12(8):618-25.

[124] Roy M, Chen H, Sippel RS. *Current understanding and management of medullary thyroid cancer*. 2013, Oncologist. 18(10):1093-100.

[125] Sugawara M, Geffner DL, Martinez D, Hershman JM. *Novel treatment of medullary*

thyroid cancer. 2009, Curr Opin Endocrinol Diabetes Obes. 16(5):367-72.

[126] Siegel R, Naishadham D, Jemal A. *Cancer statistics*. 2013, CA Cancer J Clin. 63(1):11-30.

[127] Eckstein N, Röper L, Haas B, et al. *Clinical pharmacology of tyrosine kinase inhibitors becoming generic drugs: the regulatory perspective*. 2014, Journal of Experimental & Clinical Cancer Research 33(1):15.

[128] Wells SA Jr, Robinson BG, Gagel RF, Dralle H, Fagin JA, Santoro M, Baudin E, Elisei R, Jarzab B, Vasselli JR, Read J, Langmuir P, Ryan AJ, Schlumberger MJ. *Vandetanib in patients with locally advanced or metastatic medullary thyroid cancer: a randomized, double-blind phase III trial*. 2012, J Clin Oncol. 10;30(2):134-41.

[129] Elisei R, Schlumberger MJ, Müller SP, et al. *Cabozantinib in Progressive Medullary Thyroid Cancer*. 2013, Journal of Clinical Oncology. 31(29):3639-3646.

[130] Bible KC, Ryder M. Evolving molecularly targeted therapies for advanced-stage thyroid cancers. 2016, Nat Rev Clin Oncol. 13(7):403-16.

[131] Schlumberger M, Carlomagno F, Baudin E, Bidart JM, Santoro M. *New therapeutic approaches to treat medullary thyroid carcinoma*. 2008, Nat Clin Pract Endocrinol Metab. 4(1):22-32.

[132] Kucerova, L., Feketeova, L., Kozovska, Z., Poturnajova, M., Matuskova, M., Nencka, R., & Babal, P. In Vivo 5FU-Exposed Human Medullary Thyroid Carcinoma Cells Contain a Chemoresistant CD133+ Tumor–Initiating Cell Subset. 2014, Thyroid *24*(3), 520–532.

[133] Giuffrida D, Prestifilippo A, Scarfia A, Martino D, Marchisotta S. *New Treatment in advanced Thyroid Cancer.* 2012, Journal of Oncology. 2012:391629.

[134] Zatelli MC, Luchin A, Piccin D, Tagliati F, Bottoni A, Vignali C, Bondanelli M, degli Uberti EC. *Cyclooxygenase-2 inhibitors reverse chemoresistance phenotype in medullary thyroid carcinoma by a permeability glycoprotein-mediated mechanism*. 2005, J Clin Endocrinol Metab. 90(10):5754-60.

[135] Ghoncheh M, Pournamdar Z, Salehiniya H. *Incidence and Mortality and Epidemiology of Breast Cancer in the World*. 2016, Asian Pac J Cancer Prev. 17(S3):43-6.

[136] Siegel RL, Miller KD, Jemal A. Cancer statistics, 2016. 2016, CA Cancer J Clin. 66(1):7-30.

[137] Tao Z, Shi A, Lu C, Song T, Zhang Z, Zhao J. *Breast Cancer: Epidemiology and Etiology.* 2015, Cell Biochem Biophys. 72(2):333-8.

[138] McPherson K, Steel CM, Dixon JM. *Breast cancer—epidemiology, risk factors, and genetics.* 2000, BMJ: British Medical Journal. 321(7261):624-628.

[139] Smith KL, Isaacs C. BRCA Mutation Testing in Determining Breast Cancer therapy. 2011, Cancer journal (Sudbury, Mass). 17(6):492-499.

[140] Malhotra GK, Zhao X, Band H, Band V. *Histological, molecular and functional subtypes of breast cancers.* 2010, Cancer Biology & Therapy. 10(10):955-960.

[141]Sharma GN, Dave R, Sanadya J, Sharma P, Sharma KK. *Various types and management of breast cancer: an overview*. 2010, Journal of Advanced Pharmaceutical Technology & Research. 1(2):109-126.

[142] Paik S, Shak S, Tang G, Kim C, Baker J, Cronin M, Baehner FL, Walker MG, Watson D, Park T, Hiller W, Fisher ER, Wickerham DL, Bryant J, Wolmark N. *A multigene assay to predict recurrence of tamoxifen-treated, node-negative breast cancer*. 2004, N Engl J Med. 30;351(27):2817-26.

[143] van 't Veer LJ, Dai H, van de Vijver MJ, He YD, Hart AA, Mao M, Peterse HL, van der Kooy K, Marton MJ, Witteveen AT, Schreiber GJ, Kerkhoven RM, Roberts C, Linsley PS, Bernards R, Friend SH. *Gene expression profiling predicts clinical outcome of breast cancer*. 2002, Nature. 31;415(6871):530-6.

[144]Slamon DJ, Clark GM, Wong SG, Levin WJ, Ullrich A, McGuire WL. *Human breast cancer: correlation of relapse and survival with amplification of the HER-2/neu oncogene*. 1987, Science. 9;235(4785):177-82.

[145] Chin K, DeVries S, Fridlyand J, Spellman PT, Roydasgupta R, Kuo WL, Lapuk A, Neve RM, Qian Z, Ryder T, Chen F, Feiler H, Tokuyasu T, Kingsley C, Dairkee S, Meng Z, Chew K, Pinkel D, Jain A, Ljung BM, Esserman L, Albertson DG, Waldman FM, Gray JW. *Genomic and transcriptional aberrations linked to breast cancer pathophysiologies.* 2006, Cancer Cell. 10(6):529-41

[146] Bergamaschi A, Kim YH, Wang P, Sørlie T, Hernandez-Boussard T, Lonning PE, Tibshirani R, Børresen-Dale AL, Pollack JR. *Distinct patterns of DNA copy number alteration are associated with different clinicopathological features and gene-expression subtypes of breast cancer*. 2006, Genes Chromosomes Cancer. 45(11):1033-40.

[147] Perou CM. *Molecular stratification of triple-negative breast cancers*. 2011, Oncologist. 16 Suppl 1:61-70.

[148] Sorlie T, Tibshirani R, Parker J, Hastie T, Marron JS, Nobel A, Deng S, Johnsen H, Pesich R, Geisler S, Demeter J, Perou CM, Lønning PE, Brown PO, Børresen-Dale AL, Botstein D. *Repeated observation of breast tumor subtypes in independent gene expression data sets*. 2003, Proc Natl Acad Sci U S A. 8;100(14):8418-23.

[149] Foulkes WD, Stefansson IM, Chappuis PO, Bégin LR, Goffin JR, Wong N, Trudel M, Akslen LA. *Germline BRCA1 mutations and a basal epithelial phenotype in breast cancer.* 2003, J Natl Cancer Inst. 1;95(19):1482-5.

[150] Cancer Genome Atlas Network. *Comprehensive molecular portraits of human breast tumours.* 2012, Nature. 4;490(7418):61-70.

[151] Fertig EJ, Lee E, Pandey NB, Popel AS. *Analysis of gene expression of secreted factors associated with breast cancer metastases in breast cancer subtypes*. 2015, Sci Rep. 15;5:12133.

[152] Wu T, Wang X, Li J, Song X, Wang Y, Wang Y, Zhang L, Li Z, Tian J. *Identification of Personalized Chemoresistance Genes in Subtypes of Basal-Like Breast Cancer Based on Functional Differences Using Pathway Analysis*. 2015, PLoS One. 30;10(6):e0131183.

[153] Velaei K, Samadi N, Barazvan B, Soleimani Rad J. *Tumor microenvironment-mediated chemoresistance in breast cancer*. 2016, Breast. 30:92-100.

[154] Giordano SH, Buzdar AU, Smith TL, Kau SW, Yang Y, Hortobagyi GN. *Is breast cancer survival improving?.* 2004, Cancer. 1;100(1):44-52.

[155] Hortobagyi GN. *Treatment of breast cancer*. 1998, N Engl J Med. 1;339(14):974-84.

[156] Nabholtz JM. *Docetaxel-anthracycline combinations in metastatic breast cancer*. 2003, Breast Cancer Res Treat. 79 Suppl 1:S3-9.

[157] Piccart M. The role of taxanes in the adjuvant treatment of early stage breast cancer. 2003, Breast Cancer Res Treat. 79 Suppl 1:S25-34.

[158] Kuo MT. *Roles of multidrug resistance genes in breast cancer chemoresistance*. 2007, Adv Exp Med Biol. 608:23-30.

[159] Gómez-Miragaya J, Palafox M, Paré L, et al. *Resistance to Taxanes in Triple-Negative Breast Cancer Associates with the Dynamics of a CD49f+ Tumor-Initiating Population.* 2017, Stem Cell Reports. 8(5):1392-1407.

[160] Kuo MT. *Roles of multidrug resistance genes in breast cancer chemoresistance*. 2007, Adv Exp Med Biol. 608:23-30.

[161] Zatelli MC, Luchin A, Tagliati F, Leoni S, Piccin D, Bondanelli M, Rossi R, degli Uberti EC. *Cyclooxygenase-2 inhibitors prevent the development of chemoresistance phenotype in a breast cancer cell line by inhibiting glycoprotein p-170 expression*. 2007, Endocr Relat Cancer. 14(4):1029-38.

[162] Zatelli MC, Molè D, Tagliati F, Minoia M, Ambrosio MR, degli Uberti E. *Cyclo-oxygenase 2 modulates chemoresistance in breast cancer cells involving NF-kappaB*. 2009, Cell Oncol. 31(6):457-65.

[163] Vascotto SG, Beckham Y, Kelly GM. *The zebrafish's swim to fame as an experimental model in biology*. 1997, Biochem Cell Biol. 75(5):479-85.

[164] Grunwald DJ, Eisen JS. Headwaters of the zebrafish -- emergence of a new model vertebrate. 2002, Nat Rev Genet. 3(9):717-24.

[165] Amsterdam A, Hopkins N. *Mutagenesis strategies in zebrafish for identifying genes involved in development and disease*. 2006, Trends Genet. 22(9):473-8.

[166] Streisinger G, Walker C, Dower N, Knauber D, Singer F. *Production of clones of homozygous diploid zebra fish (Brachydanio rerio).* 1981, Nature. 28;291(5813):293-6.

[167] Chakrabarti S, Streisinger G, Singer F, Walker C. Frequency of γ-Ray Induced Specific *Locus and Recessive Lethal Mutations in Mature Germ Cells of the Zebrafish, BRACHYDANIO RERIO*. 1983, Genetics. 103(1):109-123.

[168] Walker C, Streisinger G. *Induction of Mutations by γ-Rays in Pregonial Germ Cells of Zebrafish Embryos.* 1983, Genetics. 103(1):125-136.

[169] runwald DJ, Streisinger G. *Induction of recessive lethal and specific locus mutations in the zebrafish with ethyl nitrosourea*. 1992, Genet Res. 59(2):103-16.

[170] *Solnica*-Krezel L, Schier AF, Driever W. *Efficient recovery of ENU-induced mutations from the zebrafish germline.* 1994, Genetics. 136(4):1401-20.

[171]Stuart GW, McMurray JV, Westerfield M. *Replication, integration and stable germ-line transmission of foreign sequences injected into early zebrafish embryos*. 1988, Development. 103(2):403-12.

[172] Streisinger G, Singer F, Walker C, Knauber D, Dower N. *Segregation analyses and gene-centromere distances in zebrafish*. 1986, Genetics. 112(2):311-9.

[173] Laale, HW. The *biology and use of zebrafish, Brachydanio rerio in fisheries research. A literature review.* 1977, J. Fish. Biol. **10**, 121–174.

[174] Scholz S, Fischer S, Gündel U, Küster E, Luckenbach T, Voelker D. *The zebrafish embryo model in environmental risk assessment--applications beyond acute toxicity testing.* 2008, Environ Sci Pollut Res Int. 15(5):394-404.

[175] Kimmel CB, Ballard WW, Kimmel SR, Ullmann B, Schilling TF. *Stages of embryonic development of the zebrafish*. 1995, Dev Dyn. 203(3):253-310.

[176] Spence R, Gerlach G, Lawrence C, Smith C. *The behaviour and ecology of the zebrafish, Danio rerio*. 2008, Biol Rev Camb Philos Soc. 83(1):13-34.

[177] Collins JE, White S, Searle SM, Stemple DL. *Incorporating RNA-seq data into the zebrafish Ensembl genebuild*. 2012, Genome Res. 22(10):2067-78.

[178] Howe K, Clark MD, Torroja CF, Torrance J, Berthelot C, Muffato M, Collins JE, Humphray S, McLaren K, Matthews L, McLaren S, Sealy I, Caccamo M, Churcher C, et al. *The zebrafish reference genome sequence and its relationship to the human genome.* 2013, Nature. 25;496(7446):498-503.

[179] Sipes NS, Padilla S, Knudsen TB. *Zebrafish: as an integrative model for twenty-first century toxicity testing*. 2011, Birth Defects Res C Embryo Today. 93(3):256-67.

[180] Nishimura Y, Inoue A, Sasagawa S, Koiwa J, Kawaguchi K, Kawase R, Maruyama T, Kim S, Tanaka T. *Using zebrafish in systems toxicology for developmental toxicity testing.* 2016, Congenit Anom (Kyoto). 56(1):18-27.

[181] OECD (1992) *OECD guideline for the testing of chemicals. Section 2: effects on biotic systems. OECD Test Guideline 203: fish, acute toxicity test.* Paris, France: Organization for Economic Cooperation and Development,

[182] OECD (2013) *OECD Guidelines for the testing of chemicals. Section 2: effects on biotic systems test no. 236: Fish embryo acute toxicity (FET) test*. Paris, France: Organization for Economic Cooperation and Development.

[183] Braunbeck T, Kais B, Lammer E, Otte J, Schneider K, Stengel D, Strecker R. *The fish embryo test (FET): origin, applications, and future*. 2015, Environ Sci Pollut Res Int. 22(21):16247-61.

[184] Braunbeck T, Boettcher M, Hollert H, Kosmehl T, Lammer E, Leist E, Rudolf M, Seitz N. *Towards an alternative for the acute fish LC(50) test in chemical assessment: the fish embryo toxicity test goes multi-species -- an update*. 2005, ALTEX. 22(2):87-102.

[185] Knöbel M, Busser FJ, Rico-Rico A, Kramer NI, Hermens JL, Hafner C, Tanneberger K, Schirmer K, Scholz S. *Predicting adult fish acute lethality with the zebrafish embryo: relevance of test duration, endpoints, compound properties, and exposure concentration analysis*. 2012, Environ Sci Technol. 4;46(17):9690-700.

[186] Nagel R. *DarT: The embryo test with the Zebrafish Danio rerio--a general model in ecotoxicology and toxicology*. 2002, ALTEX. 19 Suppl 1:38-48.

[187] Yin H, Kauffman KJ, Anderson DG. *Delivery technologies for genome editing*. 2017, Nat Rev Drug Discov. 16(6):387-399.

[188]Guha TK, Wai A, Hausner G. *Programmable Genome Editing Tools and their Regulation for Efficient Genome Engineering.* 2017, Comput Struct Biotechnol J. 12;15:146-160.

[189]Takata M, Sasaki MS, Sonoda E, Morrison C, Hashimoto M, Utsumi H, Yamaguchi-Iwai Y, Shinohara A, Takeda S. *Homologous recombination and non-homologous end-joining pathways of DNA double-strand break repair have overlapping roles in the maintenance of chromosomal integrity in vertebrate cells.* 1998, EMBO J. 15;17(18):5497-508.

[190]Szostak JW, Orr-Weaver TL, Rothstein RJ, Stahl FW. *The double-strand-break repair model for recombination*. 1983, Cell. 33(1):25-35.

[191]Lieber MR, Ma Y, Pannicke U, Schwarz K. *Mechanism and regulation of human non-homologous DNA end-joining*. 2003, Nat Rev Mol Cell Biol. 4(9):712-20.

[192]Maeder ML, Gersbach CA. *Genome-editing Technologies for Gene and Cell Therapy*. 2016, Molecular Therapy. 24(3):430-446.

[193]Long C, Amoasii L, Mireault AA, McAnally JR, Li H, Sanchez-Ortiz E, Bhattacharyya S, Shelton JM, Bassel-Duby R, Olson EN. *Postnatal genome editing partially restores dystrophin expression in a mouse model of muscular dystrophy*. 2016, Science. 22;351(6271):400-3.

[194] Isken O, Maquat LE. *Quality control of eukaryotic mRNA: safeguarding cells from abnormal mRNA function.* 2007, Genes Dev. 1;21(15):1833-56.

[195] Kato T, Takada S. *In vivo and in vitro disease modeling with CRISPR/Cas9*. 2017, Brief Funct Genomics. 16(1):13-24.

[196] Hsu PD, Lander ES, Zhang F. *Development and applications of CRISPR-Cas9 for genome engineering*. 2014, Cell. 5;157(6):1262-78.

[197] Ishino Y, Shinagawa H, Makino K, Amemura M, Nakata A. *Nucleotide sequence of the iap gene, responsible for alkaline phosphatase isozyme conversion in Escherichia coli, and identification of the gene product*. 1987, J Bacteriol. 169(12):5429-33.

[198] Barrangou R, Fremaux C, Deveau H, Richards M, Boyaval P, Moineau S, Romero DA, Horvath P. *CRISPR provides acquired resistance against viruses in prokaryotes*. 2007, Science. 23;315(5819):1709-12.

[199] Jinek M, Chylinski K, Fonfara I, Hauer M, Doudna JA, Charpentier E. *A programmable dual-RNA-guided DNA endonuclease in adaptive bacterial immunity*. 2012, Science. 17;337(6096):816-21.

[200] Gasiunas G, Barrangou R, Horvath P, Siksnys V. *Cas9-crRNA ribonucleoprotein complex mediates specific DNA cleavage for adaptive immunity in bacteria*. 2012, Proc Natl Acad Sci U S A. 25;109(39):E2579-86.

[201] Doudna JA, Charpentier E. *Genome editing. The new frontier of genome engineering with CRISPR-Cas9*. 2014, Science. 28;346(6213):1258096.

[202] Ran FA, Hsu PD, Lin CY, Gootenberg JS, Konermann S, Trevino AE, Scott DA, Inoue A, Matoba S, Zhang Y, Zhang F. *Double nicking by RNA-guided CRISPR Cas9 for enhanced genome editing specificity*. 2013, Cell. 12;154(6):1380-9.

[203] Graham DB, Root DE. *Resources for the design of CRISPR gene editing experiments*. Genome Biology. 2015;16:260.

[204] Ablain J, Durand EM, Yang S, Zhou Y, Zon LI. *A CRISPR/Cas9 vector system for tissue-specific gene disruption in zebrafish*. 2015, Dev Cell. 23;32(6):756-64.

[205] Cho SW, Kim S, Kim JM, Kim JS. *Targeted genome engineering in human cells with the Cas9 RNA-guided endonuclease.* 2013, Nat Biotechnol. 31(3):230-2.

[206] Cong L, Ran FA, Cox D, Lin S, Barretto R, Habib N, Hsu PD, Wu X, Jiang W, Marraffini LA, Zhang F. *Multiplex genome engineering using CRISPR/Cas systems*. 2013, Science. 15;339(6121):819-23.

[207] Jiang W, Bikard D, Cox D, Zhang F, Marraffini LA. *RNA-guided editing of bacterial genomes using CRISPR-Cas systems.* 2013, Nat Biotechnol. 31(3):233-9.

[208] Mali P, Yang L, Esvelt KM, Aach J, Guell M, DiCarlo JE, Norville JE, Church GM. *RNA-guided human genome engineering via Cas9*. 2013, Science. 15;339(6121):823-6.

[209] ang H, Yang H, Shivalila CS, Dawlaty MM, Cheng AW, Zhang F, Jaenisch R. *One-step generation of mice carrying mutations in multiple genes by CRISPR/Cas-mediated genome engineering*. 2013, Cell. 9;153(4):910-8.

[210] Gagnon JA, Valen E, Thyme SB, Huang P, Akhmetova L, Pauli A, Montague TG, Zimmerman S, Richter C, Schier AF. *Efficient mutagenesis by Cas9 protein-mediated oligonucleotide insertion and large-scale assessment of single-guide RNAs*. 2014, PLoS One. 29;9(5):e98186.

[211] Ablain J, Durand EM, Yang S, Zhou Y, Zon LI. *A CRISPR/Cas9 vector system for tissue-specific gene disruption in zebrafish*. 2015, Developmental cell. 32(6):756-764.

[212] ZFIN https://zfin.org/ZDB-GENE-040426-1776

[213]Laemmli UK. *Cleavage of structural proteins during the assembly of the head of bateriophage T4*. 1970, Nature, 227, 680–5.

[214] Chari R, Mali P, Moosburner M, Church GM. *Unraveling CRISPR-Cas9 genome ngineering parameters via a library-on-library approach*. 2015, Nature Methods 12(9):823-6.

[215] https://crispr.med.harvard.edu/sgRNAScorerV1

[216] Brinkman EK, Chen T, Amendola M, van Steensel B. *Easy quantitative assessment of genome editing by sequence trace decomposition*. 2014, Nucleic Acids Res 16;42(22):e168.

[217] https://tide-calculator.nki.nl/

[218] Westerfield M. *The Zebrafish Book a Guide for the Laboratory Use of Zebrafish (Danio Rerio)*. 2007, *5th Edition*. Eugene: University of Oregon Press.

[219] Bentzien F, Zuzow M, Heald N, Gibson A, Shi Y, Goon L, Yu P, Engst S, Zhang W, Huang D, Zhao L, Vysotskaia V, Chu F, Bautista R, Cancilla B, Lamb P, Joly AH, Yakes FM. *In vitro and in vivo activity of cabozantinib (XL184), an inhibitor of RET, MET, and VEGFR2, in a model of medullary thyroid cancer*. 2013, Thyroid. 23(12):1569-77.

[220] Giorgi C, Bonora M, Missiroli S, Poletti F, Ramirez FG, Morciano G, Morganti C, Pandolfi PP, Mammano F, Pinton P. *Intravital imaging reveals p53-dependent cancer cell death induced by phototherapy via calcium signaling*. 2015, Oncotarget. 30;6:1435-45.

[221] Kuchay S, Giorgi C, Simoneschi D, Pagan J, Missiroli S, Saraf A, Florens L,Washburn MP, Collazo-Lorduy A, Castillo-Martin M, Cordon-Cardo C, Sebti SM, Pinton P, Pagano M. *PTEN counteracts FBXL2 to promote IP3R3- and Ca(2+)-mediated apoptosis limiting tumour growth.* 2017, Nature. 22;546(7659):554-558.

[222] Missiroli S, Bonora M, Patergnani S, Poletti F, Perrone M, Gafà R, Magri E, Raimondi A, Lanza G, Tacchetti C, Kroemer G, Pandolfi PP, Pinton P, Giorgi C. *PML at Mitochondria-Associated Membranes Is Critical for the Repression of Autophagy and Cancer Development*. 2016, Cell Rep 30;16(9):2415-27.

[223] Lin Y, Devin A, Rodriguez Y, Liu Z. *Cleavage of the death domain kinase RIP by Caspase-8 prompts TNF-induced apoptosis*. 1999, Genes & Development. 13(19):2514-2526.

[224] Wolff S, Erster S, Palacios G, Moll UM. *p53's mitochondrial translocation and MOMP action is independent of Puma and Bax and severely disrupts mitochondrial membrane integ*rity. 2008, Cell Res. 18(7):733-44.

[225] Ashcroft M, Taya Y, Vousden KH. *Stress Signals Utilize Multiple Pathways to Stabilize p53*. 2000, Molecular and Cellular Biology. 20(9):3224-3233.

[226] Kaul SC, Deocaris CC, Wadhwa R. *Three faces of mortalin: a housekeeper, guardian and killer.* 2007, Exp Gerontol. 42(4):263-74.

[227] Yi X, Luk JM, Lee NP, Peng J, Leng X, Guan XY, Lau GK, Beretta L, Fan ST. *Association of mortalin (HSPA9) with liver cancer metastasis and prediction for early tumor recurrence*. 2008, Mol Cell Proteomics. 7(2):315-25.

[228] Czarnecka AM, Campanella C, Zummo G, Cappello F. *Mitochondrial chaperones in cancer: from molecular biology to clinical diagnostics*. 2006, Cancer Biol Ther. 5(7):714-20.

[229] Iosefson O, Azem A. *Reconstitution of the mitochondrial Hsp70 (mortalin)-p53 interaction using purified proteins--identification of additional interacting regions*. 2010, FEBS Lett. 19;584(6):1080-4.

[230] Yang L, Li H, Jiang Y, Zuo J, Liu W. *Inhibition of mortalin expression reverses cisplatin resistance and attenuates growth of ovarian cancer cells*. 2013, Cancer Lett. 9;336(1):213-21.

[231] Ojala T, Polinati P, Manninen T, Hiippala A, Rajantie J, Karikoski R, Suomalainen A, Tyni T. *New mutation of mitochondrial DNAJC19 causing dilated and noncompaction cardiomyopathy, anemia, ataxia, and male genital anomalies*. 2012, Pediatr Res. 72(4):432-7.

[232] Miyata N, Tang Z, Conti MA, Johnson ME, Douglas CJ, Hasson SA, Damoiseaux R, Chang CA, Koehler CM. *Adaptation of a Genetic Screen Reveals an Inhibitor for Mitochondrial Protein Import Component Tim44*. 2017, J Biol Chem. 31;292(13):5429-5442.